EIDESSTATTLICHE ERKLÄRUNG

Ich erkläre an Eides statt, dass ich die vorliegende Arbeit selbstständig verfasst, andere als die angegebenen Quellen/Hilfsmittel nicht benutzt, und die den benutzten Quellen wörtlich und inhaltlich entnommenen Stellen als solche kenntlich gemacht habe. Das in TUGRAZonline hochgeladene Textdokument ist mit der vorliegenden Masterarbeit identisch.

Datum

Unterschrift

Danksagung

An dieser Stelle möchte ich mich all jenen bedanken, die mich bei der Verfassung dieser Arbeit unterstützt haben bedanken.

Zuerst gebührt mein Dank Professor Viktor Hacker, der mich beim Erstellen der Arbeit betreut und diese begutachtet hat. Für hilfreiche Anregungen und konstruktive Kritik möchte ich mich herzlich bedanken.

Des Weiteren möchte ich mich bei Dr. Christoph Grimmer und allen weiteren Mitarbeitern des Instituts für Chemische Verfahrenstechnik an der TU Graz bedanken. Sie standen mir Hilfsbereit zur Seite und sorgten für ein angenehmes und angeregtes Arbeitsumfeld.

Ein Besonderer Dank gilt der proionic GmbH und der österreichischen Forschungsförderungsgesellschaft (FFG) für ihre Finanzielle Unterstützung.

Abschließend möchte ich mich bei meinen Eltern Heinrich Grandi und Sonja Kugler Grandi bedanken, die mein Studium ermöglicht haben und mich immer unterstützt haben.

Maximilian Grandi, BSc

Graz, 07.09.2016

Abstract

Since their discovery in the 1960's and their rediscovery in the early 1990's, direct borohydride fuel cells (DBFC) have been topic of many publications in the last decade [1]–[8]. They are attractive because of high energy storage densities and high theoretical open circuit voltage of 1.64 V. Because the fuel used is liquid, storage and transport are safe and easy [9]. However, they are still far from the commercial deployment. The reason is mainly the complexity of the borohydride oxidation reaction (BOR). To reach the fully oxidized state of the metaborate numerous transition states are formed. Additionally, the reaction pathway of the BOR depends on the chemical, physical and structural properties of the used electro catalyst and the support material. An important factor is the occurrence of hydrogen as a result of the concurring hydrolysis reaction, a side reaction that needs to be supressed.

The goal of this work was the synthesis of different carbon supported mono – and bimetallic nanoparticles as electro catalysts for the borohydride oxidation reaction. Platinum, gold, palladium, bismuth and indium were investigated.
The nanoparticles were synthesized by the instant method, a colloidal deposition method.
A focus was laid on the inhibition of the hydrogen evolution. Therefore, these electro catalysts were characterized using cyclic voltammetry (CV), rotating disc electrode cyclic voltammetry (RDE-CV) and in-situ polarisation measurements combined with an online hydrogen detection system. The in-situ measurements were performed in an in-house designed DBFC.

A comparison of different borohydride sources was made. Four different ionic liquids of the type NR_4BH_4 were provided by the proionic GmbH. These compounds are known to show an increased solubility and stability in alkaline solutions, resulting in an increased energy density of the fuel. The kinetic parameters of said borohydride sources were studied using rotating disk electrodes and compared to $NaBH_4$.

Kurzfassung

Seit deren Aufkommen in den 1960er Jahren und deren Wiederentdeckung in den Anfängen der 90er, waren Direkt Borhydrid Brennstoffzellen (DBFC) das Thema mehrerer Publikationen des letzten Jahrzehnts. Die Attraktivität dieser elektrochemischen Zellen ist durch die hohe Energiespeicherdichte und hohe theoretische Zellspannung von 1,64 V gegeben. Weil der Brennstoff flüssig ist, sind Transport und Lagerung sicher und unkompliziert. Jedoch sind diese Brennstoffzellen weit von einer praktischen und kommerziellen Umsetzung entfernt. Das liegt vor Allem an der komplexen Kinetik der Borhydrid Oxidationsreaktion (BOR). Um das Endprodukt Metaborat zu erhalten werden mehrere Zwischenprodukte gebildet. Außerdem hängt der Reaktionsmechanismus von den chemischen, physikalischen und strukturellen Eigenschaften des eingesetzten Katalysators und dessen Trägermaterials ab. Ein wichtiger Faktor ist das Auftreten von Wasserstoffentwicklung als Folge der konkurrierenden Hydrolysereaktion. Diese Nebenreaktion muss unterdrückt werden.

Das Ziel dieser Arbeit war die Synthese von mehreren mono- und bimetallischen Nanopartikeln auf Kohlenstoff als Katalysatoren für die Borhydrid Oxidationsreaktion. Die untersuchten Metalle waren Platin, Gold, Palladium Bismut und Indium.
Die Nanopartikel wurden mit der Instant Methode, einem kolloidalen Abscheidungsverfahren, hergestellt. Besondere Aufmerksamkeit wurde der Inhibition der Wasserstoffentwiklung geschenkt. Die Charakterisierung erfolgte mittels Zyklovoltametrie (CV), rotierende Scheibenelektroden Zyklovoltametrie (RDE-CV) und in-situ Polarisationsmessung welche mit einem Wasserstoffdetektionssystem kombiniert wurde. Die in-situ Messungen wurden mit einer selbst entworfenen DBFC durchgeführt.

Ein Vergleich verschiedener Borhydridquellen wurde durchgeführt. Vier verschiedene ionische Flüssigkeiten des Typs NR_4BH_4 wurden von der proionic GmbH zur Verfügung gestellt. Diese Verbindungen zeigen eine höhere Löslichkeit und Stabilität in alkalischen Lösungen. Dies führt zu einer erhöhten Energiedichte des Brennstoffs. Die kinetischen Parameter dieser Borhydridquellen wurden mittels rotierender Scheibenelektroden Zyklovoltametrie bestimmt und mit denen von $NaBH_4$ verglichen.

Table of content

1 Introduction

The mitigation of climate change effects and the creation of a sustainable and resource efficient society is one challenging task for the present scientific society worldwide. Following this goal, the deployment of renewable energy sources such as solar, wind and biomass for a large scale energy production has been driven forward by governments and organizations. However, these technologies are not reliable continuously, meaning there will be major fluctuations in the electrical power grid. For this purpose clean and efficient energy storage and conversion systems are needed [10]. In the mobility sector an environmentally friendly and safe alternative to fossil fuel driven systems has to be found.

Rechargeable batteries like lithium ion or nickel metal hydride batteries are often mentioned as a potential candidate but these systems need scarce resources. According to *S. Gupta* The main concern is lithium, of which the demand has already doubled in the last few years [11].

Fuel cells have long been proposed as storage and conversion systems for said purposes due to their high efficiency, adjustable storage capacity, high specific energy and the relatively clean and CO_2 free exhaust gases [12].

One major drawback of "conventional" fuel cells such as the polymer electrolyte membrane fuel cell (PEMFC) which are on the verge of commercialization, is the need for platinum. The use of alkaline media in fuel cells is a solution for this issue, because it allows the application of metals that are not stable in acidic conditions.

Another issue arises concerning the storage of the gaseous hydrogen. In the last decades a lot of research was conducted in the field of hydrogen storage systems. In the course of these studies many physical and chemical solutions have been investigated [13],[14]. *U. Eberle et al.* divided these solutions into physical and chemical storage systems [9].

The physical systems are listed as:

- Compressed gaseous Hydrogen (CGH_2): 35 - 70 MPa, room temperature
- Liquid Hydrogen (LH_2): 0.1 MPa, -253 °C
- Cryoadsorption on high surface area materials (CA): several MPa, liquid nitrogen temperatures

The **CGH_2** solution is technically by far the most mature system. It is very suitable for mobile applications due to the simplicity of the system and ambient operating temperature. To obtain acceptable specific energy densities it has to be stored at high pressures of 35 - 70 MPa.

Current compressed hydrogen systems do not meet requirements concerning system cost, volumetric storage density and fuel cost. Also the gravimetric density remains unsatisfactory [12]. The **LH_2** system, due to the higher densities of liquids, could address the challenges of gaseous systems. The biggest drawback of this system is the very low operation temperature, which leads to heat flow from the environment into the tank and evaporation of the hydrogen. Thus the increasing pressure has to be reduced by venting. Due to the low phase change enthalpy of around 0.45 MJ/kg of liquid to gaseous even small heat flows lead to evaporation.

Another physical storage method is the **cryoadsorbtion on high surface area materials**. As the name suggests, the operation temperature is around the boiling point of liquid nitrogen and pressures of several MPa. The exact temperature and pressure depends on the adsorption enthalpy, which varies with the material. Currently mainly Zeolite, carbon materials (nanotubes, nanohorns, carbon cloths and others), Metal-Organic Frameworks (MOFs) and Polymers with intrinsic microporosity (PIMs) are mentioned as such materials. None of these showed technically relevant storage densities [9].

The chemical hydrogen storage offers a broad variety of possibilities compared to the physical methods. These are listed as follows:

- Amide-borane adducts
- Amides/imides
- Liquid organic hydrogen carriers (LOHCs)
- Hydrocarbons (with reforming)
- Hydride systems

Amide-borane adducts are mainly BH_3NH_3 and $NH_3B_3H_7$. Due to their extraordinary hydrogen content they are highly promising for storage purposes. Ammonia-borane can be thermally decomposed at 130°C in a decomposition process involving multiple steps [15]. Because of the exothermic nature of the reaction, it is not suitable for reversible hydrogen storage. Using ammonia-triborane, hydrolytic hydrogen release is possible [16]. Using alumina supported rhodium compounds as catalyst a storage capacity of 6.1 wt% H_2 was realized. The risk of ammonia reaching the fuel cell inquires safety precautions and gas cleaning. Furthermore, the borate regeneration remains an unsolved issue.

Amide/imide systems work using mainly lithium imide (Li_3N) as hydrogen absorbent [17]. This absorption leads to a mixture of lithium hydride and lithium amide. Due to high desorption

enthalpies (approx. 60kJ/mol) the equilibrium pressure at 250°C reaches only 0.1 mPa. Additionally ammonia evolution is thermodynamically favoured [18]. Therefore, it is not suitable for practical application using a PEMFC.

The hydrogenation/dehydrogenation of cyclic hydrocarbons is another interesting approach. These liquid organic compounds (for example benzene/cyclohexane) have storage capacities of around 7 wt% H_2. They are intended for stationary storage, for example at a refuelling station. The dehydrogenated form needs to be transported back to a recycling station. However, the problem related to these systems is the high dehydrogenation temperature. For a complete release of H_2 over 300°C are required [19]. Nevertheless, it is one of the few technologies that have reached competitive prices on the market.

A technology that has been around for a long time and is already used for H_2 production is the **reforming of hydrocarbons**. However for a mobile application the creation of a small reactor with minimal heat losses is a difficult task [9].

Hydride systems are a solution with a big variety of possibilities regarding the hydrogen carrier. Metal hydrides have been studied intensively for this purpose, but due to the high specific weight of the transition metals used only 2 wt% storage density could be achieved. Therefore, the use of complex hydrides is more promising. One example with high storage densities is $LiBH_4$ with 8.4 wt%. One big challenge using hydride systems is the regeneration process. After releasing the hydrogen the carrier cannot be regenerated on board but needs an industrial size plant [20]. Furthermore, the solid hydrolysis product can lead to a precipitate in the storage tank. Using $NaBH_4$ these problems can be solved partially. The hydrogen can be released easily by bringing it in contact with a catalyst and it is stable in alkaline solutions [9], [20].

However, one major drawback of all these chemical storage solutions is the need for a reactor or catalyst system to release the stored hydrogen. This implies the need of additional space and produces additional costs. A potential solution is the direct oxidation of the hydrogen carrier on an anode producing the dehydrogenated form of the carrier. This can be achieved by the direct borohydride fuel dell (DBFC) [5]–[7].

2 Theoretical aspects

2.1 The Borohydride Oxidation Reaction (BOR)

As described above, for the use of hydrogen as fuel there are already many technologically mature fuel cell systems available. However, there is one intrinsic problem associated with the use of hydrogen: The gravimetric storage density of the most mature storage solution (CGH_2) is still not satisfactory. In contrast to this $NaBH_4$ is reported to have reached storage densities of 7.3 wt% H_2. The volumetric storage density is superior to that of the CGH_2 system [9].

Another issue is that fuel cells using H_2 reach open circuit voltages of around 0.9 V (small variations occur with the use of different systems), which is low compared to other electrochemical storage systems (e.g. lithium ion batteries). Although the kinetics of the hydrogen oxidation is favourable, the oxygen reduction reaction (ORR) shows high overpotentials even on platinum surfaces. A way to achieve higher OCVs could be the use of borohydride as fuel. First of all, the properties of the BH_4^- ion imply the use of alkaline media due to chemical stability reasons. This is favourable for the ORR due to the better kinetics in alkaline media. Furthermore, non- noble metals could be used as ORR catalysts, which reduce the costs of the system drastically. The standard redox potential of the BOR, is -1.24 V vs. SHE (see Eq.1).

$$BH_4^- + 8\,OH^- \rightarrow BO_2^- + 6\,H_2O + 8\,e^- \qquad E_0 = -1{,}24\,V \qquad \text{(Eq.1)}$$

$$2\,O_2 + 4\,H_2O + 8\,e^- \rightarrow 8\,OH^- \qquad E_0 = 0{,}40\,V \qquad \text{(Eq.2)}$$

Combined with the ORR in alkaline media this leads to equilibrium cell voltage of 1.64 V. The standard potential, cannot be reached in practical applications due to kinetic limitations. Especialy from the very poor kinetics of the BOR leading to a high overpotential [6], [7], [21]. The reactions mechanisms are very complex and still not fully understood. The BH_4^- ion is oxidized in a multiple step reaction involving various boron species as intermediates. The mechanisms are even more complex due to the influence of the pH value and the different behaviour on different metal surfaces. The two most studied surfaces in literature are Pt and Au [1]–[4], [6]–[8]. Of minor importance are reports of BOR on other metals like Pd, Ru, Ni, Co, Hg, Ag, Rh, Ir and Cu [5], [6], [22], [23]. These metals can be divided into two groups of metals: those catalytically active towards the heterogeneous hydrolysis and those inactive to it. Among those not active for heterogeneous hydrolysis are Hg, Cu, Au and possibly Ag [6]. However, in contradiction to this, *Chatenet et al.* [24] and *Lima et al.* [25] found that Au was active towards hydrolysis performing online electrochemical mass spectrometry experiments.

For DBFCs it is important, that the hydrolysis does not occur, because the produced hydrogen can leave the electrode surface before being oxidized and lead to faradaic losses and safety issues. Therefore, research effort is made towards electro catalysts that are selective for direct oxidation.

2.1.1 The BOR on Hydrolytically Active Surfaces

Finkelstein et al. [7] stated that BOR does not take place on metal surfaces that are not active for hydrogen ionization (such as Cu) until potentials near to oxygen evolution are reached. Therefore, they proposed the reaction in Eq.3. The adsorbed surface hydrogen is ionized leaving an adsorbed BH_3. The potential of the electrochemical reaction would be a mixed potential between BH_3 and H, which explains why the equilibrium potential is not reached.

$$BH_4^- + Pt \leftrightarrow Pt - BH_3 + H^+ + 2e^- \quad \text{(Eq.3)}$$

Therefore, they proposed that BOR on platinum surfaces involves the following CE-type mechanism (Eq.4 to Eq.6).

$$\text{(C) } BH_4^- + H_2O \rightarrow BH_3OH^- + H_2 \quad \text{(Eq.4)}$$

$$\text{(E) } H_2 + 2OH^- \rightarrow 2H_2O + 2e^- \quad \text{(Eq.5)}$$

$$\text{(E) } BH_3OH^- + 3OH^- \rightarrow BO_2^- + 3/2H_2 + 2\,H_2O + 3e^- \quad \text{(Eq.6)}$$

According to this, the intermediate BH_3 should be found near the catalyst surface. In-situ fourier transformed infra-red spectroscopy (FTIR) measurements showed that the intensity of BH_3 and BH_2 peaks increased with the applied potential on Pt surfaces [26].

Following the density functional theory (DFT) calculations [27]–[29], it was proposed, that the adsorbed surface hydrogen could either react with each other to form H_2 (g) (see Eq.7) or that it could be oxidized electrochemically following Eq.8 [25]. The competition between these two reactions determines if hydrolysis or oxidation takes place.

$$H_* + H_* \leftrightarrow H_2\,(g) \quad \text{(Eq.7)}$$

$$H_* + OH^- \leftrightarrow H_2O + e^- \quad \text{(Eq.8)}$$

The $*$ indicates an active site of the catalyst.

In both cases the surface hydrogen originates from B–H bond breaking in earlier steps. The following sequence of reactions was found to be energetically favoured on Pt(111) surfaces (Eq.9 to Eq.11) [27], [29]:

$$BH_4^- + 4* \leftrightarrow BH* + 3H* + e^- \quad \text{(Eq.9)}$$

$$BH* + OH^- \leftrightarrow BOH* + H* + e^- \quad \text{(Eq.10)}$$

$$BOH* + 2OH^- \leftrightarrow B(OH)_{3}* + 2e^- \quad \text{(Eq.11)}$$

On gold surfaces the B–H bonds are broken step by step after adsorption forming Au–H and Au–BH_x intermediates [28]. The surface hydrogen can be oxidized in combination with OH^-. The sequence is shown in Eq.12 to Eq.18 where one electron (e^-) is generated per step with a total of 8.

$$BH_4^- \leftrightarrow BH_{4}* + e^- \quad \text{(Eq.12)}$$

$$OH^- + BH_{4}* \leftrightarrow BH_{3}* + e^- + H_2O \quad \text{(Eq.13)}$$

$$OH^- + BH_{3}* \leftrightarrow BH_{2}* + e^- + H_2O \quad \text{(Eq.14)}$$

$$OH^- + BH_{2}* \leftrightarrow BH_2OH* + e^- \quad \text{(Eq.15)}$$

$$OH^- + BH_2OH* \leftrightarrow BH(OH)_{2}* + e^- \quad \text{(Eq.16)}$$

$$OH^- + BH(OH)_{2}* \leftrightarrow B(OH)_{2}* + e^- + H_2O \quad \text{(Eq.17)}$$

$$OH^- + B(OH)_{2}* \leftrightarrow B(OH)_3 + e^- \quad \text{(Eq.18)}$$

In this sequence the surface hydrides are instantly oxidized with OH^- and are not shown. In real conditions the formed Au–H can also react with one another under bond formation to give H_2 (see Eq.7). This is in concordance with the experimental results of *Chatenet* [24] and *Lima* [25].
In the studies of other hydrolytically active metals no other reaction mechanism is proposed and no quantum mechanical simulations are reported. However, it is plausible, that they follow one of the described pathways.

2.1.2 The BOR on hydrolytically inactive surfaces

The search for a catalyst that does not hydrolyse BH_4^- is of great importance, because of safety and fuel efficiency issues. If hydrogen is continuously produced in a DBFC stack, the need for overpressure venting will lead to considerable fuel loss over time. Furthermore, the evolution reaction puts high mechanical stress on the catalyst layer affecting the long term stability of the anode.

As already stated above, Au is not seen as a faradaic efficient BOR catalyst due to the fact that in contradiction to earlier studies H_2 evolution does occur. The metals that are mentioned as being inactive are Ag, Cu and Hg [6]. The absence of H_2 evolution would make them promising for DBFC technology, but they show too high onset potentials for the BOR [30]. Ag for example is reported by *Chatenet et al.* [31] to have an onset potential of -0.2 V vs NHE. Using Rotating Disc Electrode Cyclic Voltammography (RDE-CV) it was found that silver shows two oxidation waves. One pseudo wave centred at around 0.1 V vs. NHE and a second wave at around 0.4 V vs. NHE. This was attributed to the formation of Ag_2O at around 0.2 V vs. NHE. The number of exchanged electrons calculated for the pseudo wave is smaller than the one for the second wave. This led to the conclusion, that pristine Ag promotes hydrolysis, while Ag_2O is inactive towards it. Therefore, the potential region which is not hydrolytically active is at almost oxygen evolution potential. This excludes silver as good choice for a BOR catalyst.

Similar conclusions can be made for copper and mercury[7], [32], [33].

Furthermore, no measurement was done to prove the inactivity towards hydrolysis. All studies found in literature merely refer to visual observations. But as one can see from the example of Au, visual observations are often subjective and can lead to false conclusions. Therefore, an online measurement of the hydrolysis activity is essential for the determination of a proper catalyst.

2.1.3 The Effect of Alloying

The fact that alloying of two or even three catalytically active metals yields a new catalyst with different properties is well-known [6], [22], [34]–[37]. First of all, by combining two metals with different atomic radii the crystal structure changes slightly. Sometimes this leads to a different adsorption mechanism of the reactant. As an example *Merino-Jimenez et al.* [22] found that the adsorption of borohydride on a Pd-Ir bimetallic electro catalyst differs for various nanoparticle surfaces. On the $Pd_2Ir_1(111)$ surface the adsorption follows Eq.19, while on the $Pd_2Ir_2(111)$ surface the reaction in Eq.20 takes place.

$$BH_4^- + * \rightarrow BH_{3*} + H_* + e^- \qquad \text{(Eq.19)}$$

$BH_4^- + * \rightarrow BH_4* + e^-$ (Eq.20)

The adsorption free energy of the BH_4^- ion was calculated for both surfaces and compared it to a pure Pd surface. At -0.5 V vs. SHE the adsorption free energy on Pd(111), $Pd_2Ir_1(111)$ and $Pd_2Ir_2(111)$ is -1.77 eV, -1.12 eV and -0.89 eV, respectively. This example shows how the composition of the surface affects the binding strength of the reactant to the catalyst.

Other bimetallic catalysts studied were Platinum alloyed with Iridium, Nickel or Gold [6]. The alloyed platinum was compared to pure Platinum by recording linear sweeps at constant rotation rates and varying borohydride concentrations. It was found that the Pt-Au alloy shows a peak current slightly shifted to more negative peaks. The plots of peak current versus BH_4^- concentration showed, that the slope was steeper for Pt-Au then for pure Pt. The calculated number of exchanged electrons amounted to eight on Pt-Au. The presence of Nickel in the Platinum catalyst had the effect to shift the peak to an even more negative potential and the potential shift was the largest for Pt-Ir.

2.1.4 Hydrolysis Inhibition for the Borohydride Oxidation Reaction

As already stated, the inhibition of the hydrolysis as a concurring reaction to the direct oxidation is of great importance for the realisation of a safe and efficient DBFC. The first factor deciding if hydrolysis or direct oxidation takes place is the concentration of OH^- at the electrode. As it can be seen in Eq.7 and Eq.8, the deciding step is the reaction of OH^- with the adsorbed hydrogen. Therefore, if the concentration of OH^- is high in relation to surface hydrogen concentration, the probability of this reaction is increased. Hence, the pH value is an important factor. This was already reported in 1965 [32], [33]. For the ratios $[OH^-]/[BH_4^-]$ above 4.4 the borohydride oxidation reaction is an eight electron process on a mercury drop electrode. When the ratio is below 4.4 the hydrolysis reaction gradually gains importance.

Another way to control the hydrolysis of BH_4^- is the addition of thiourea [5]–[7], [27], [29], [34], [35], [38]–[42]. The sulphur atom makes it a good ligand for complexation and can easily adsorb on many transition metal surfaces. Therefore, it blocks the sites for surface hydride formation. Following potential relaxation experiments by *Gao et al., Finkelstein et al.* stated that concentrations as small as 10μM block 90% of the surface hydride sites [43]. However, by doing so it also inhibits borohydride oxidation, which partially depends on hydride formation especially at low potentials. Nevertheless, in the course of this work the use of thiourea was inevitable at

higher borohydride concentrations, because the hydrolysis reaction was too dominant to allow significant measurements.

A different approach to inhibit hydrolysis is the alloying of Pt and other hydrolysis active metals with those that inhibit hydrogen adsorption. This has been done in alkaline batteries to prevent charge loss because of the hydrogen evolution on metallic zink in alkaline solutions since the early 1990s [44]–[47]. The addition of In, Al, Pb, Hg, Ca or Bi into the Zinc powder notably reduces gas evolution on the electrode. The inhibitor metal is commonly added in quantities of 9wt%. This inhibition of hydrogen evolution is not limited to zinc. Pt and Pd for example are extensively used as heterogeneous dehydrogenation catalysts and it is known that the coverage of their surface by Bi leads to increased catalytic activity and a considerable inhibition of hydrogen adsorption and desorption [48]. This path is also interesting for borohydride oxidation catalysts, as it could lead to a selective catalyst for borohydride direct oxidation. The influence of Bi alloying on the borohydride oxidation kinetics was investigated in a previous publication [48]. $Pt_{0.9}Bi_{0.1}/C$, $Pd_{0.9}Bi_{0.1}/C$ and $Pd_{0.8}Bi_{0.2}/C$ bimetallic nanoparticles were sythesized using the "water-in-oil" micro emulsion method. They were then compared to commercial Pt/C and Pd/C catalysts. Using TEM-EDX characterisation it was found that within $Pd_{0.8}Bi_{0.2}/C$ and $Pt_{0.9}Bi_{0.1}/C$ isolated nanoclusters of Bi_2O_3 had formed.

During the electrochemical characterisation in 1M NaOH the surface hydride formation peaks on Pt did not show on the Pt-Bi catalyst, indicating the effect of bismuth. For the Pd-Bi catalyst similar results were obtained. It was shown, that the hydrogen adsorption and desorption peak of pure Pd did not show in the Bi modified Pd. It was also shown that in presence of $NaBH_4$ the first peak that is normally found on Pt did disappear for the Bi modified Pt. This first peak has often been related to oxidation of hydrogen formed by BH_4^- hydrolysis [7], [8], [25]. The number of exchanged electrons calculated at higher potentials was also higher for the Bi modified catalyst.

Another study performed on Bi modified Pt for borohydride direct oxidation came to similar conclusions [41].

As one can see from these studies, the combination of a catalytically active metal with one that inhibits surface hydrogen adsorption can lead to a very desirable result. This leads to the assumption that indium and the other metals listed before can lead to good results in terms of hydrolysis suppression.

2.2 Ionic Liquids

Ionic liquids (ILs) are salts that are liquid at temperatures below 100 °C and atmospheric pressure. The first mention of a ionic substance with melting point of 55°C is ethanolammonium nitrate. It was discovered in 1888 by *S. Gabriel and L. Weiner* [49]. Since then a large number of ionic liquids have been synthesized. Yet the number of proposed applications has only been growing since the early 1990's[50].

For this work we used methoxyethyltrimetylammonium borohydride (METMA-BH_4), dimethoxyethyltrimethylammonium borohydride (DMETMA-BH_4) and trimethylpropyammonium borohydride (TMPA-BH4). These ILs were synthesized by the proionic GmbH. A structure of the cations is given in **Figure 1**.

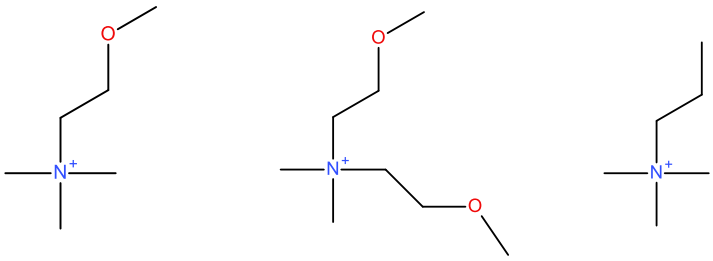

***Figure 1**: Cation structure of the ILs provided by proionic GmbH; from left to right: METMA-BH_4, DMETMA-BH_4 and TMPA-BH_4*

Using these ILs as borohydride containing species has two main advantages over sodium borohydride. First of all, the solubility of in water of both, the BH_4^- and the product BO_2^-. is enhanced by the presence of the quaternary ammonium. This is very important for increasing the storage density without increasing the risk of accumulation of a precipitate in the system. The other advantage is that the stability of BH_4^- is drastically increased by the introduction of these large cations. One reason is ion pair formation. The other is, that the large cations are chemically "soft" compared to the small sodium or lithium cations.

The quaternary ammonium ions have a very large voltage window and are therefore stable at the generated voltage.

This is why ILs are an optimal choice for long term storage of hydrogen with very high storage densities.

3 Experimental

3.1 Materials and Methods

3.1.1 The electrochemical measurement equipment

All electrochemical measurements were performed using a Gamry Reference 600 potentiostat. For the hydrogen detection cell a Gamry Interface1000E was used to record the chronoamperogram. The HydroFlex reversible hydrogen electrode (RHE) from Gaskatel GmbH was used for all measurements with a reference electrode. As counter electrode in the cyclic voltammetry and rotating disc cyclic voltammetry a glassy carbon rod from Gaskatel GmbH was employed. The Working Electrode was a 5mm glassy carbon disc electrode from Pine Industries that was coated with the catalyst to be measured. The modulated speed rotator (MSR) from Pine Industries was used for the rotation speed control.

3.1.2 The Single Test Cell

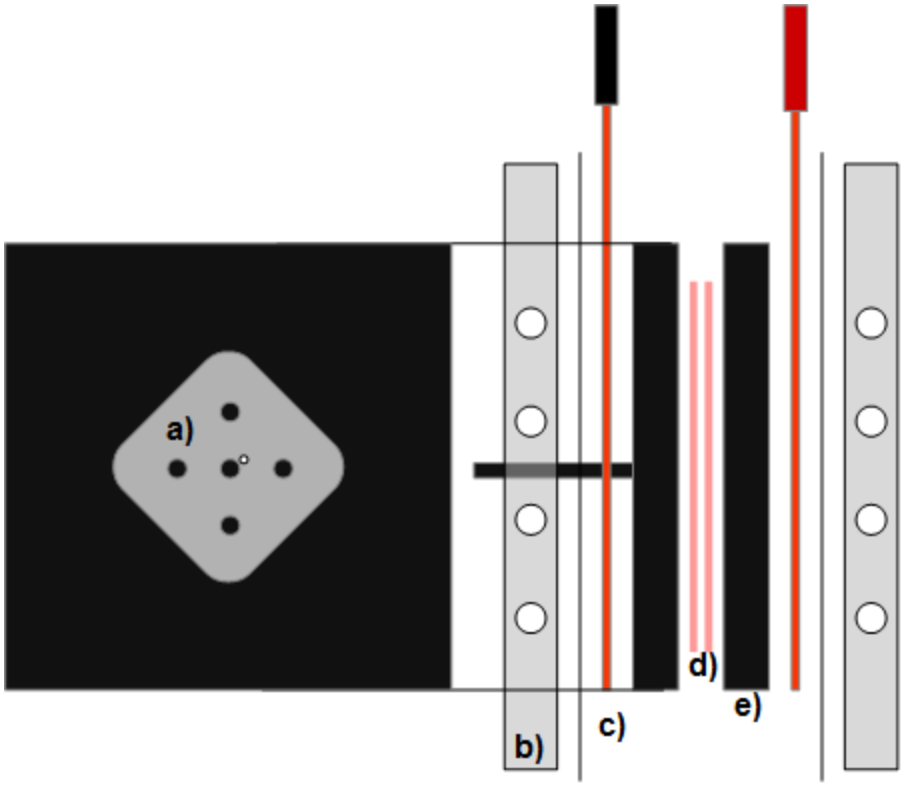

***Figure 2**: Schematic of the MEA testing cell with: a) Graphite anodic flow field with five pins for flow density homogenisation and a small drilling acting as Luggin capillary, b) aluminium end plates with thermostat water channels, c) copper current collectors d) silicon gaskets e) graphite cathodic flow field*

A schematic of the cell is shown in Figure 2. It was fabricated in-house in a workshop. The cathode flow field channels had a standard serpentine structure as also used in PEM fuel cells. For electric

conductivity it was made of graphite. The anodic flow field seen in **Figure 2** a) had no channels, but rather a pin type flow field. The five pins had the task to homogenize the flow density over the 4 cm^2 wide area of the flow field.

The fuel inlet and outlet were situated on the lower and upper edge of the anodic compartment, respectively. The reason for the new flow field design was to remove hydrogen that evolved during measurements, preventing blockage of the electrode surface. Hydrogen that evolved during measurements, simply raised to the outlet and was transported out of the cell. The design was developed using CFD and is extensively described elsewhere [51]. The pins provided the necessary electrical contact and lead to a more homogenous distribution of the flow density.

Near the central pin a small drilling was further prolonged by a plastic tube to the outside of the closed cell. The drilling and tube acted as Luggin capillary and the tube was connected with a compartment for the reference electrode.

Both the anodic and cathodic flow field were carved out of a graphite plate using a CNC milling machine.

The end plates made of aluminium as seen in **Figure 2 b)** had two functions. First, to hold all the components together tightly and second to ensure proper heat management. They were screwed together with eight steel screws that were isolated with Teflon to prevent short circuit. Additionally, a Teflon sheet was placed between the end plates and the copper current collectors for isolation purpose.

For heat management the end plates had four parallel channels that were provided with temperature controlled water from a thermostat.

The thickness of the silicon gaskets matched that of anode and cathode, respectively.

3.1.3 The Hydrogen Detection System

The online hydrogen detection cell was developed in-house and previously published [52]. It consisted of a PEMFC with a commercial MEA of 25 cm^2 active area. The hydrogen containing test gas was transported to the working electrode and is electrochemically converted.

The working electrode of the cell was supplied with the test gas in combination with an inert carrier gas (N_2). On the counter electrode a hydrogen flow was applied. The potential of the working electrode was kept at 430 mV vs the counter electrode, which also acted as a pseudo reference electrode, resulting in the immediate oxidation of any hydrogen on the working electrode following Eq.21.

$$H_2 \leftrightarrow 2H^+ + 2e^- \qquad E^0=0.000V \text{ vs SHE} \qquad \text{(Eq. 21)}$$

On the counter electrode the generated protons were reduced to hydrogen and the generated current was measured. This current was proportional to the hydrogen flow on the working electrode, according to faradaic laws.

To get a system with relatively fast response times the cell was connected directly with the fuel tank of the DBFC as illustrated in **Figure 3**.

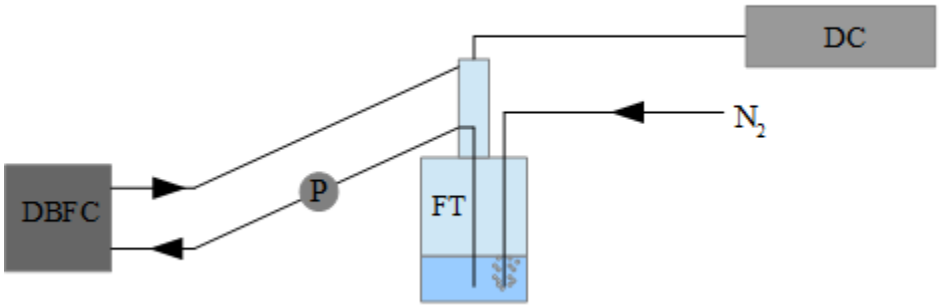

***Figure 3**:* Schematic of the hydrolysis detection system. P = pump, DBFC = Direct Borohydride fuel Cell, DC = detection cell, FT = fuel tank

The hydrogen generated on the anode of the DBFC was transported back into the fuel tank together with the remaining $NaBH_4$. The nitrogen that was bubbled through the fuel acted as carrier gas for the hydrogen reaching the fuel tank. Both were transported to the detection cell through an outlet on the top of the fuel tank. The hydrogen generated at every operating point of the polarisation curve was detected online during measurements.

3.2 Catalyst preparation

3.2.1 Preparation of the Anode Catalysts

A schematic of the catalyst preparation method is shown in **Figure 4**.

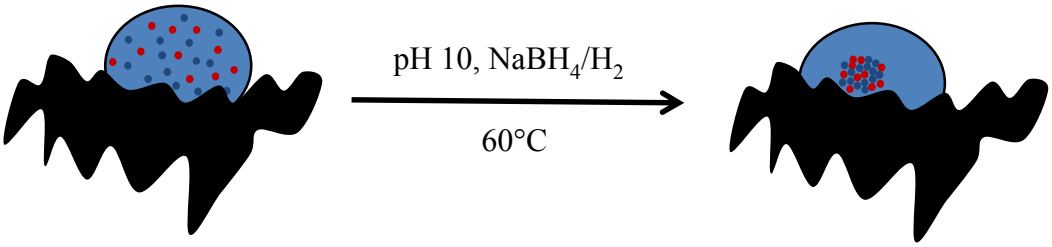

Figure 4: *Schematic of the electrocatalyst synthesis by the instant method. It consists of two steps: first the deposition of the metal hydroxide, then the reduction of the metal to give nanoparticles with homogeneous size distribution*

In **Table 1** a glossary of the catalysts synthesized is presented.

All catalysts were prepared by the instant method [53]. In short, the right amount of Vulcan XC72R was transferred into a round flask and mixed with water and the appropriate amount of precursor salts. To reduce the surface tension and allow a better suspension a small amount of 2-propanol was added in the proportion 1:30 2-propanol:water.

Cat. + No.	Precursor 1	Precursor 2	Support	Red. agent	Base
Au/C (40%)	$HAuCl_4$	-	Vulcan XC72R	H_2	NaOH
CGr	(48 mg Au)		(72 mg)		
$Pt_{0.5}Au_{0.5}$/C (40%)	H_2PtCl_6	$HAuCl_4$	Vulcan XC72R	$NaBH_4$	NaOH
CGr 24	(23.9 mg Pt)	(24.1 mg Au)	(72 mg)		
$Pt_{0.25}Au_{0.75}$/C (40%)	H_2PtCl_6	$HAuCl_4$	Vulcan XC72R	$NaBH_4$	NaOH
CGr 25	(11.9 mg Pt)	(36.1 mg Au)	(72 mg)		
Pd/C (40%)	$PdCl_2$	-	Vulcan XC72R	H_2	NaOH
CGr 22	(48 mg Pd)		(72 mg)		
$Pt_{0.5}Pd_{0.5}$/C (40%)	H_2PtCl_6	$PdCl_2$	Vulcan XC72R	H_2	NaOH
CGr 23	(31 mg Pt)	(17 mg Pd)	(72 mg)		
$Pt_{0.9}Bi_{0.1}$/C (40% Pt)	H_2PtCl_6	$BiCl_3$	Vulcan XC72R	$NaBH_4$	$LiCO_3$
CGr 50			(mg)		
$Pt_{0.8}Bi_{0.2}$/C (40% Pt)	H_2PtCl_6	$BiCl_3$	Vulcan XC72R	$NaBH_4$	$LiCO_3$
CGr 51			(mg)		
$Pt_{0.9}In_{0.1}$/C (40% Pt)	H_2PtCl_6	$InCl_3$	Vulcan XC72R	$NaBH_4$	$LiCO_3$
CGr 52			(mg)		
$Pt_{0.8}In_{0.2}$/C (40% Pt)	H_2PtCl_6	$InCl_3$	Vulcan XC72R	$NaBH_4$	$LiCO_3$
CGr 53			(mg)		

Table 1: *List of the synthesized electrocatalysts for direct borohydride oxidation with composition, reducing agent and base used for pH adjustment.*

The mixture was sonicated for 30 min while cooled with an ice bath to prevent solvent loss from heat generation. The pH value was adjusted while stirring by adding drops of a 1 M $LiCO_3$ water suspension or 0.1M NaOH until it reached 10-11. The mixture was heated to 60°C and stirred for 4 hours. The pH value was constantly monitored and adjusted if necessary.

After 4 hours 0.5 M $NaBH_4$ solution was added dropwise. The amount of $NaBH_4$ was chosen to be 5 equivalents of metal to ensure complete reduction. The dispersion was stirred overnight at room temperature.

For selected catalysts hydrogen was used as reducing agent (see **Table 1**). For this purpose, hydrogen from a balloon was bubbled through the reaction mixture until saturation was assumed. The balloon was then refilled to keep the sealed reaction apparatus under hydrogen atmosphere over the reaction time (4 hours).

The final product was isolated by centrifugation and decantation. To remove all formed by-products, it was suspended and centrifuged at least three times after which the clean product was dried at 50°C.

The final step for all bimetallic catalysts was annealing under nitrogen atmosphere. The annealing conditions for the different catalysts are listed in **Table 2**.

Cat. + No.	Annealing Temp. / °C	Time / h	Heating rate / °C/min
$Pt_{0.5}Au_{0.5}$/C (40%)	300	2,5	2
$Pt_{0.25}Au_{0.75}$/C (40%)	500	2,5	2
$Pt_{0.5}Pd_{0.5}$/C (40%)	350	2	5
$Pt_{0.9}Bi_{0.1}$/C (40% Pt)	500	5	2
$Pt_{0.8}Bi_{0.2}$/C (40% Pt)	500	5	2
$Pt_{0.9}In_{0.1}$/C (40% Pt)	500	5	2
$Pt_{0.8}In_{0.2}$/C (40% Pt)	500	5	2

***Table 2**:* Annealing conditions of the prepared catalysts. All were annealed under nitrogen atmosphere

3.2.1 Preparation of the Cathode Catalyst (MnO_2/C (30%))

The Cathode catalyst was chosen to be MnO_2/C because it proved to be active towards ORR and showed the best tolerance for BH_4^- in a previous publication [51].

This catalyst was prepared by suspending Vulcan XC72R in a 1:1 mixture of water and ethanol. After the stoichiometric amount of $Mn(NO_3)_2$ had been added the reaction mixture was stirred and heated to 80°C. Then the solvent was boiled down until a slurry was obtained which was collected and dried at 60°C. The resulting powder was heat treated at 400°C for 2 hours under N_2 atmosphere with a heating rate of 5°C/min.

3.3 Cyclic Voltammetry (CV) and Rotating Disk Electrode Cyclic Voltammetry (RDE-CV)

The synthesized catalysts were characterized via Cyclic Voltammetry (CV) in degassed 1M NaOH and via Rotating Disk Electrode Cyclic Voltammetry (RDE-CV) in presence of 5mM BH_4^-. They were compared to a commercial Pt/C (nominally 50%, on carbon black) catalysts from Alfa Aesar. The source of BH_4^- was changed to see the effect of using ionic liquids. In the course of this thesis sodium borohydride alongside with METMA-BH_4, DMETMA-BH_4 and TMPA-BH_4 (see section 2.3) were used. In **Table 3** an overview of the measurements performed with the different BH_4^- sources is given.

A thorough study of the BOR with the ionic liquids as borohydride source on all catalysts prepared could not be performed in the time period of this study. Therefore, a selection of Pt/C, Au/C, Pd/C and $Pt_{0.5}Au_{0.5}$/C has been made.

Catalyst	Loading / µg/cm²	$NaBH_4$	METMA-BH_4	DMETMA-BH_4	TMPA-BH_4
Pt/C	28	✓	✓	✓	✓
Au/C	56	✓	✓	✓	✓
Pd/C	28	✓	✓	✓	✓
$Pt_{0.5}Au_{0.5}$/C	42	✓	✓	✓	✓
$Pt_{0.25}Au_{0.75}$/C	42	✓	✗	✗	✗
$Pt_{0.5}Pd_{0.5}$/C	28	✓	✗	✗	✗
$Pt_{0.9}Bi_{0.1}$/C	112	✓	✗	✗	✗
$Pt_{0.8}Bi_{0.2}$/C	112	✓	✗	✗	✗
$Pt_{0.9}In_{0.1}$/C	112	✓	✗	✗	✗
$Pt_{0.8}in_{0.2}$/C	112	✓	✗	✗	✗

Table 3 *List of the performed measurements on all synthesized catalysts. ✓ = CV and RDE-CV performed with this BH_4^- source; ✗ = no CV and RDE -CV performed.*

All CV measurements were performed in a three electrode setup using a reversible hydrogen reference electrode.

3.3.1 Preparation of the working electrode

The working electrode was prepared by drop coating a catalyst ink on the glassy carbon disc electrode. The catalyst ink was obtained by suspending the catalyst powder in a 3:7 mixture of water:2-propanol. After 10 minutes of ultrasonification 5 µL of the ink were dropped onto the disc electrode two times with a drying time of ten minutes in between. While drying the disc electrode was kept at 700 rpm rotation speed. After the two dropping steps, the working electrode was dried for another forty minutes to receive a stable catalyst layer. The loading for every catalyst can be seen in **Table 3**.

3.3.2 Cyclic Voltammetry (CV) in the pure Electrolyte

To obtain surface related currents a CV was recorded in oxygen free electrolyte. Therefore, 50 mL of 1M NaOH were transferred into the measurement cell and purged with nitrogen for thirty minutes. The temperature was thermostatically controlled at 30°C. Twenty cleaning cycles were performed from 0.05 to 1.20 V vs RHE at 50 mV/s to remove possible impurities.
The final CV was recorded from 0.05 to 1.20 V vs RHE at a scan rate of 10 mV/s.

3.3.3 Rotating Disc Electrode Cyclic Voltammetry (RDE-CV) in presence of BH_4^-

After the CV in inert electrolyte had been recorded, 1 mL of a 0.255 M BH_4^- solution was added to achieve a final concentration of 0.005 M. After thoroughly mixing the measurement solution, one stationary CV was recorded from -0.05 to 1.6 V vs RHE at 10 mV/s. Then CVs with the same parameters were recorded at 100, 200, 400, 600, 900 and 1200 rpm.

3.4 MEA Preparation and Testing

3.4.1 Preparation of the anodes

The prepared anodes are listed in **Table 4**. The anodes had the dimensions 3x3 cm^2. The support material was carbon cloth purchased from Fuel Cells Etc. and the anode was obtained by a simple drop coating process to receive a catalyst loading of 1 mg/cm^2. To achieve homogeneous catalyst distribution, the 3x3 cm^2 piece of carbon cloth was fixed onto four hollow needles that were glued upside down to a plain plank as it can be seen in **Figure 5**.

Support	Binder / ionomer	Catalyst loading
	Pt/C, CGE 1	
Carbon cloth, 3x3 cm^2	30% Tokuyama AS-4	1mg Pt /cm^2
	$Pt_{0.8}Bi_{0.2}$/C, CGE 2	
Carbon cloth, 3x3 cm^2	30% Tokuyama AS-4	1mg Pt /cm^2
	$Pt_{0.9}Bi_{0.1}$/C, CGE 3	
Carbon cloth, 3x3 cm^2	30% Tokuyama AS-4	1mg Pt /cm^2
	$Pt_{0.8}In_{0.2}$/C, CGE 4	
Carbon cloth, 3x3 cm^2	30% Tokuyama AS-4	1mg Pt /cm^2
	$Pt_{0.9}In_{0.1}$/C, CGE 5	
Carbon cloth, 3x3 cm^2	30% Tokuyama AS-4	1mg Pt /cm^2

Table 4: *Overview of the anodes prepared for the fabrication of the MEAs.*

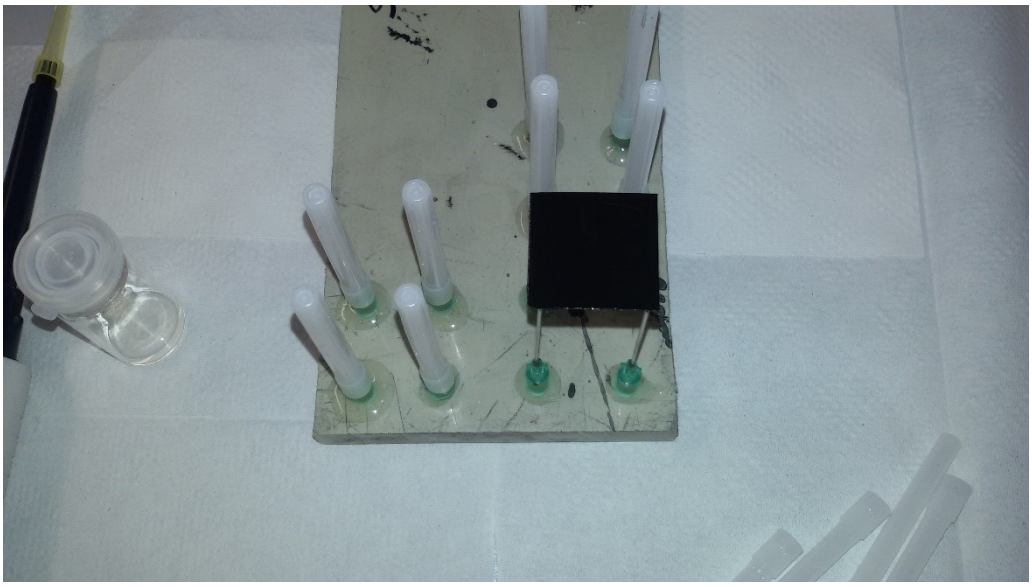

Figure 5: *Picture of an electrode support fixed on hollow needles to achieve a homogeneous distribution during the drop coating process.*

The catalyst ink was evenly dropped on the fixated support material. A usual dropping process consisted of 5 steps of 300µL dropping volume each and the electrode was dried for 10 min at 40°C between every dropping step. After the last step the electrode was dried at 40°C overnight.
The ink was prepared by suspending the right amount of catalyst powder in 2-propanol. Catalyst concentrations were fixed to receive the desired loading on the final electrode with addition of 10 wt% to compensate for losses. The ionomer AS-4 (Tokuyama) was added to get 30wt% content referred to the active mass (support + catalyst). The ionomer acted as binder and provided ionic conductivity inside the electrode. To homogenize the ink, it was sonicated for 15 minutes before using it for the drop coating method previously described.

3.4.2 Preparation of the cathodes

The cathode was prepared by rolling a catalyst/binder/ionomer paste onto a 3x3 cm^2 piece of Toray paper. The Toray paper acted as gas diffusion layer and prevented possible leakage of the liquid fuel/electrolyte into the cathode flow field.
The paste was obtained by mixing 733.8 mg MnO_2/C (30%), 91.7 mg PTFE (Dyneon GmbH, paste TF2021Z) and 1.82 g of a 5wt% AS-4 (Tokuyama) solution with a spatula until a rubberlike consistency was achieved. The paste was rolled with a roller and folded in the middle 10 times to achieve a homogeneous catalyst distribution. A schematic of the roller is shown in **Figure 6**.

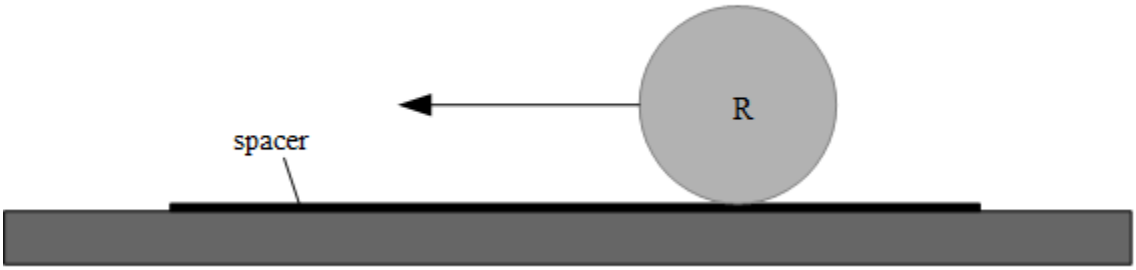

Figure 6: *Schematic of the roller and spacer to get a plain sheet of active mass.*

The spacers had different thicknesses and during the process the thickness was gradually reduced to a final value of 1.55 mm. The paste was rolled onto the Toray paper with the 1.55 mm spacer between working plane and roller. To calculate the catalyst loading of the final cathode the Toray paper was weighed before this step.
The moist catalyst layer of the cathode was placed between two sheets of cellulose filter and pressed at room temperature with a pressure of 120 kg/cm^2 for 15 minutes. This was done twice

to ensure proper drying. The pieces of the catalyst layer that were sticking out were cut away with a scalpel and a ruler. The final step was sintering with a pressure of 120 kg/cm^2 at 100°C for 30 minutes. All final cathodes had a catalyst loading of 16±0.2 mg/cm^2.

3.4.3 Preparation of the MEA

The MEA was assembled using an anion exchange membrane from Tokuyama.

After a 4x4 cm^2 piece of membrane had been prepared, the anode and the cathode were placed onto it facing each other. Care was taken that the two electrodes were placed coinciding each other followed by pressing at 100°C and a pressure of 120 kg/cm^2 for 30 minutes.

In **Table 5** a list of the prepared MEAs is given.

MEA No.	Anode / Membrane / Cathode
1	CGE1 / Tokuyama / MnO_2
2	CGE2 / Tokuyama / MnO_2
3	CGE3 / Tokuyama / MnO_2
4	CGE4 / Tokuyama / MnO_2
5	CGE5 / Tokuyama / MnO_2

Table 5: *Overveiw of the MEAs prepared for the in - situ measurements. See* ***Table 4*** *for anode specifications*

3.4.4 Recording of polarisation curves and online measurement of hydrolysis activity

Fuel volume / mL	$[BH_4^-]$ / mol*l^{-1}	[thiourea] / mmol*l^{-1}	[NaOH] / mol*l^{-1}
80	1	5	1

Table 6: *Fuel volume and composition for one polarisation curve measurement.*

The MEA was placed between the two flow fields taking care that the silicon gaskets were positioned properly to avoid leakage of fuel/electrolyte. All other parts were assembled according to **Figure 2** in the materials and methods section. The screws were tightened uniformly and carefully while measuring the thickness of the complete cell. After the reference electrode compartment was connected with the Luggin capillary via a silicon tube, 1M NaOH was pumped through the anode compartment at a flow rate of 10 mL/min for 1 hour to alkalize and moisturize the membrane and the ionomer inside the electrodes. To prevent the electrolyte from flowing into the reference electrode compartment, the connection to it was sealed. During the last 20 minutes of alkalisation the oxygen flow was set to 50 mL/min and held through the measurement.

The hydrogen detection cell was powered up before the fuel was pumped through the DBFC by supplying the counter electrode with hydrogen and the working electrode with nitrogen through the fuel tank (a precise description is given in the materials and methods section). The warm up time for the detection cell was 15 minutes. The OCV of the detection cell was recorded during warm up and the measurement was started after it reached values below 150 mV. The voltage of the detection cell was set to 430 mV while the current was recorded. The baseline current was recorded for 10 minutes before the borohydride tank containing 1M $NaBH_4$ and 0.005M Thiourea in 1M NaOH was connected to the cell and pump. The fuel was pumped through the cell with a flow of 10 mL/min and the first 15 mL were thrown away to flush out any residual alkalization electrolyte. Afterward the connection to the reference electrode compartment was opened to ensure electrolytic contact.

The internal resistance was measured and a polarisation curve was recorded at 30°C and 40°C with online hydrogen detection. The polarization curves at 30°C were performed as a warm up for the actual measurement at 40°C. Every current step was held for 5 minutes while the voltage and the anode potential were recorded. A stable current for 5 minutes was necessary to allow the formed hydrogen to reach the detection cell for the corresponding current step.

4 Results and Discussion

4.1 Cyclic Voltammetry of the Prepared Anode Catalysts

4.1.1 Cyclic Voltammetry of Pt/C

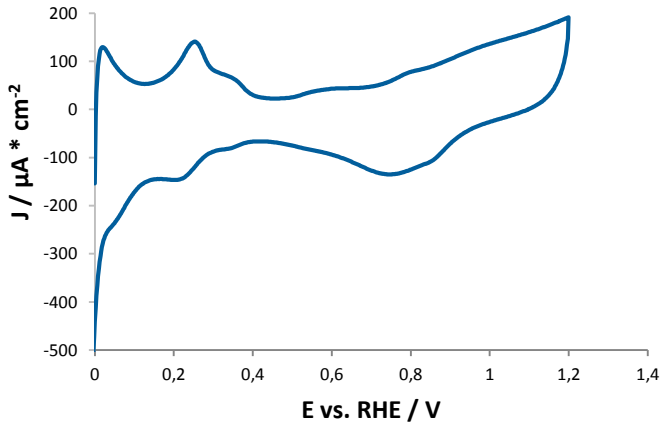

Figure 7: *Cyclic voltammogram of Pt/C (50%) from Alfa Aesar in 1M NaOH, 28 µg/cm², 0 to 1.2 V vs RHE, 10 mV/s*

The second cycle of the CVs of Pt/C (50%) from Alfa Aesar is illustrated in **Figure 7**. It shows the characteristic peaks of platinum. The cathodic and anodic peaks around 0 V vs RHE can be ascribed to hydrogen evolution and re-oxidation.

The anodic peak at 0.25 V vs RHE is typically attributed to the oxidation of the Pt-H monolayer formed in the cathodic sweep. From 0.22 to 0.35 V vs RHE the formation and re-oxidation of the monolayer in alkaline media undergoes two potential dependant mechanisms as represented by the two oxidation/reduction waves. These waves correspond to the hydrogen adsorption/desorption on the 111 plane and the 100 plane respectively.

The anodic wave starting at 0.7 V vs RHE corresponds to the oxidation of the Pt surface to gradually form a monolayer of Pt-OH and Pt-O. The corresponding cathodic reaction, i.e. the reduction of Pt, results in the broad cathodic peak at 0.75 V vs RHE [54].

4.1.2 Cyclic Voltammetry of Au/C

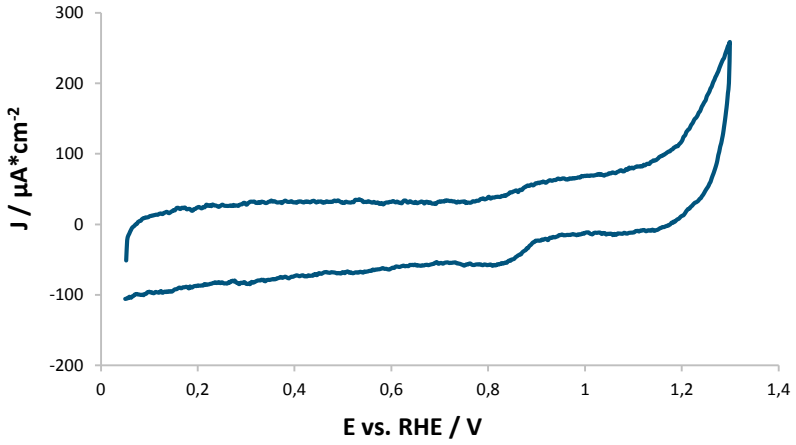

Figure 8: *Cyclic voltammogram of Au/C (40%) in 1M NaOH, 56 µg/cm², 0 to 1.2 V vs RHE, 10 mV/s*

In the CV of Au/C (40%) a slight shift of the horizontal symmetry line to more positive current densities can be seen at 0.9 V vs RHE. The CV is shown in **Figure 8**. The shift indicates residual oxygen in the solution despite the nitrogen purging. Although the gas tube was checked thoroughly for eventual leaks, the problem could not be fixed over the course of the present studies. Because the shift amounted only to approx. 5 µA/cm² it had no substantial effect on the results.

The CV itself is typical for gold as it shows no sign of a hydrogen monolayer formation. This is one point that lead many studies to the assumption that Au was not active for borohydride hydrolysis. The oxidation of the gold surface begins at approximately 1.1 V vs RHE.

4.1.3 Cyclic Voltammetry of Pd/C

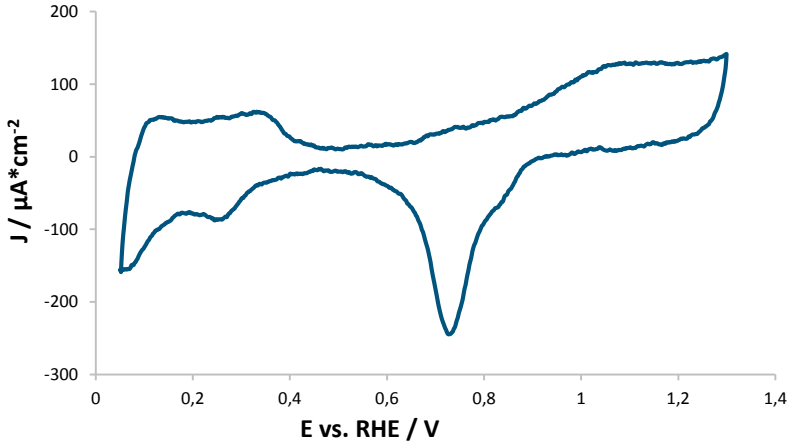

Figure 9: *Cyclic voltammogram of Pd/C (40%) in 1M NaOH, 28 µg/cm², 0 to 1.3 V vs RHE, 10 mV/s*

Pd/C (40%) shows similar peaks as the CV of Pt/C in **Figure 7**. By looking at the CV of Pd/C in **Figure 9** one will notice that the peak intensities of Pd/C oxidation and reduction are higher than those in the platinum CV The Pd oxidation and reduction is probably faster than the corresponding reactions on Pt. Therefore, the corresponding peaks have a higher intensity.

For the interpretation of this CV it is important to remember the well-known ability of Pd to incorporate hydrogen in its crystalline structure. The desorption of hydrogen is clearly identifiable in two anodic peaks with a plateau from 0.1 to 0.35 V vs RHE. The peak at 0.35 V vs RHE can be barely distinguished. This peak is typically assigned to the desorption of absorbed hydrogen from Pd(111), although *Simoes et al.* found the peak 0.1 V more positive than in the here presented results [48]. The desorption of adsorbed hydrogen leads to the formation of the anodic peak at 0.1 V vs RHE.

The corresponding cathodic peaks at 0.25 and 0.07 V vs RHE show two distinct waves of hydrogen adsorption and absorption.

The smaller peak is attributed to the adsorption and the larger one to absorption of hydrogen inside the Pd lattice. The oxidation of Pd to PdOH/PdO corresponds to the plateau from 1.1 to 1.3 V vs. RHE. In the cathodic sweep the peak of the reduction to Pd is formed at 0.73 V vs RHE.

4.1.4 Cyclic Voltammetry of $Pt_{0.5}Au_{0.5}/C$ (40%)

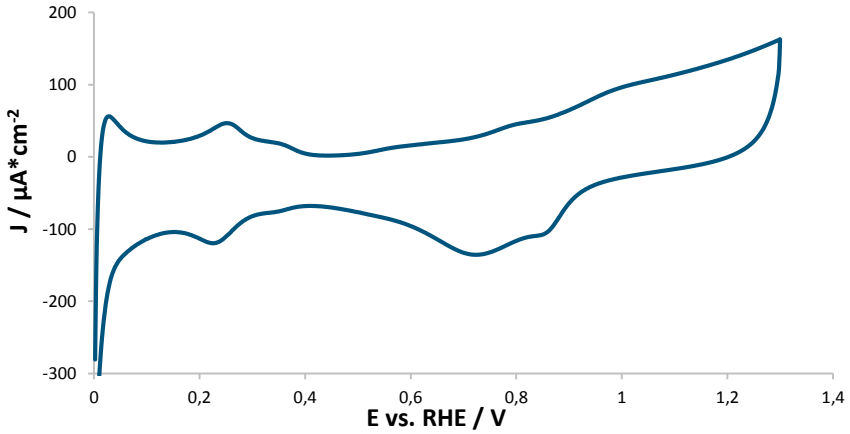

Figure 10: *Cyclic voltammogram of $Pt_{0.5}Au_{0.5}/C$ (40%) in 1M NaOH, 42 µg/cm², 0 to 1.3 V vs RHE, 10 mV/s*

From a look at the CV of $Pt_{0.5}Au_{0.5}/C$ (40%) in **Figure 10** it becomes evident, that the CV typical for gold is overlaid by the platinum CV. The expected inhibition of surface hydride formation did clearly not occur.

4.1.5 Cyclic Voltammetry of $Pt_{0.5}Pd_{0.5}/C$

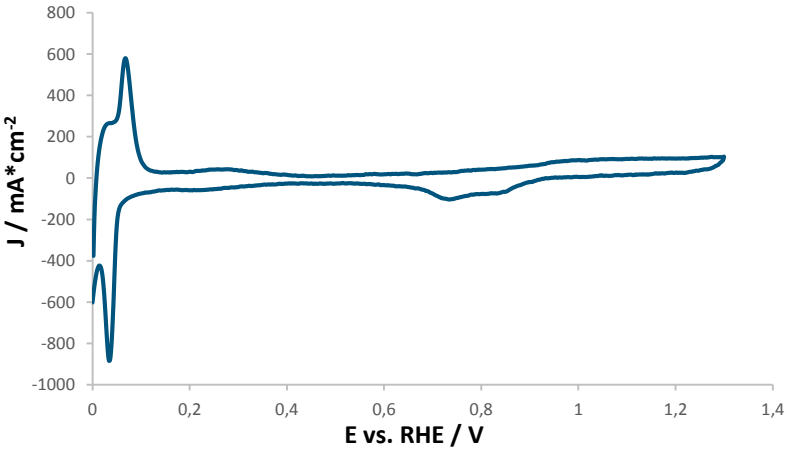

Figure 11: *Cyclic voltagrammogram of $Pt_{0.5}Pd_{0.5}/C$ in 1M NaOH, 28µg/cm², 0 to 1.3 V vs RHE, 10 mV/s*

The CV of $Pt_{0.5}Pd_{0.5}/C$ in supporting electrolyte is shown in **Figure 11**. It is interesting because of the large cathodic and anodic hydrogen adsorption/desorption peaks at 40 mV vs RHE (cathodic) and at 70mV vs RHE (anodic). Either the adsorption/desorption reaction has a greatly increased reaction rate, or the absorption into the Pd-lattice is facilitated by the presence of Pt. At around 0.3 V vs RHE the typical peak for desorption of the hydrogen absorbed inside the palladium lattice can be slightly distinguished. The peaks for Pd/Pt oxidation/reduction form with a typical onset potential at 0.9 V vs RHE.

The strong hydrogen adsorption/desorption peaks lead us to the conclusion, that BH_4^- hydrolysis should be promoted by $Pt_{0.5}Pd_{0.5}/C$.

4.1.6 Cyclic Voltammetry of $Pt_{0.25}Au_{0.75}/C$

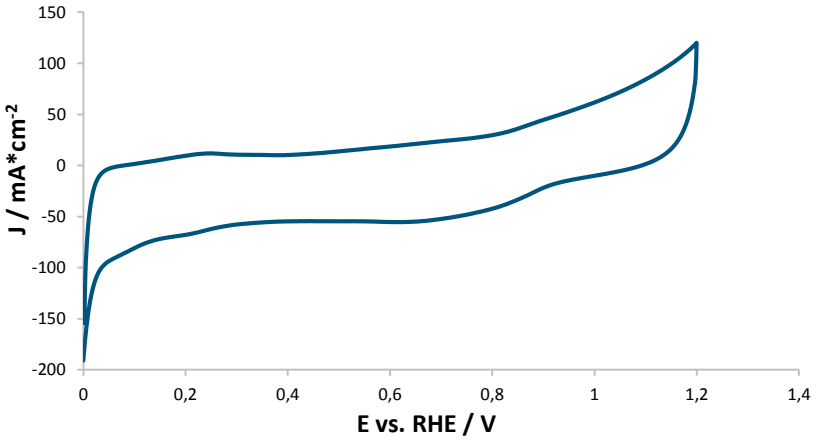

Figure 12: *Cyclic voltagrammogram of $Pt_{0.25}Au_{0.75}/C$ in 1M NaOH, 42 µg/cm², 0 to 1.3 V vs RHE, 10 mV/s*

The CV of $Pt_{0.25}Au_{0.75}/C$ in supporting electrolyte clearly shows the signs of a greater gold content compared to $Pt_{0.5}Au_{0.5}/C$. In **Figure 12** The typical Pt peaks are only slightly visible and it mainly looks like the CV of Au/C discussed in a previous section. This shows that the higher gold content reduces the number of active Pt sites, but does not inhibit surface hydrogen formation on the Pt atoms.

4.1.7 Cyclic voltammetry of $Pt_{0.9}Bi_{0.1}/C$

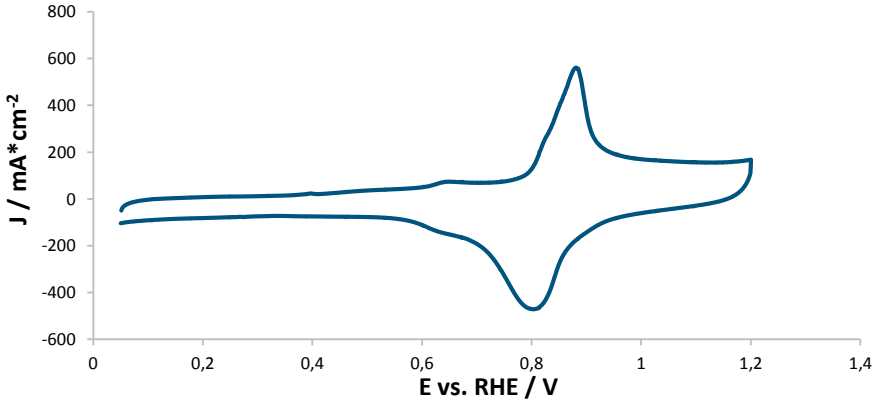

Figure 13: *Cyclic voltagrammogram of $Pt_{0.9}Bi_{0.1}/C$ (40 wt% Pt) in 1M NaOH, 112 µg/cm², 0 to 1.3 V vs RHE, 10 mV/s*

The CV of $Pt_{0.9}Bi_{0.1}/C$ in **Figure 13** shows that obviously the hydrogen adsorption/desorption on the Pt-surface is strongly inhibited, because no peak is formed. This is a quite desirable effect because the BH_4^- hydrolysis reaction is dependent on the surface hydride formation.

The results presented here match those of *Simoes et al.* [48]. In both studies Pt-Bi nanoparticles with the same atomic ratios were synthesized.

XPS measurements of Bi modified Pt(111) surfaces were also performed to study the structure of such alloys [55]. It was found that Bi would rather be found on the surface than in the core. Furthermore, it did not affect the electronic structure of the Pt atoms meaning that the inhibition of the surface hydride formation originates from lattice effects on the Pt-lattice and not from an electronic d-band shift.

At 0.9 V vs RHE a distinct anodic peak is visible with a corresponding cathodic peak. These two peaks and their position indicate a reversible redox pair and were attributed to Bi oxidation and reduction. By looking at the Pourbaix-diagram of bismuth one can see that at pH-values over 13 Bi is stable until 0.4 V vs RHE. At higher potentials BiOOH(s) is formed. The results of our CV experiment suggest that it is stable at even higher potentials. The Pourabix-diagram also shows that BiOOH(s) forms no soluble phase with increasing potential [56]. This could be confirmed by our studies because during the cleaning cycles no considerable reduction of the Bi-peaks had been noticed.

The anodic plateau following the presumed Bi oxidation peak is the typical PtO/OH formation peak found in all other CV of Pt containing surfaces.

One other noticeable feature of the Bi and In modified catalysts is the high double layer current, coming the high catalyst loadings in comparison to the other measured catalysts.

4.1.8 Cyclic Voltammetry of $Pt_{0.8}Bi_{0.2}/C$

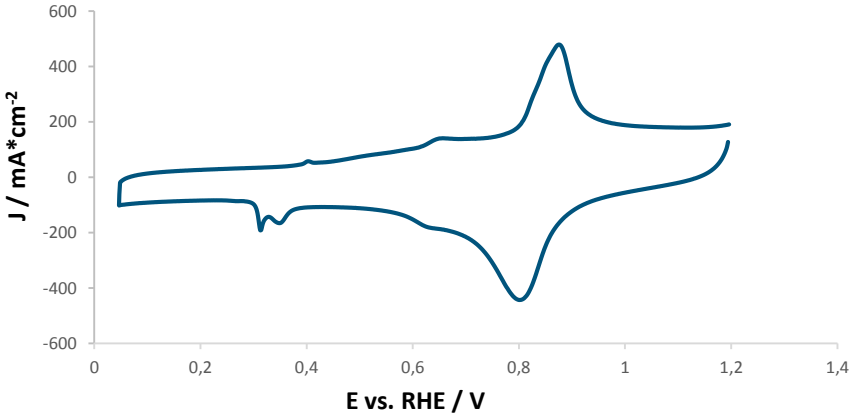

Figure 14: *Cyclic voltagrammogram of $Pt_{0.8}Bi_{0.2}/C$ (40 wt% Pt) in 1M NaOH, 112 µg/cm², 0 to 1.3 V vs RHE, 10 mV/s*

The CV of $Pt_{0.8}Bi_{0.2}/C$ in **Figure 14** shows basically the same form as that of the catalyst with lower Bi content. As expected, the surface hydride formation is as strongly inhibited as for $Pt_{0.9}Bi_{0.1}/C$ because of the higher coverage of the platinum particles with bismuth.

The bismuth oxidation and reduction peaks form at the same potential as for the $Pt_{0.9}Bi_{0.1}/C$, and have approximately the same intensity as in the $Pt_{0.9}Bi_{0.1}/C$ CV.

4.1.9 Cyclic voltammetry of $Pt_{0.9}In_{0.1}/C$

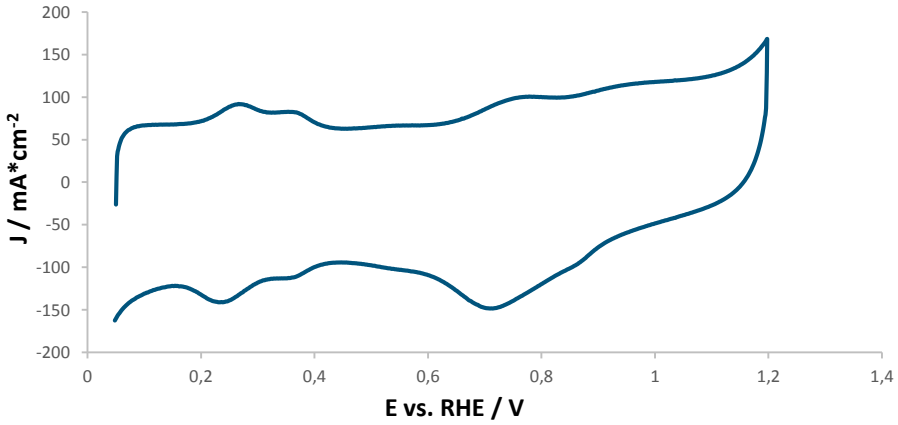

Figure 15: *Cyclic voltagrammogram of $Pt_{0.9}In_{0.1}/C$ (40 wt% Pt) in 1M NaOH, 112 µg/cm², 0 to 1.3 V vs RHE, 10 mV/s*

In **Figure 15** the CV of $Pt_{0.9}In_{0.1}/C$ (40wt% Pt) interestingly shows great similarity to the one of pure platinum. However, the surface hydride formation is not as distinct, which is the effect of indium.

Furthermore, high current densities of double layer formation can be observed. It is the same effect as observed for the Pt-Bi catalysts.

4.2 Cyclic Voltammetry in Presence of $NaBH_4$

4.2.1 Cyclic Voltammetry of Pt/C with 5mM $NaBH_4$

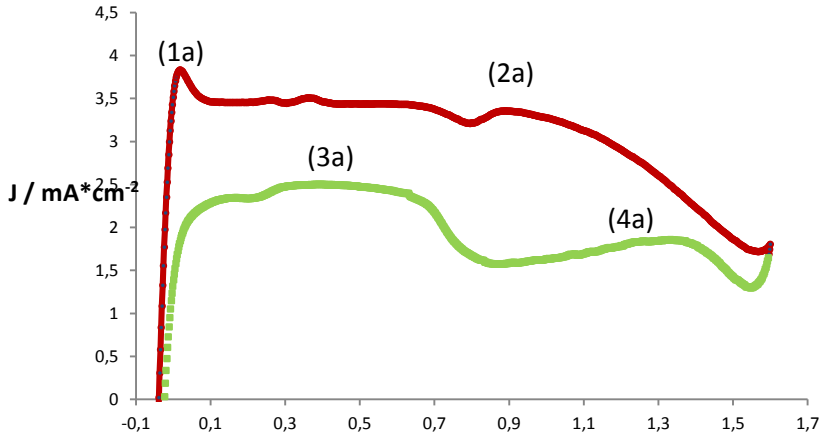

Figure 16: *Cyclic voltagrammogram of Pt/C (50 wt%) in 5mM $NaBH_4$ and 1M NaOH, 28 µg/cm², -0.05 to 1.6 V vs RHE, 10 mV/s*

The stationary CV of the commercial Pt/C (50 wt%) in 5mM $NaBH_4$ and supporting electrolyte can be seen in **Figure 16**.

The borohydride oxidation reaction (BOR) has been discussed in several publications [7], [8], [40]. As expected from the low standard potential, the onset potential for the BOR is below 0 V vs RHE. In the anodic sweep two peaks are visible. According to a previous studies results, the peak (1a) at 0.02 V vs. RHE can be attributed to the oxidation of H_2 formed in the CE mechanism shown in Eq. 4 [8]. This conclusion was drawn after recording CVs at different scan rates showing that the peak potential moved to higher potentials with increasing scan rate, a sign of a CE mechanism. Furthermore, the peak potential coincides with the peak of hydrogen oxidation in the CV in supporting electrolyte. This is also the case for here presented measurements as it can be seen by comparing **Figure 7** and **Figure 16**. The anodic plateau between peaks (1a) and (2a) should be the oxidation of BH_3OH^- [8]. Direct BH_4^- oxidation does only occur at potentials higher than 0.8 V vs RHE, due to the surface hydroxide/oxide formation on the Pt surface that starts at 0.7 V vs RHE (peak 2a).

In the cathodic sweep two anodic plateaus can be distinguished. In most studies they have been associated to the oxidation of adsorbed intermediates. Peak (3a) corresponds to the oxidation of adsorbed BH_3OH^- and peak (4a) has not been discussed further.

Another investigation of BOR on Pt associated the anodic plateau between peaks (1a) and (2a) to the direct oxidation of BH_4^- in connection with the formation of surface hydrides. Peak (2a) itself was attributed to the direct oxidation of BH_4^- without involving surface hydrides by both. The concept of surface hydrides was also proposed in the first stages of BOR investigations in the

1960s [1]. The fact that the OCV of borohydride on Pt surfaces is more negative than that of H_2 and that it decreases with increasing BH_4^- concentration substantiates this proposition. It means that at least parts of the current come from adsorbed species.
It also correlates well with the DFT simulation model, where BH_4^- is adsorbed under formation of surface hydrides [27].

4.2.2 Cyclic Voltammetry of Au/C with 5mM $NaBH_4$

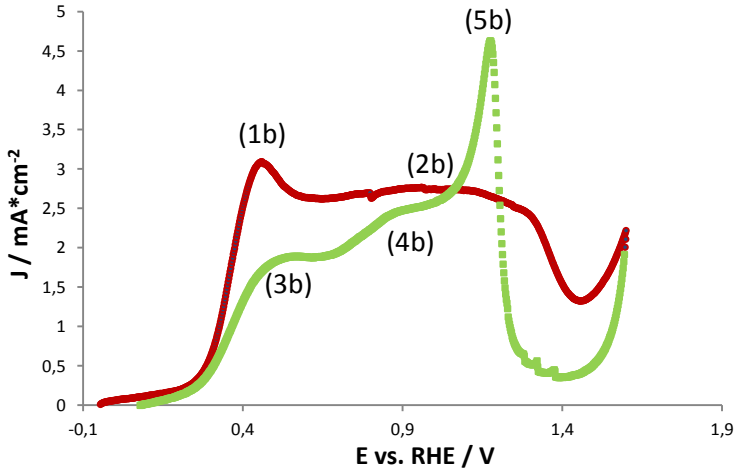

Figure 17: *Cyclic voltagrammogram of Au/C (40 wt%) in 5mM $NaBH_4$ and 1M NaOH, 56 µg/cm², -0.05 to 1.6 V vs RHE, 10 mV/s*

By comparing the CVs of the gold catalyst in
Figure *17* whit those of platinum in **Figure 15** a few differences can be noticed. First of all, the onset potential is shifted to approx. 0.3 V vs RHE. This is a considerably higher potential than that of the hydrogen evolution. This can be expected if gold is seen as a non-hydrolytically active surface or as a surface that cannot oxidize hydrogen without a considerable overpotential. Nevertheless, bubble formation on gold surfaces was observed in some studies [3], [7], [24], [31], [42], which could be confirmed by the results of this work. The work of *Chatenet et al.* [24] builds a strong case against the theory of gold being inactive for BH_4^- hydrolysis. In it the hydrogen release reaction was measured online by coupling mass spectroscopy with the electrochemical measurement and considerable amounts of hydrogen evolution over the measured potential range were found.
According to some studies in literature peak (1b) at 0.42 V vs RHE originates from the direct 8 electron oxidation of BH_4^- while the following anodic plateau is attributed to the oxidation of adsorbed intermediates (see Eq. 12 to 18) [8].

In the cathodic sweep the sharp anodic peak (5b) is easily distinguishable. It was stated that it comes from the oxidation of adsorbed BH_3OH^-. The two following anodic plateaus (3b) and (4b) were not discussed in the cited literature. However, the authors suppose that it comes from the oxidation of other intermediates, most likely $BH_2(OH)_2^-$ and $BH(OH)_3^-$. They are formed following the reaction sequence from Eq. 12 to Eq. 18.

Another explanation for the formation of peak (1b) is given by *Chatenet et al's* work [24]. The number of exchanged electrons was calculated and it was found to be between 3 and 4. That lead to the conclusion, that the oxidation is incomplete and stops at $BH_2(OH)_2^-$ and $BH(OH)_3^-$. These intermediates are further oxidised at higher potentials forming peak (2b). Following online electrochemical mass spectroscopy measurements to detect hydrogen, it was proposed that BH_3OH^- is formed by heterogeneous hydrolysis and oxidized in a 3 or 4 electron oxidation. In the experiments presented in this work peak (2b) is less distinct and does not quite substantiate *Chatenet's* theory. But the observation of bubbles on the electrode supports the hydrolysis involved in their pathway.

Furthermore, the studies in literature have calculated a different number of electrons for the peak (1b) originating from different values of the diffusion coefficient used for calculations.

4.2.3 Cyclic Voltammetry of Pd/C with 5mM $NaBH_4$

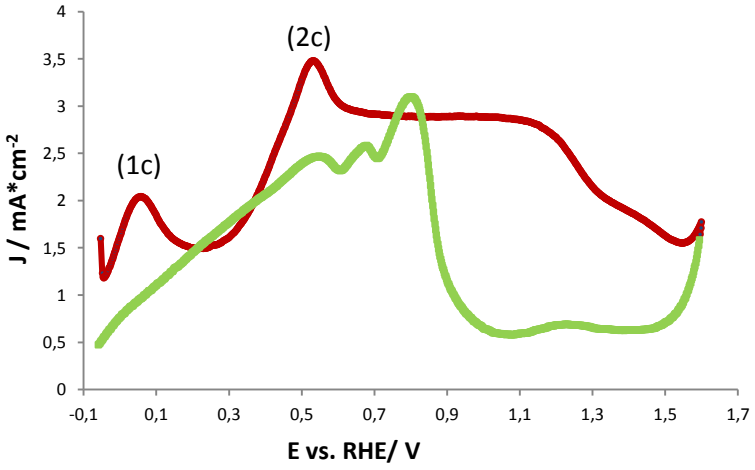

Figure 18: *Cyclic voltagrammogram of Pd/C (40 wt%) in 5mM $NaBH_4$ and 1M NaOH, 28 µg/cm², -0.05 to 1.6 V vs RHE, 10 mV/s*

The CV of Pd/C in BH_4^- containing electrolyte in **Figure 18** is quite interesting because it shows 2 anodic peaks that seem to come from two different oxidation mechanisms. Peak (1c) with a peak potential of 0.08 V vs RHE seems to come from an incomplete oxidation process while the complete oxidation of borohydride occurs only at potentials above 0.55 V vs RHE shown by peak (2c). This concept of high potential and low potential oxidation was introduced in the course of

the investigations of the BOR on a Pd-surface [57]. Additionally, the peak current densities and the current densities of the following plateaus differ by the factor 2. This can be explained by assuming that in the low potential oxidation only $BH_2(OH)_2^-$ is formed, as confirmed by the previous investigation [57]. The complete BOR occurs at the high potential region. Hydrogen absorption and desorption could play an important role for this phenomenon, because the lattice parameters of the Pd crystal are highly influenced by the incorporation of hydrogen into the interstitial spaces. By looking at the CV of Pd/C in pure 1M NaOH it can be noticed that desorption of hydrogen is completed at approximately 0.45 V vs RHE. This coincides with the onset potential for the high potential oxidation of borohydride. Therefore, a link between the structural change and the change of the oxidation behaviour is highly probable.

4.2.4 Cyclic Voltammetry of $Pt_{0.5}Au_{0.5}$/C with 5mM $NaBH_4$

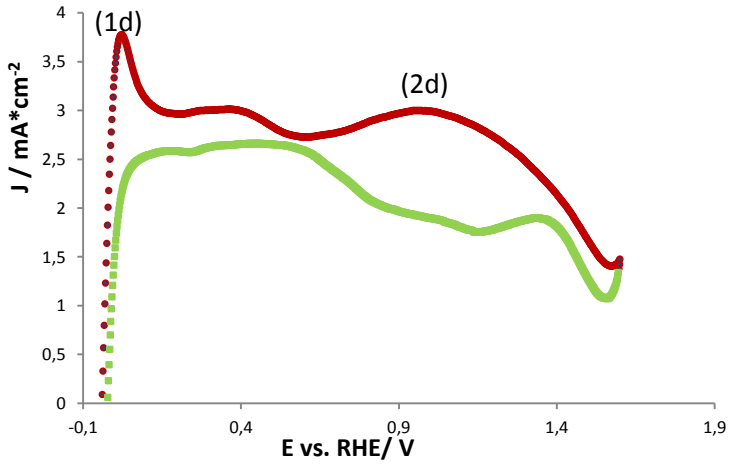

Figure 19: *Cyclic voltagrammogram of $Pt_{0.5}Au_{0.5}$/C (40 wt%) in 5mM $NaBH_4$ and 1M NaOH, 42 µg/cm², -0.05 to 1.6 V vs RHE, 10 mV/s*

The CV of the $Pt_{0.5}Au_{0.5}$/C catalyst seen in **Figure 19** seems to be an overlap of the CVs of both metals contained in the catalyst. The anodic peak (1d) at 0.03 V vs RHE is similar to peak (1a) in the CV of Pt/C in **Figure 16** and can be discussed in the same way (see section 3.3.1). The following anodic plateau from 0.15 to 0.4 V vs RHE is comparable to the one in the CV of Pt/C with a slightly lower current density. Furthermore, there is a small increase in current density at increasing potentials peaking at 0.4 V vs RHE. That is approximately the peak potential of peak (1b) in the CV of Au/C in

Figure 17. The peak current densities also match each other what indicates a relation between the two. The following drop in current density with the minimum at 0.6 V vs RHE has the same current density and potential range as the anodic plateau after peak (1b) in

Figure 17 indicating that the BOR follows the same reaction mechanism in this potential range.

At 1 V vs RHE peak (2d) is formed, which is assumed to be an overlap of peak (2a) in the CV of Pt/C and peak (2b) from the CV of Au/C.

These differences in the current density of the peaks and the formation of the minimum at 0.6 V vs RHE lead to the assumption that at around 0.4 to 0.6 V vs RHE the energetically favoured pathway is the one for BOR on gold. At low potentials around 0.03 V vs RHE the energetically favoured pathway seems to be the one for BOR on platinum. At the other potentials the reaction mechanisms appear to concur with one another. For more clearance of this theory more data would be necessary. XPS analysis of the surface structure of the particles and electronic structure of the metals in the alloy would provide further information of the reaction mechanism.

While in the anodic sweep a fluctuating overlap of the CVs of the pure metals can be observed, the cathodic sweep seems to look more like Pt/C. Therefore, it can be assumed that the same intermediates are oxidized.

4.2.5 Cyclic Voltammetry of $Pt_{0.25}Au_{0.75}$/C with 5mM $NaBH_4$

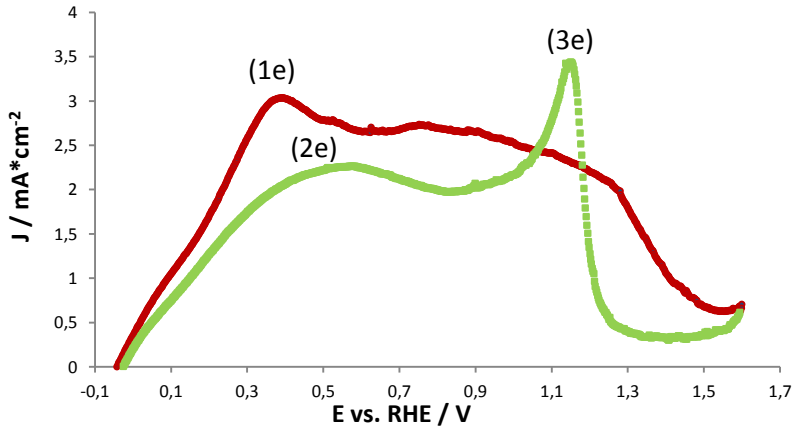

Figure 20: *Cyclic voltagrammogram of $Pt_{0.25}Au_{0.75}$/C (40 wt%) in 5mM $NaBH_4$ and 1M NaOH, 42 µg/cm2, -0.05 to 1.6 V vs RHE, 10 mV/s*

The stationary CV of $Pt_{0.25}Au_{0.75}$/C with 5 mM $NaBH_4$ can be seen in **Figure 20**. The higher gold content shows its effect in the CV. The form of the CV comparable to the one of pure gold except that the onset potential for the BOR is shifted from 0.3 to 0.0 V vs RHE. The following kinetically limited region has a broad potential range of 400 mV. This can be explained by the assumption of a mixed mechanism comparable to $Pt_{0.5}Au_{0.5}$/C. With increasing potential, the mechanism of the BOR on gold gains importance resulting in peak (1e). Although it is shifted slightly to more negative potentials, it has the same current density as peak (1b) in the CV of Au/C. The shift

amounts to 70 mV and could result from changes in the electronic structure or the lattice parameter of the gold crystal.

The rest of the CV can basically be discussed the same way as the CV of pure gold. Only slight changes in current density are observed. Peak (2e) in the cathodic sweep is probably an overlap of peak (3a) found in the Pt/C CV and the plateaus (3b) and (4b) identified in the Au/C CV.

The sharp anodic peak (3e) in the cathodic sweep can be discussed the same way as peak (5b) in the CV of Au/C.

During the experiment bubble formation was observed which substantiates the findings of *Chatenet et al.* that Gold is active for hydrolysis [24].

4.2.6 Cyclic Voltammetry of $Pt_{0.5}Pd_{0.5}$/C with 5mM $NaBH_4$

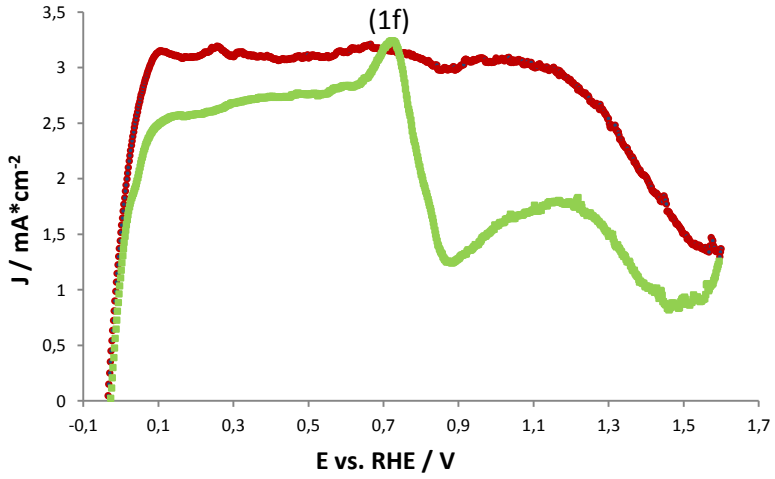

Figure 21: *Cyclic voltagrammogram of $Pt_{0.5}Pd_{0.5}$/C (40 wt%) in 5mM $NaBH_4$ and 1M NaOH, 42 µg/cm², -0.05 to 1.6 V vs RHE, 10 mV/s*

The results of $Pt_{0.5}Pd_{0.5}$/C in **Figure 21** show a CV that is very similar to the CV of Pt/C and can be discussed in the same way. The differences are the lower current density and the occurrence of peak (1f) in the cathodic sweep. This peak can also be found in the CV of Pd/C. In general, Pd has a negative effect on the catalytic activity of Pt and no effect on the hydrolysis reaction. This was deduced by the vigorous formation of bubbles during the experiments.

4.2.7 Cyclic Voltammetry of $Pt_{0.8}Bi_{0.2}/C$ with 5mM $NaBH_4$

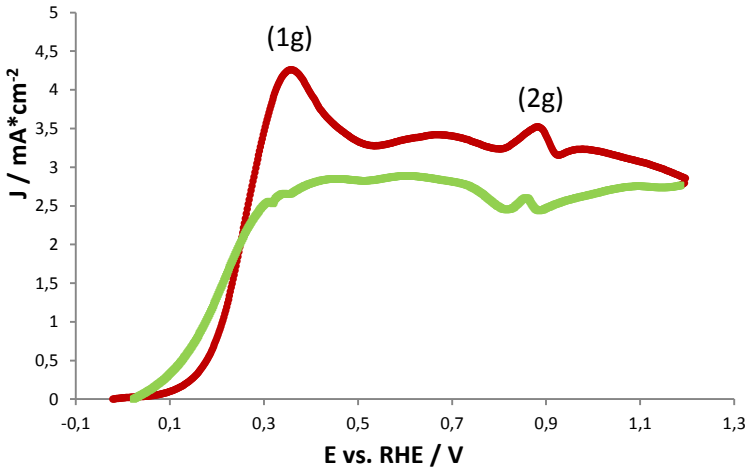

Figure 22: *Cyclic voltagrammogram of $Pt_{0.8}Bi_{0.2}/C$ (40 wt% Pt) in 5mM $NaBH_4$ and 1M NaOH, 112 µg Pt/cm², -0.05 to 1.6 V vs RHE, 10 mV/s*

The results of the ex – situ experiments for $Pt_{0.8}Bi_{0.2}/C$ in **Figure 22** showed interesting features. On this catalyst with high Bi content, the onset potential is shifted to 40 mV vs RHE being a positive shift of approximately 100 mV compared to the onset potential on Pt/C. This shows the high kinetic limitations that result from bismuth. However, in comparison to Au/C the onset potential is about 0.25 V more negative. At 0.37 V vs RHE the first oxidation peak (1g) forms. Because no hydrogen can be formed it should originate from borohydride direct oxidation to at least an intermediate. This is further oxidized at higher potentials forming the following anodic plateau.

Peak (2g) is the Bi oxidation peak, which is really distinct. Therefore, it is easily distinguishable in all CVs with Bi- containing catalysts.

In the cathodic sweep an almost constant anodic plateau is formed. Further oxidation of intermediates occurs.

The performance is heavily affected by bismuth, but no bubble formation could be observed. This finding indicates that the introduction of bismuth is a good way to inhibit hydrolysis. A gradual reduction of the Bi content to a minimum should lead to a very promising catalyst for a practical application of a DBFC.

4.2.8 Cyclic Voltammetry of $Pt_{0.9}Bi_{0.1}/C$ with 5mM $NaBH_4$

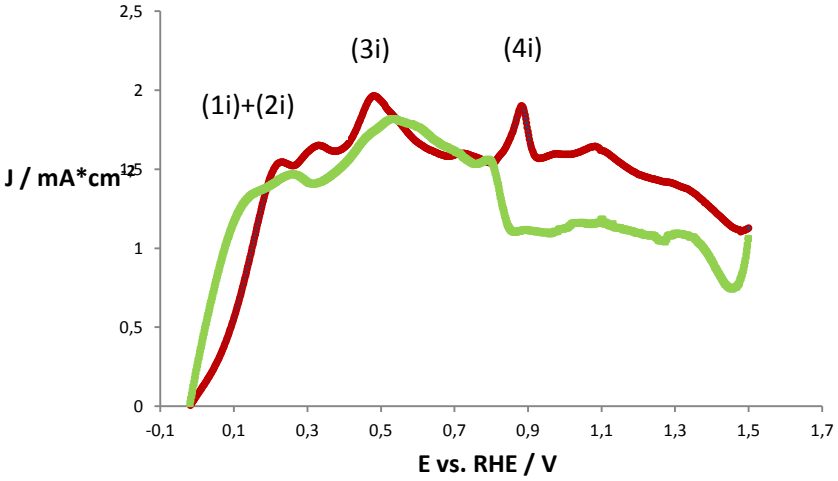

Figure 23: *Cyclic voltagrammogram of $Pt_{0.8}Bi_{0.2}/C$ (40 wt% Pt) in 5mM $NaBH_4$ and 1M NaOH, 112 µg Pt/cm², -0.05 to 1.6 V vs RHE, 10 mV/s*

The same way as for the high Bi content catalyst also the CV of $Pt_{0.9}Bi_{0.1}/C$ in **Figure 23** showed interesting results. In it the effects of the inhibition of surface hydride formation can be seen. The onset potential for the BOR is shifted from -50 mV to -20 mV vs RHE. Furthermore, strong kinetic limitations can be observed at low potentials as the current density did not rise considerably below 0.1 V vs RHE. This is the region where peak (1a) on pure platinum is formed. As discussed in section 3.2.1 it corresponds to surface hydride oxidation. The absence of a surface hydride oxidation peak is a sign of the inhibition of their formation. At 0.2 V and 0.35 V vs RHE two oxidations waves are visible and form peaks (1i) and (2i). They are probably generated by an incomplete BOR forming an intermediate. The full oxidation seems to occur at 0.5 V vs RHE, where peak (3i) is formed. Peak (4i) occurs at bismuth oxidation potentials and can be attributed to it.

In the cathodic sweep the peaks occur at approx. the same potentials as in the anodic sweep. Apparently the same reactions restart as the working electrode reaches the corresponding potential. Due to the high loading of catalyst it was difficult to obtain a stable catalyst layer. A binder was not used because the comparability with the other catalyst measurements would have been affected significantly. Therefore, small losses of catalyst throughout the measurement were tolerated. This lead to the apparently better performance of $Pt_{0.8}Bi_{0.2}/C$, where no catalyst was lost during the measurement.

In general, the kinetic performance of the catalyst is negatively affected by the alloying with Bi. However, no bubble formation could be observed over the measurement. This is a sign that the

low Bi content has the same effect for hydrolysis inhibition as the high Bi content. The losses in performance are tolerable by taking the gains from an absence of hydrolysis into account.

4.2.9 Cyclic Voltammetry of $Pt_{0.9}In_{0.1}/C$ with 5mM $NaBH_4$

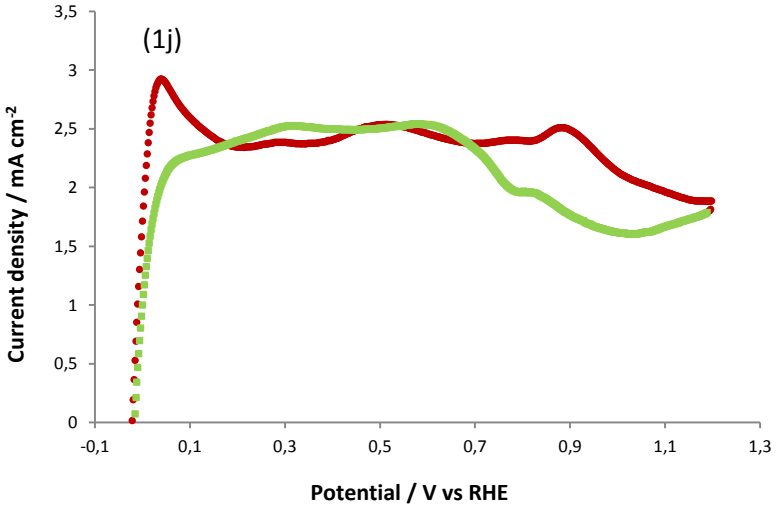

Figure 24: *Cyclic voltagrammogram of $Pt_{0.8}Bi_{0.2}/C$ (40 wt% Pt) in 5mM $NaBH_4$ and 1M NaOH, 112 µg Pt/cm², -0.05 to 1.6 V vs RHE, 10 mV/s*

The stationary CV of $Pt_{0.9}Bi_{0.1}/C$ in 5mM $NaBH_4$ can be seen in **Figure 24**. The introduction of indium in the platinum matrix was expected to have a similar effect as the introduction of bismuth. However, peak (1j) occurs at the same potential as peak (1a), which is mainly attributed to hydrogen oxidation. This means the surface hydride formation is not inhibited by the presence of indium. If we look at the result of the online hydrogen detection experiments in **Figure 43** we can see that at low current densities no hydrogen was evolved on the In modified catalyst. The surface hydrides that are formed are immediately oxidized and cannot form hydrogen. That means the sites for surface hydride formation have enough distance from on another not to allow hydrogen recombination.

The CV looks very similar to that of Pt/C. The remaining peaks can be discussed in the same way as those in section 4.2.1.

4.3 Rotating Disk Electrode Cyclic Voltammetry (RDE-CV)

A summary of the results of the Levich (L) - and Koutecky-Levich (K-L) analysis of all catalysts are summarized in **Table 7**. L and K-L equations are given in Eq. 21 and 22.

Pt		**Au**	
k_h / cm*s^{-1}	$91*10^{-2}$	**k_h / cm*s^{-1}**	$1.9*10^{-2}$
n_L (0.38 V)	7.3	**n_L (1.05 V)**	7.2
n_{KL} (0.11 V)	6.7	**n_{KL} (0.76V)**	7.4
n_L (0.6 V)	7.3	-	-
n_L (0.98 V)	6.7	-	-
Pd		**$Pt_{0.5}Au_{0.5}$**	
k_h / cm*s^{-1} (0.55 V)	$1.3*10^{-1}$	**k_h / cm*s^{-1}**	-
n_L (0.4 V)	4.3	**n_L (0.38 V)**	8.0
n_L (0.84 V)	8.0	**n_L (0.6 V)**	8.0
n_{KL} (0.15 V)	6.7	**n_L (0.9 V)**	8.1
n_{KL} (0.55 V)	7.5	**n_{KL}**	-
$Pt_{0.25}Au_{0.75}$		**$Pt_{0.5}Pd_{0.5}$**	
-	-	**k_h / cm*s^{-1}**	-
n_l (0.86 V)	7.5	**n_l (0.5 V)**	6
-	-	**n_l (0.8 V)**	7
$Pt_{0.8}Bi_{0.2}$		**$Pt_{0.9}Bi_{0.1}$**	
k_h / cm*s^{-1}	$1.4*10^{-1}$	**k_h / cm*s^{-1}**	$1.4*10^{-2}$
n_l (0.37 V)	6.9	**n_l (0.37 V)**	4.4
n_l (0.75 V)	8.9	**n_l (0.75 V)**	6.9
n_{kl} (0.2 V)	3.1	**n_{kl} (0.2 V)**	5.3
$Pt_{0.9}In_{0.1}$			
k_h / cm*s^{-1}	-		
n_l (0.5 V)	7.7		
n_l (0.65 V)	7.8		
n_{kl} (0.02 V)	-		

Table 7: *Summary of the results of Levich and Koutecky-Levich analysis of all catalysts; RDE CVs were performed in 5mM $NaBH_4$ and 1M NaOH.*

The analysis was performed at potentials with linear L and K-L-plots.

To give a quick insight into the performance of our catalysts in comparison to Pt/C we compared the anodic sweeps 1200 rpm in

Figure 25. The catalysts were grouped in Au containing, Pd containing and Bi and In containing catalysts to make it more clearly arranged. The best performing catalyst of each group were then compared with one another.

One can clearly see the good performance of the $Pt_{0.5}Au_{0.5}$/C in comparison to the other gold containing catalysts and Pt/C. The alloying of Pd and Pt proved to give a catalyst with a weaker performance. Pure Pd showed an interesting split into two potential regions that are defined by an

incomplete 4 electron oxidation in the low-potential region. The full 8 electron oxidation above potentials of 0.7 V vs RHE yielded higher current densities than Pt/C.

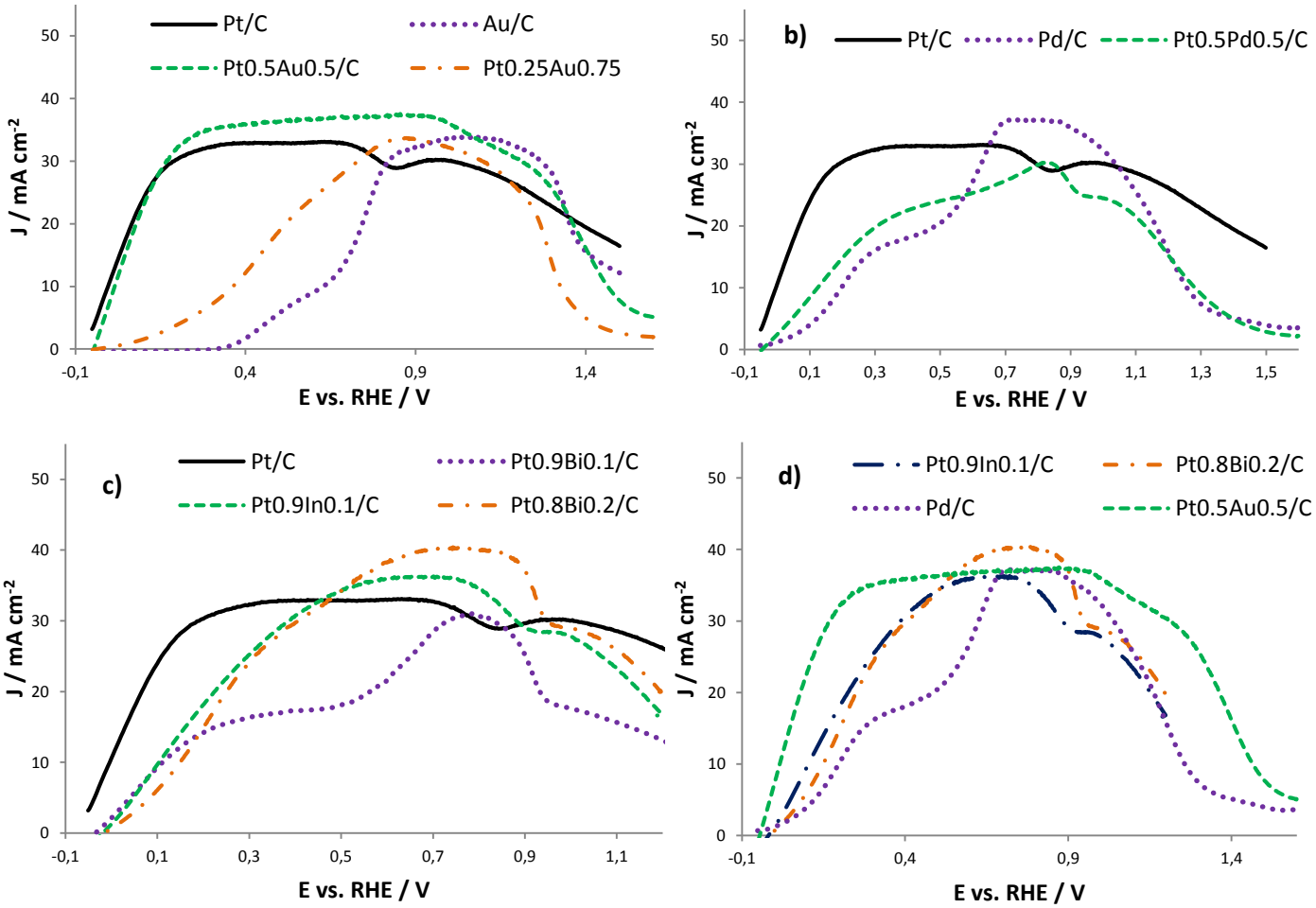

Figure 25: *Comparison of the anodic sweeps at 1200 rpm for all catalysts grouped in:* ***a)*** *gold containing catalysts,* ***b)*** *Pd containing catalysts,* ***c)*** *Bi and In containing catalysts and* ***d)*** *comparison of the best performing catalysts of each group.*

The comparison of the Bi and In containing catalysts seems perplexing due to the fact that the performance seems to increase with the amount of Bi in the catalyst. This was due to the fact that with $Pt_{0.9}Bi_{0.1}/C$ no stable catalyst layer could be achieved on the RDE surface. During the rotation rate increase parts of the catalyst layer were lost to the electrolyte and therefore decreased the loading. Nevertheless, information could be gathered from these experiments. The alloying of Pt with In and Bi showed very similar results by slightly increasing kinetic limitations for lower anode potentials compared to Pt/C. At potentials higher 0.45 V vs RHE they both outperformed Pt/C. This and the complete absence of bubble formation during measurements qualify them as promising catalysts for a hydrolysis-free DBFC system.

A more detailed discussion for every single catalyst can be found in the following sections of this work.

4.3.1 RDE-CV of Pt/C (50%) with 5mM $NaBH_4$

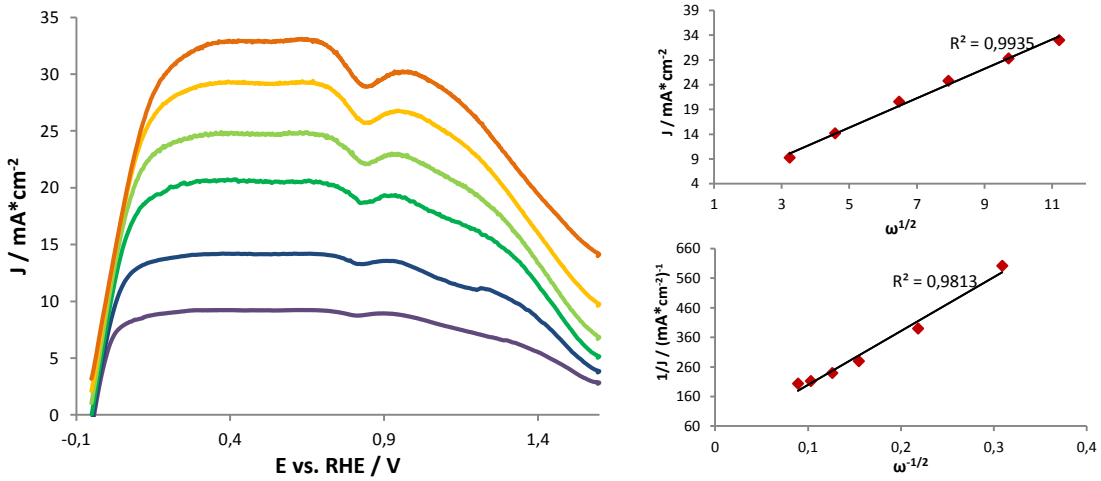

Figure 26: *Rotating Disc Electrode Cyclic Voltagrammogram, Levich and Koutecky-Levich plots of Pt/C (50 wt%) in 5mM $NaBH_4$ and 1M NaOH, 28 µg/cm², -0.05 to 1.5 V vs RHE, 10 mV/s; rotation rates are: 100, 200, 400, 600, 900 and 1200 rpm*

The RDE CV curves of the commercial Pt/C (50%) from Alfa Aeasar and the Levich and Koutecky Levich plots are presented in **Figure 26**.

The onset potential is approx. -0.05 V vs RHE. The aqueous electrolyte poses an obstacle for measuring the exact onset potential due to the very low overpotential of hydrogen evolution on platinum. This circumstance creates challenges for the K-L-analysis too. Due to the overlapping of hydrogen evolution and hydrogen re-oxidation with the BOR current the K-L-plots are not linear at low potentials up to 0.1 V vs RHE. It was tried to start the CV at 0.0 V vs RHE, but no onset potential could be seen because the current at 0.0 V vs RHE increases with the rotation rate.

At potentials above 0.1 V a linear K-L plot could be achieved. The electron yield at 0.11 V vs RHE is 6.7 which seems plausible. Hence the calculated value for the heterogeneous rate constant (k_h) was considered accurate. The diffusion limited region starts at 0.38 V vs RHE and there are two regions that are divided by a drop of current density at 0.84 V vs RHE, which was also observed in literatue [*7*]. There a high-potential and a low-potential region was introduced to the BOR on Pt. The form of the drop suggests that it originates from a species in solution rather than a surface oxidation of an intermediate. This is in concordance the theory of the different mechanisms on the metallic Pt and the PtOH/O as already discussed in section 3.21 [40].

Levich analysis of the low potential region shows a yield of 7.3 electrons. According to the assumption that in the low potential region BH_3OH^- is the species being oxidized [8], only 6 electrons would be exchanged. The remaining "one" electron can be explained if we take into account that the hydrogen formed in the CE mechanism (see Eq. 4 to 6 in section 2.2.1) is also

oxidized on platinum. The complete 8 electrons cannot be achieved because the hydrogen is partially transported away, especially at higher rotation rates.

In another publication it was observed that above 0.9 V vs RHE hydrogen evolution increased noticeably [7]. It was argued that in the mass transport normed RDE plots (by dividing current density with the square root of the rotation rate), a CE mechanism can be identified. The intensity of the diffusion limited current density decreases with increasing rotation rate. This means a precursor of an electrochemically active substance is transported away before it can form the electrochemically active species. However, this phenomenon could not be observed in the results presented in **Figure 56** in the attachments. A difference between the experiments performed by the in literature and this work was the use of bulk platinum. Because Pt nanoparticles were used for the here presented investigations, the reaction rates are much higher. The evenly decreasing intensity in **Figure 56** is a sign that the produced current is a mixture of direct borohydride oxidation and oxidation of BH_3OH^- formed in the CE mechanism. By increasing the rotation rate more hydrogen is transported away before it can be oxidized, leading to the reduction of the peak intensity.

4.3.2 RDE-CV of Au/C (40%) with 5mM $NaBH_4$

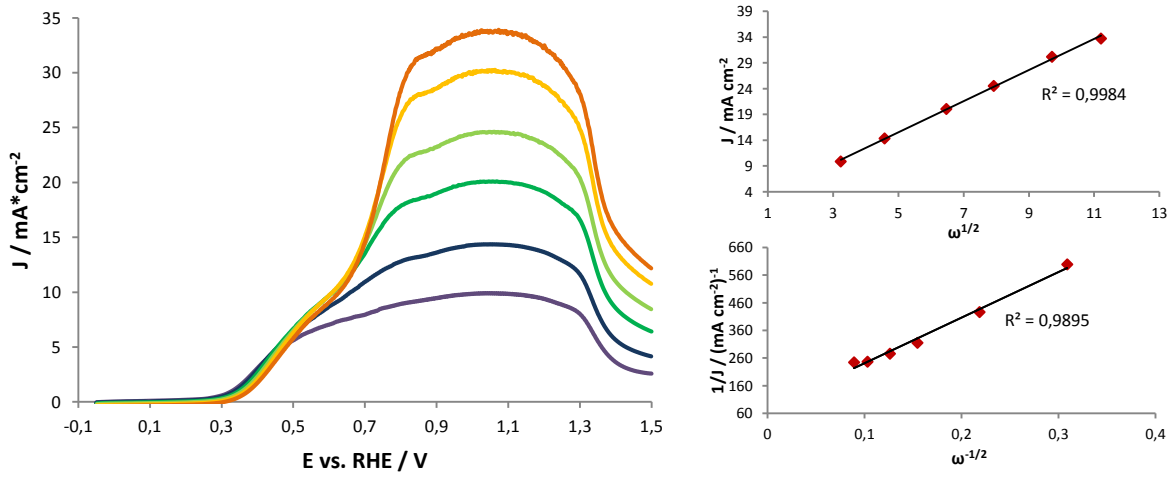

Figure 27: *Rotating disc electrode cyclic voltagrammogram, Levich and Koutecky-Levich plots of Au/C (40 wt%) in 5mM $NaBH_4$ and 1M NaOH, 28 µg/cm², -0.05 to 1.5 V vs RHE, 10 mV/s; rotation rates are: 100, 200, 400, 600, 900 and 1200 rpm*

As it was already seen in the stationary CV of Au/C in borohydride containing electrolyte the onset potential is approx. at 0.3 V vs RHE. Interestingly, the current density between onset potential and 0.7 V vs RHE is independent of the rotation rate and forms a small plateau. This is a sign of strong kinetic limitations. The form of the mass transport normed RDE plot in

Figure 57 in the attachments suggests a CE mechanism for this region. The peak intensity decreases rapidly with increasing rotation rate. This is similar to mass transport limited RDE plots of platinum found in literature [7]. The potential region coincides with peak (1b) in the stationary CV of Au/C in

Figure 17 (see section 3.2.2). This is somewhat inconsistent with the explanation of peak (1b) where it is assumed to come from direct borohydride oxidation [8]. Online electrochemical mass spectroscopy showed hydrogen evolution on gold and a DFT simulated mechanism on gold gave insights into the nature of the peak form [24], [28]. According to the DFT model surface hydrides are formed by adsorption of BH_4^- on gold. These can recombine to form a H_2 molecule, which can be transported away before being oxidized. The effect increases with the rotation rate, especially on gold which is slow for hydrogen oxidation.

After this kinetic limitation a diffusion limited region forms between approx. 0.7 and 1.2 V vs RHE.

These results deviate from those of other results found in literature because there, two diffusion limited regions were found [7]. Instead of the strong kinetic limitations they show a diffusion limited plateau between 0.4 and 0.7 V vs RHE. Levich-analysis of this plateau gave an electron yield of 4. Similar results were found an other study [3].

Krishnan et al. found only one diffusion limited plateau similar to the present work [42]. The difference is that their diffusion limited region lies between 0.4 V and 1.2 V vs RHE and no kinetic limitation could be observed. During their RRDE experiments with a gold ring they measured a current on the ring electrode that increased with the disc electrode potential. The ring electrode potential was held at 0.130 V vs RHE at which the current can be assigned to BH_3OH^- formed by BH_3 leaving the disc electrode surface. According to this result, the oxidation at higher potentials should be incomplete. This explanation is inconsistent with results from this study and other results in literature [7]. The parameters calculated by L and K-L-analysis are given in **Table 7**. They imply that the BOR on Au/C is almost complete. This are similar results as for Pt/C. It could be related to a loss of hydrogen.

However, the great difference of experimental results of all presented studies puts the proposed theories into question. One important difference of some studies is the use of bulk electrodes, while others, including the present work, deployed gold nanoparticles.

To clear these inconsistencies more data will be needed in the future.

4.3.3 RDE-CV of Pd/C (40%) with 5mM $NaBH_4$

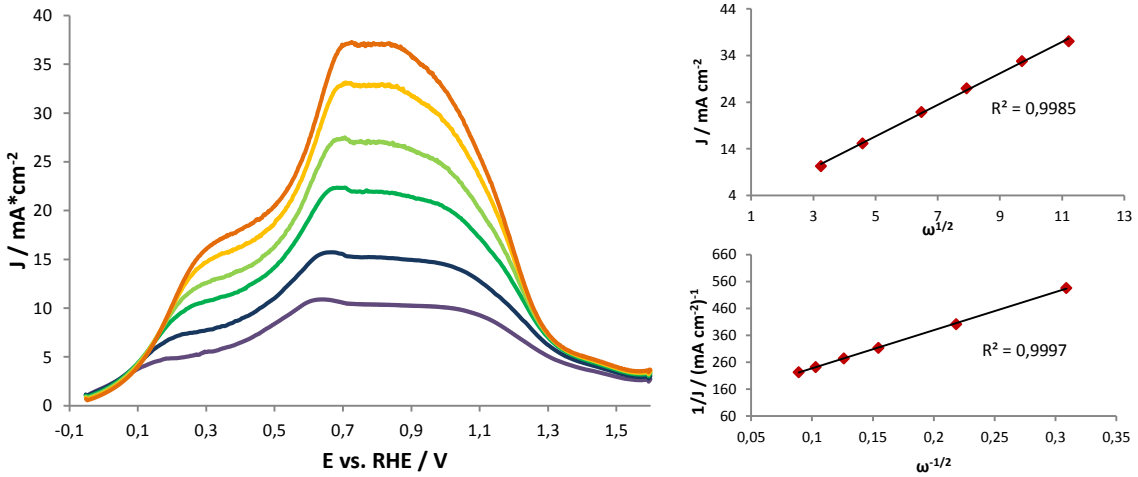

Figure 28: *Rotating disc electrode c voltagrammogram, Levich and Koutecky-Levich plots of Pd/C (40 wt%) in 5mM $NaBH_4$ and 1M NaOH, 28 µg/cm², -0.05 to 1.6 V vs RHE, 10 mV/s; rotation rates are: 100, 200, 400, 600, 900 and 1200 rpm*

In the RDE-CV of Pd/C it is clearly visible that the low- and the high-potential region are also formed at all rotation rates and the onset potential is below 0.0 V vs RHE. The RDE CVs of Pd/C resulted in a publication which can be found in the references [57]. In the low potential region, the oxidation only yields $BH_2(OH)_2^-$ in a 4 electron oxidation and the complete 8 electron oxidation occurs in the high potential region. The calculated number of electrons in **Table 7** matches this assumption. At 0.4 V vs RHE 4.2 electrons are yielded while at 0.7 V vs RHE almost complete oxidation with 7.8 electrons is observed.

4.3.4 RDE-CV of $Pt_{0.5}Au_{0.5}$/C (40%) with 5mM $NaBH_4$

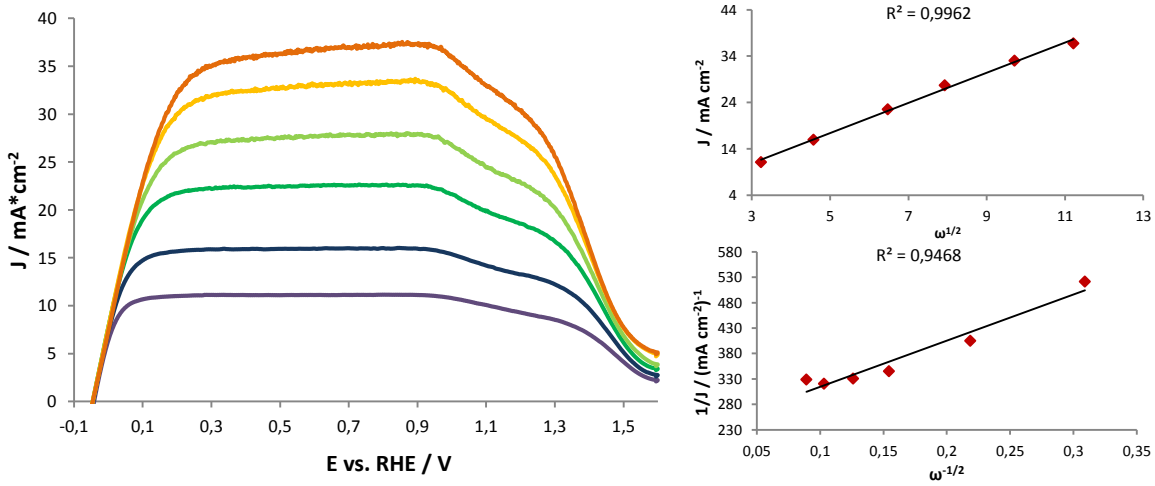

Figure 29: *Rotating disc electrode cyclic voltagrammogram, Levich and Koutecky-Levich plots of $Pt_{0.5}Au_{0.5}$/C (40 wt%) in 5mM $NaBH_4$ and 1M NaOH, 42 µg/cm², -0.05 to 1.6 V vs RHE, 10 mV/s; rotation rates are: 100, 200, 400, 600, 900 and 1200 rpm*

The form of the curves is similar to the RDE CVs of pure platinum. The current density of the diffusion limited plateaus is higher for $Pt_{0.5}Au_{0.5}$/C. This leads to a higher electron yield in the L and K-L analysis (compare **Table 7**).

While for Pt/C the onset Potential could not be determined exactly due to strong hydrogen evolution, this was not the case for the $Pt_{0.5}Au_{0.5}$/C catalyst. The onset potential can be determined as -0.05 V vs RHE. Due to the gold alloying the overpotential of the hydrogen evolution from the aqueous electrolyte is higher. Therefore, the kinetically limited area shows no increase in onset current density with increasing rotation rate, as we saw for Pt/C.

A broad diffusion limited area can be identified from 0.3 to 0.9 V vs RHE. At higher rotation rates there is a slight increase of the current density that peaks at 1 V vs RHE, which is approximately the potential of the peak of the diffusion limited area of Au/C.

The drop that occurs at 0.8 V vs RHE in the RDE CV of Pt/C is not observed. As discussed in section 3.2.1 and 3.3.1, this drop is probably due to the surface change from Pt to PtOH/O. However, on the $Pt_{0.5}Au_{0.5}$/C the oxidation can continue on the gold particles until the phase transition is finished.

In general, the alloying with gold has shown very positive effects. The electron yield was increased and the diffusion limited area was broadened without shifting the onset potential.

This is why the Platinum load was decreased and the performance increased. But during the measurements hydrogen bubble formation was observed.

4.3.5 RDE-VC of $Pt_{0.25}Au_{0.75}$/C (40%) with 5mM $NaBH_4$

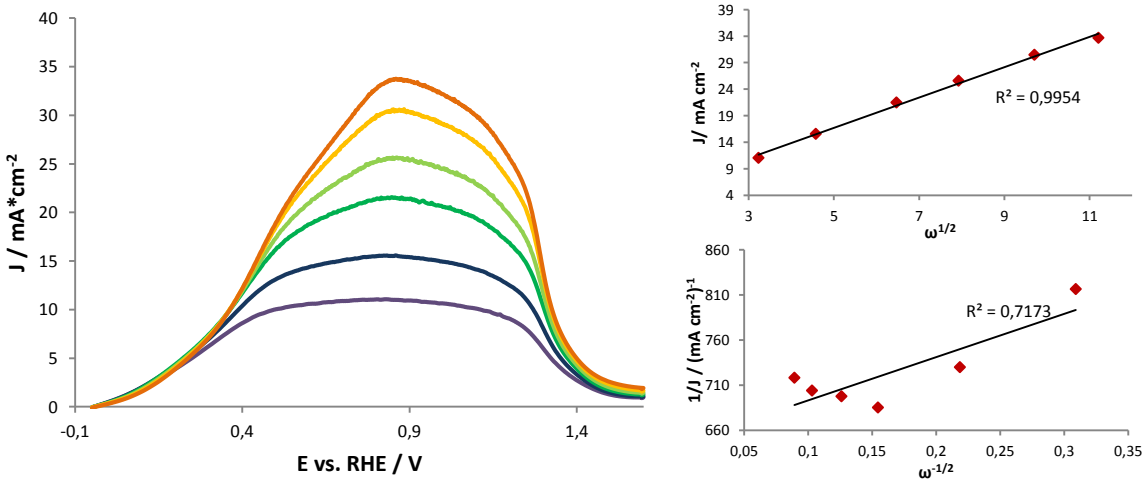

Figure 30: *Rotating disc electrode cyclic voltagrammogram, Levich and Koutecky-Levich plots of $Pt_{0.25}Au_{0.75}$/C (40 wt%) in 5mM $NaBH_4$ and 1M NaOH, 42 µg/cm², -0.05 to 1.5 V vs RHE, 10 mV/s; rotation rates are: 100, 200, 400, 600, 900 and 1200 rpm*

Comparable to $Pt_{0.5}Au_{0.5}$/C, the onset potential of the BOR is below the redox potential of hydrogen evolution. The higher gold content in this catalyst has a negative effect on the activity. Extreme kinetic limitations similar to those found for Au/C in section 3.3.2 were observed from the onset potential to 0.3 V vs RHE, which is probably due to an oxidation mechanism involving hydrogen formation that cannot be oxidized fast enough on the surface. Between 0.3 and 0.7 V vs RHE the kinetic limitations were less strong. Compared to the Au/C with extreme kinetic limitations in this region, an improvement could be observed by the introduction of Pt.

At higher rotation rates the curves seem to change slightly to a shape similar to that of the Pd/C RDE-CVs. This was identified as an effect of the high gold content. While all active sites of Pt are already occupied due to the high BH_4^- supply, the active sides of gold cannot oxidize BH_4^- at low potentials without considerable kinetic limitations. This shape change leads to a small diffusion limited region at around 0.83 V vs RHE. L and K-L analysis proved difficult at lower potentials, due to the shape change and unusual kinetical limitations. Therefore, L analysis was only performed at 0.86 V vs RHE resulting in an electron yield of 7.5.

The fact that complete BH_4^- oxidation is only reached at high potentials and that bubble formation is observed on the electrode surface during measurements, excludes this catalyst from deployment in a DBFC. $Pt_{0.5}Au_{0.5}$/C proved to be superior.

4.3.6 RDE-CV of $Pt_{0.5}Pd_{0.5}$/C (40%) with 5mM $NaBH_4$

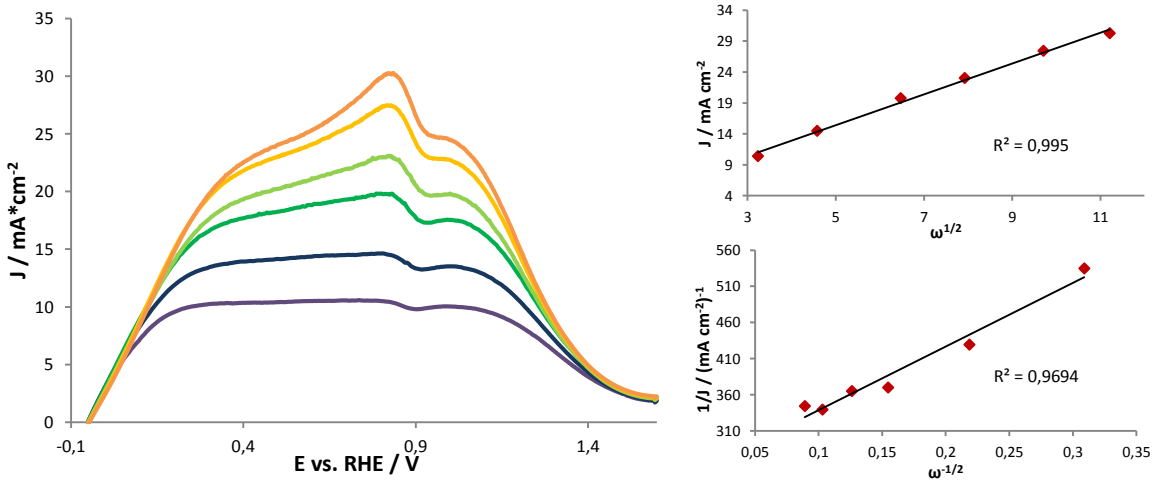

***Figure 31**: Rotating disc electrode cyclic voltagrammogram, Levich and Koutecky-Levich plots of Pt0.5Pd0.5/C (40 wt%) in 5mM NaBH4 and 1M NaOH, 28 µg/cm2, -0.05 to 1.5 V vs RHE, 10 mV/s; rotation rates are: 100, 200, 400, 600, 900 and 1200 rpm*

On the Pt-Pd-alloy catalyst an onset potential of -0.05 V vs RHE and a kinetically limited region that extends to approximately 0.3 V vs RHE was observed. An interesting observation is the shape change at higher rotation rates comparable to $Pt_{0.25}Au_{0.75}$/C in section 3.3.5. Due to the high BH_4^-

supply at high rotation rates the Pt sites are occupied while the Pd sites can oxidize borohydride only until the $BH_2(OH)_2^-$ intermediate. L analysis was difficult at these potentials due to the shape change but possible for rotation rates from 100 to 600 rpm. The electron yield was 6 at 0.5 V vs RHE. This is strong evidence for the theory of a mixed mechanism. On Pt sites the BOR follows through an 8 electron mechanism, while on the Pd sites $BH_2(OH)_2^-$ blocks the surface and is not further oxidized until higher potentials are reached. At 0.8 V vs RHE where the electron yield was 7.

During the whole measurement vigorous bubble formation could be observed. This leads to the conclusion that Pd-Pt alloys are not a candidate for practical application in DBFCs.

4.3.7 RDE-CV of $Pt_{0.8}Bi_{0.2}$/C (40 wt% Pt) with 5mM $NaBH_4$

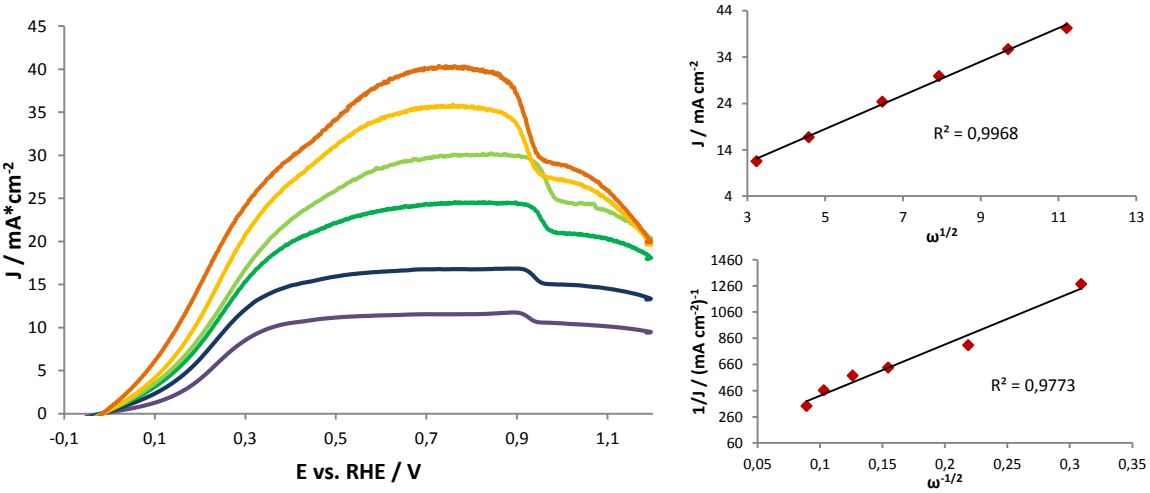

Figure 32: *Rotating disc electrode cyclic voltagrammogram, Levich and Koutecky-Levich plots of Pt0.8Bi0.2/C (40 wt%) in 5mM $NaBH_4$ and 1M NaOH, 112 µg Pt/cm², -0.05 to 1.2 V vs RHE, 10 mV/s; rotation rates are: 100, 200, 400, 600, 900 and 1200 rpm*

The onset potential of the oxidation is at around -10 mV vs RHE followed by a broad kinetically limited potential region. The potential interval of the region seems to increase with the rotation rate. At high rotation rates the oxidation seems to form a high and a low potential region comparable to Pd/C, $Pt_{0.5}Pd_{0.5}$/C and $Pt_{0.25}Au_{0.75}$/C. Therefore, we assume the same explanation as for the Pt-Pd and Pt-Au catalyst (see section 3.3.5 and 3.3.6). The reason is the surface coverage by bismuth [48], which limits the number of active Pt sites.

L and K-L plots show a linear trend (results are given in table 5). L analysis at 0.37 V vs RHE gave 6.9 electrons and at 0.75 V vs RHE it increases to 8.9 electrons. This non-faradaic electron yield could come from fluctuations of the diffusion coefficient related to the changing ambient conditions. It is not probable that they come from bismuth oxidation because it occurs at potentials above 0.8 V vs RHE. The oxidation current does also decrease rapidly above the peak potential

for the bismuth oxidation. This could be a sign that metallic bismuth is involved in a direct borohydride oxidation mechanism.

K-L analysis at 0.2 V vs RHE showed that at these low potentials the kinetic limitations are considerable. Only 3.1 electrons are exchanged per molecule. By looking at Eq. 12 to 18 one can see that the mechanism has to stop at BH_{2*} to generate only these few electrons. However, to prove this assumption the species formed at 0.2 V vs RHE has to be clearly detected.

4.3.8 RDE-CV of $Pt_{0.9}Bi_{0.1}$/C (40 wt% Pt) with 5mM $NaBH_4$

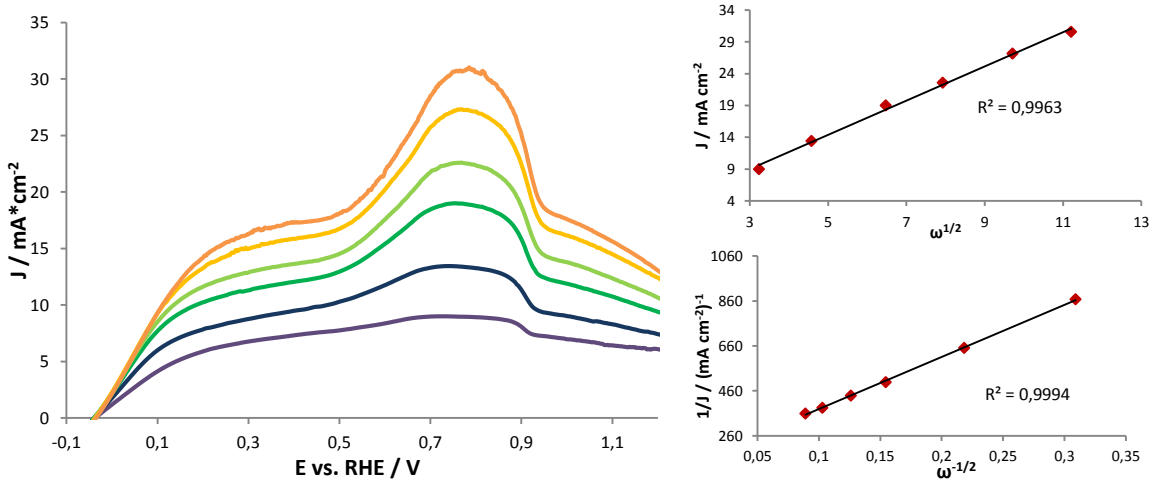

Figure 33: *Rotating disc electrode cyclic voltagrammogram, Levich and Koutecky-Levich plots of Pt0.9Bi0.1/C (40 wt%) in 5mM $NaBH_4$ and 1M NaOH, 112 µg/cm², -0.05 to 1.2 V vs RHE, 10 mV/s; rotation rates are: 100, 200, 400, 600, 900 and 1200 rpm*

$Pt_{0.9}Bi_{0.1}$/C (40 wt% Pt) showed complications with the stability of the catalyst layer on the RDE lead to a lower catalyst loading during all measurements. Therefore, all K-L and L parameters are lower than those of the higher Bi content catalyst.

The form of these CVs in **Figure 33** is similar to the higher Bi-content catalyst. There are two potential regions, which can be discussed in the same way. The effect is stronger for this measurement because of the catalyst loss as soon as rotation was started.

The electron yield at 0.37 V vs RHE amounts to 4.4, while at 0.75 V vs RHE 6.9 electrons are exchanged. This combined with the absent bubble formation lead to the conclusion, that $Pt_{0.9}Bi_{0.1}$/C was a promising catalyst for a practical DBFC application. In addition, K-L analysis at 0.2 V vs RHE revealed that 5.3 electrons are exchanged. This shows that the kinetic limitations are abated with lower Bi content.

4.3.9 RDE-CV of $Pt_{0.9}In_{0.1}$/C (40 wt% Pt) with 5mM $NaBH_4$

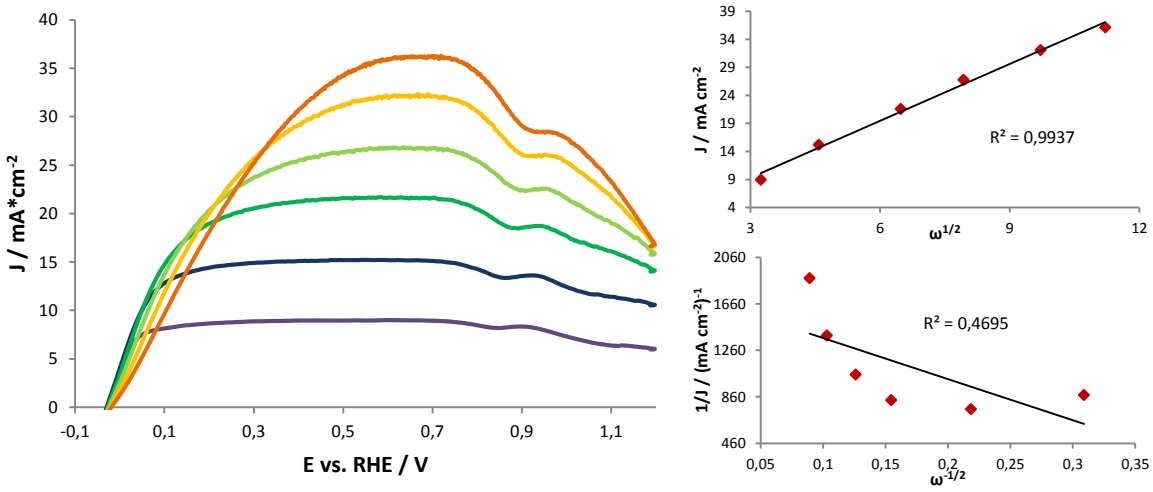

Figure 34: *Rotating disc electrode cyclic voltagrammogram, Levich and Koutecky-Levich plots of Pt0.9In0.1/C (40 wt%) in 5mM $NaBH_4$ and 1M NaOH, 112 µg/cm², -0.05 to 1.2 V vs RHE, 10 mV/s; rotation rates are: 100, 200, 400, 600, 900 and 1200 rpm*

The anodic sweeps of the RDE CV of the $Pt_{0.9}In_{0.1}$/C (40 wt% Pt) can be seen in **Figure 34**.

In general, they show a better performance than bismuth modified catalysts. The onset potential lies at -20 mV vs RHE. In the region from the onset potential to 0.4 V vs RHE an increase in kinetic limitation with the rotation rate can be observed. This can be attributed to an impurity in the electrolyte. The poison was identified as Cl^- as a by-product of the catalysts synthesis is NaCl. Apparently this was not fully removed in the centrifugation process. That is why K-L analysis was not possible. The oxidation reaches almost a complete 8 electron oxidation at 0.5 V vs RHE, where L-analysis resulted in an electron yield of 7.7. The maximum is reached at 0.65 V vs RHE with 7.8 exchanged electrons.

Comparable to other In or Bi modified catalysts, no hydrolysis could be observed during the measurements making it a promising candidate for practical DBFC applications.

4.4 Stationary Cyclic Voltammetry with BH_4^- containing ionic liquids

A structure of ionic liquids used as borohydride source was already presented in **Figure 1** in the theoretical aspect (see section 2.3).

The catalysts which were measured with the ionic liquids as BH_4^- source are listed in table 3. Resulting stationary CVs are shown in **Figure 44** to **Figure 55** in the attachment.

The CVs of the platinum catalyst show the same peaks for the ionic liquids METMA-BH_4, TMPA-BH_4 and $NaBH_4$. Peak (1a) only differs in the intensity from the corresponding peaks for the ILs. The current density of the anodic plateau following the peak is a bit lower with METMA-BH_4 and even lower with TMPA-BH_4. Apparently the presence of nitrogen containing species can lead to amine formation in small amounts, which poison the platinum surface. Especially in the CV with DMETMA-BH_4 the equivalent of peak (1a) is only slightly formed and its potential is shifted to 0.3 V vs RHE. With the present data it is not possible to predict if the impurities originate from the synthesis, decomposition during storage or if they form during electro oxidation.

On the gold catalyst a similar effect could be observed as on Pt/C. But the negative effect is not as distinct as on Pt/C. METMA-BH_4 seems to have almost no effect on the anodic plateau and only a small effect on the first anodic peak. With DMETMA-BH_4 and TMPA-BH_4 the anodic plateau and the equivalent to peak (1a) are slightly affected.

By looking at the CVs on $Pt_{0.5}Au_{0.5}$/C with the ionic liquids, one can see that the trend continues also by alloying the two metals. METMA-BH_4 seems to have the least influence on the performance of the catalysts.

On Pd/C the stationary CV with METMA-BH_4 shows a current jump at the position of peak (2c) in the CV of Pd/C with $NaBH_4$. This was probably due to an error inside the potentiostat. Nevertheless, it gives information about the BOR with METMA-BH_4. By comparing ILs with $NaBH_4$ there is obviously a great effect by all three ILs. Only METMA-BH_4 seems to have less impact on the catalyst.

So by comparing the performance in stationary conditions of all metals with the different ILs we came to the conclusion, that METMA-BH_4 has the least effect on the performance of all presented catalysts.

4.5 Rotating Disc Electrode Cyclic Voltammetry with BH_4^- containing ionic liquids

The catalysts which were measured with the ionic liquids as BH_4^- source are listed in **Table 3**. The resulting RDE CVs can be seen in **Figure 44** to **Figure 55** in the attachment and the calculated kinetic parameters are shown in **Table 8**

	$NaBH_4$	METMA- BH_4	DMETMA- BH_4	TMPA- BH_4
		Pt		
k_h / cm*s^{-1}	$91*10^{-2}$	$1.5*10^{-1}$	$1.3*10^{-1}$	-
n_L (0.38 V)	7.3	7.3	7.4	7.2
n_{KL} (0.11 V)	6.7	9.0	9.3	-
n_L (0.6 V)	7.3	7.0	6.9	6.7
n_L (0.98 V)	6.7	6.8	7.0	7.0
		Au		
k_h / cm*s^{-1}	$3.5*10^{-2}$	$1.7*10^{-2}$	$1.8*10^{-2}$	$3.4*10^{-2}$
n_L (1.05 V)	7.2	6.9	5.2	6.8
n_{KL} (0.76V)	6.4	6.9	5.1	5.7
		Pd		
k_h / cm*s^{-1}	$1.3*10^{-1}$	$6.8*10^{-2}$	$1.6*10^{-1}$	$6.3*10^{-2}$
n_L (0.4 V)	4.3	3.4	3.4	2.9
n_L (0.84 V)	8.0	7.2	7.8	7.5
n_{KL} (0.15 V)	6.7	-	-	-
n_{KL} (0.55 V)	7.5	9.4	6.4	8.0
		$Pt_{0.5}Au_{0.5}$		
k_h / cm*s^{-1}	-	-	-	-
n_L (0.38 V)	8.0	8.3	7.1	6.8
n_L (0.6 V)	8.0	8.6	7.2	6.9
n_L (0.9 V)	8.1	8.5	7.4	7.0
n_{KL}	-	-	-	-

Table 8: *Summary of the calculate kinetic parameters by Levich and Koutecky-Levich analysis for the ionic liquids in comparison with $NaBH_4$*

K-L analysis proved to be difficult on Pt/C and Au/C. K-L analysis that resulted in more than 10 electrons per BH_4^- molecule is not reported in **Table 8**. Therefore, K-L was only performed for Pt/C, Au/C and Pd/C. Values for the heterogeneous rate constant k_h for points were K-L analysis resulted in an electron yield greater 8 cannot be considered accurate. The calculations were only performed in regions with linearity of the L and K-L plots. The corresponding plots are given in the attachment.

For Pd/C not all rotation rates are included into the analysis to receive a linear plot at 0.4 V vs RHE.

The comparison of the kinetic parameters calculated by L and K-L analysis show that on Pt/C the negative effect seen in stationary conditions cannot be reproduced in dynamic conditions. A slight

difference in the form of the RDE curves with ILs can be noticed. The drop at 0.8V vs RHE proved to be more distinct when ILs were used as borohydride source. Furthermore, the current density seems to slowly decrease with increasing potential. This effect seems to rise with the rotations rate. Therefore, the electron yield decreases slightly at 0.6 V vs RHE. The decrease of electron yield is biggest for TMPA-BH_4. However, the three ionic liquids show no significant loss of performance.

Contrary to the stationary CVs on Au/C with ILs, the L and K-L analysis of the corresponding RDE CVs reveal a negative effect on the electron yield. METMA-BH_4 has the least and DMETMA-BH_4 the biggest effect on the electron yield of Au/C.

Pd/C shows a higher performance loss than Pt/C with all ionic liquids. In the high and low potential region the electron yield is reduced by 1 and the form of the RDE curves changed by using ILs. Real diffusion limited regions did not form, but they rather became peaks, indicating greater kinetic limitations.

On $Pt_{0.5}Au_{0.5}$/C only L analysis was possible. The results show that the performance is unchanged for METMA-BH_4. The slight increase of electron yield can be neglected because the deviation is below 10%. By using DMETMA-BH_4 and TMPA-BH_4 as borohydride source the performance loss is considerable. The conclusion, that alloying gold and platinum increases the tolerance for $METMA^+$, lies near.

By comparing the calculated electron yield at every rotation rate for one potential, a decrease with increasing rotation rate can be noticed at every potential, for every metal and every BH_4^- source. In **Figure 35** the corresponding diagram for the catalysts measured with ionic liquids is shown. For $NaBH_4$ on Pt/C (**Figure 35 a)**) an initial increase of electron yield in the low rotation rate region can be observed. It is caused by hydrogen bubbles that are not transported away from the electrode at low rotation rates. The bubbles increase the resistance and therefore the current measured is lower. With increasing rotation, the bubbles are then swept away from the electrode surface. Therefore, after a peak electron yield is reached, a steady loss from 400 to 2000 rpm occurs for $NaBH_4$. This loss originates from hydrogen being transported away before it can be oxidized. In the case of ILs there is no increasing electron yield for the first rotation rate steps. Apparently hydrolysis is prevented by the ammonium cations. Furthermore, the loss with increasing rotation rate is higher for all ILs, which is indicated by steeper curves. This can be explained by the increasing transport of poisonous species to the Pt surface. In addition, the lost is biggest with TMPA-BH_4.

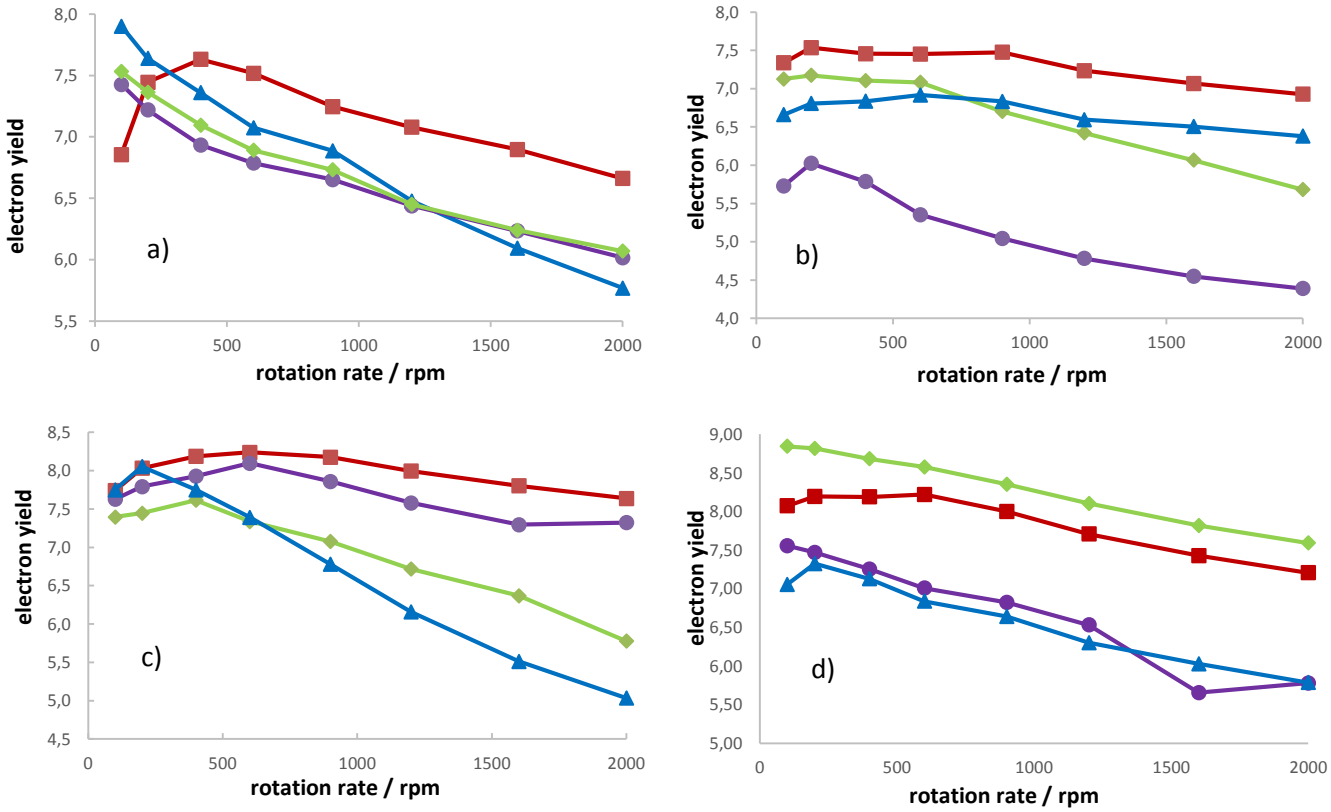

Figure 35: *Electron yield at every rotation rate on a) Pt/C at 0.6 V, b) Au/C at 1.05 V, c) Pd/C at 0.84 V and d) Pt0.5Au0.5/C at 0.6 V for: $NaBH_4$, $METMA\text{-}BH_4$, $DMETMA\text{-}BH_4$, $TMPA\text{-}BH_4$.*

On Au/C the ILs that seem to poison the catalyst are METMA and DMETMA-BH_4, while the loss of electron yield for TMPA-BH_4 does not deviate from the $NaBH_4$ curve. The decrease of electron yield for $NaBH_4$ indicates a species being transported away before it can be oxidized. This can be attributed to hydrolysis.

Pd/C clearly shows signs of poisoning with TMPA-BH_4. A slight poisoning effect can be noticed by METMA-BH_4, while DMETMA-BH_4 does not seem to affect the Pd catalyst.

Alloying of Au and Pt appears to increase the tolerance to poisoning form nitrogen species. The loss of electron yield with increasing rotation rate is approx. the same for all BH_4^- sources. METMA-BH_4 even seems to show better performance than $NaBH_4$ with an electron yield above 8. It could be due to imprecisions of the concentration or fluctuations in ambient pressure leading to different electrolyte viscosities. Nevertheless, the results qualify $Pt_{0.5}Au_{0.5}/C$ for a practical application in a DBFC that uses one of the presented ILs as fuel.

Another characteristic of the curves of ILs in comparison to $NaBH_4$ is the overall lower electron yield for all ILs on all catalysts. Due to the nature of the ILs ion pair formation occurs. The formation of ion pairs decreases the concentration of free BH_4^- anions.

4.6 In-situ polarisation curve and online hydrolysis detection

4.6.1 In-situ experiments with Pt/C as anode catalyst (MEA1)

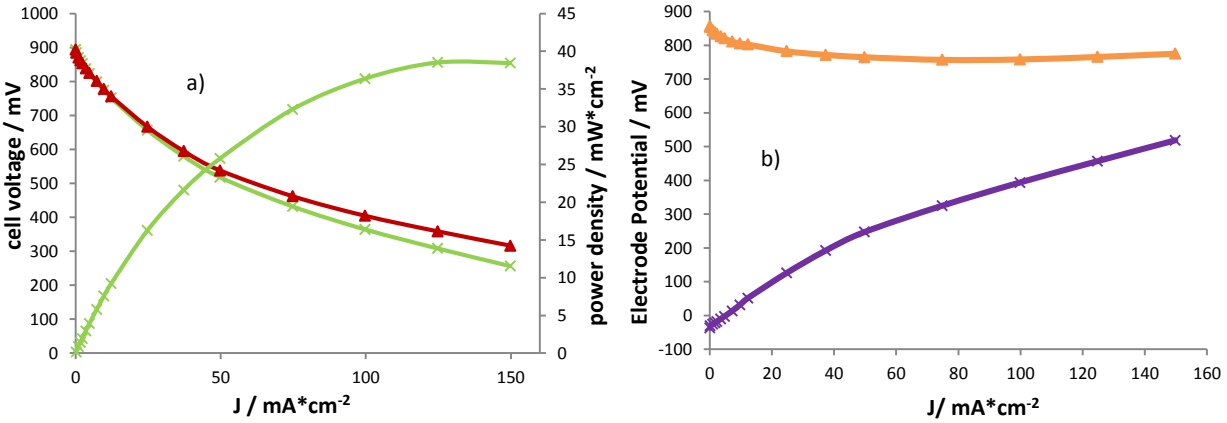

Figure 36: *Polarisation curve of MEA1 at 40°C: Pt/C (50%) anode with 1 mg/cm² Pt loading vs. a MnO_2/C cathode; Tokuyama membrane; a) polarization curve; red line = I*R compensation b) anode and cathode polarization*

As shown in **Figure 36** the OCV of MEA1 was 895 mV, which is close to the OCV of common hydrogen fuel cells. Because of the aqueous fuel the anode potential is limited to approx. 0 V vs RHE, as already discussed in section 3.2.1. In ex-situ experiments the onset potential of the BOR is approx. -50 mV vs RHE, while the OCP of the Anode in MEA1 was -37 mV vs RHE. Apparently slight oxygen crossover followed by a mixed potential formation occurs due the thin membranes. This phenomenon occurred throughout all in-situ measurements. However, the oxygen pressure was kept low and the potential increase of the anodes was insignificantly small.

Figure 36 b) shows that the kinetic loss is dominant on the anode, while the cathode catalyst shows good ORR behaviour. MnO_2/C was used because it shows excellent BH_4^- tolerance, which was proven by *Grimmer et al*. [39]. The low cathode potential loss proves this. Even though a high BH_4^- crossover can be expected from the thin anion exchange membrane (AEM) it does not change significantly.

Ohmic losses are small due to the low internal resistance of 0.15 Ω. The steepness in the linear region from 50 to 150 mA/cm² is high compared to typical steepness of linear regions in Polymer electrolyte fuel cells (PEMFCs) [58]. This is due to the poor mass transport in the liquid fuel. In all electrochemical cells the steepness of the fuel concentration gradient from the bulk liquid/gas to the electrode surface increases with higher current densities. Diffusion coefficients of gaseous fuels in are much higher compared to fuels in liquid media. Hence the concentration of fuel on the electrode surface sinks faster for direct liquid fuel cells than for PEMFCs. **Figure 36 b)** shows that this mass transport effect is much higher on the anode than on the cathode (gaseous O_2 used on the cathode). An increase of the operating temperature could alleviate this effect. A higher temperature would also benefit the kinetics. Because of the aqueous environment the boiling point

of water poses an upper limit. Other ways to improve mass transport on the anode could be to reduce the depth of the flow field channels and increase the fuel flow.

In **Figure 37** the hydrogen detection measurement of a Pt/C anode in a mixed electrolyte cell can be seen. Because of time reasons a measurement with an anode in an AEM DBFC could not be performed. Because the two cells only differ in the lack of an AEM the effect of the anode catalyst is equivalent.

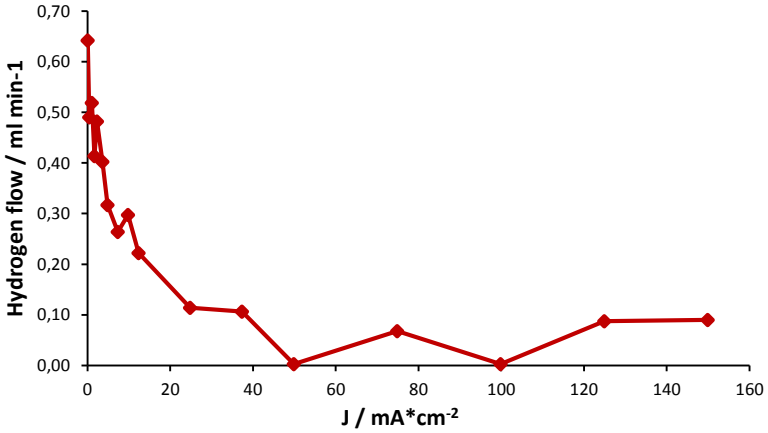

Figure 37: *Results of the online hydrogen detection measurement on a Pt/C anode; the hydrogen current at every DBFC current density step converted to hydrogen flow. Measurement performed by Robert Zacharias*

An issue of MEA1 are the great kinetic losses. To reach 12.3 mA/cm^2 the voltage drops about 140 mV from the OCV. These losses are probably caused by the high hydrolysis rate. At OCV conditions and at low current densities most of the charge is lost as evolved hydrogen. This can be seen in **Figure 37**. The hydrogen was not oxidized in the DBFC and is therefore lost. This is the main challenge for the use of platinum as catalyst. At higher current densities part of the formed hydrogen can be oxidized before it leaves the anode surface, indicated by the sinking hydrogen flow rate with increasing current density. Hydrogen loss is not fully prevented though, as a considerable amount of hydrogen reached the detection cell even at high current densities.

Because hydrolysis occurs even at OCV there would be a constant pressure increase in a resting cell. Venting would be required which leads to a loss of stored energy. Alternatively, a flushing system would be needed to remove the fuel from the anode. This would complicate the system and need additional space. Furthermore, the overall efficiency of the system would decrease due to the energy used by this flushing system. Over time the BH_4^- flushed out would still amount to great losses.

The OCV is very high compared to the MEAs that use Bi or In modified catalysts and kinetic losses are almost equal. This is why MEA1 reached the highest power density of all MEAs tested in this work. The maximum power density was 38 mW/cm^2. Compared to conventional fuel cells

this is not a high value. Because of the high volumetric storage densities of the fuel, a stationary application would be advisable.

4.6.2 in-situ experiments with $Pt_{0.8}Bi_{0.2}$/C as anode catalyst (MEA2)

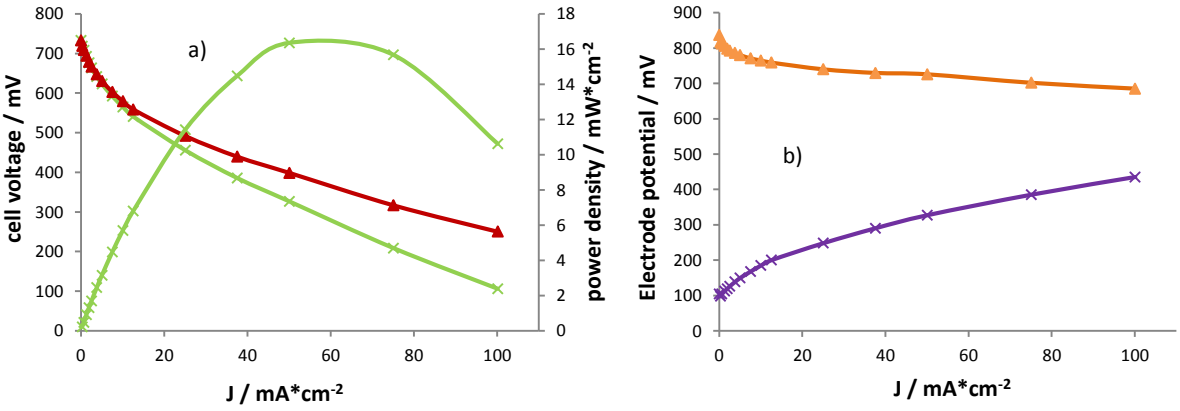

Figure 38: *Polarisation curve of MEA2 at 40°C: $Pt_{0.8}Bi_{0.2}$/C anode with 1 mg/cm² Pt-loading vs. a MnO_2/C cathode; Tokuyama membrane; a) polarization curve; red line = I*R compensation b) anode and cathode polarization*

The polarisation curve of MEA 2 shows a massive kinetic loss, which was expected due to the high bismuth and thiourea content, inhibiting surface hydride formation. Therefore, BH_4^- oxidation at low anode potentials, at which it is strongly connected to these surface hydrides, is kinetically limited. The OCV amounted to 733 mV and about 175 mV are lost from the electrode kinetics. A comparison of **Figure 38** b) and **Figure 36** b) in section 3.6.1 shows that the kinetic loss is greater on the anode than on the cathode. The latter shows a slightly lower performance then in MEA1. Because the cathodes were self-made variations in performance occurred in the course of this work. The Anode performed similarly to the anode in MEA3 with $Pt_{0.9}Bi_{0.1}$/C (see section 4.6.3), were higher power densities were reached.

A considerable ohmic loss can be seen from the polarisation curves. The internal resistance was 0.36 Ω, which resulted in a loss of 108 mV at 75 mA/cm² (compare measured curve to I*R compensated curve). Apparently the humidification and alkalisation of the AEM was not complete. To address this, issue the alkalisation time could have been prolonged, but because all other measurements showed good results it was not.

The same mass transport effects identified for MEA1 can be seen in the polarisation curve of MEA2. It is a phenomenon that is independent of the catalyst and therefore it can be found in all in-situ measurements performed with the designed testing cell.

All together these losses lead to a low maximum power density of 16 mW/cm². Yet this value can be attributed to the cathode performance, while the anode performed similarly to the one in MEA3 as mentioned above.

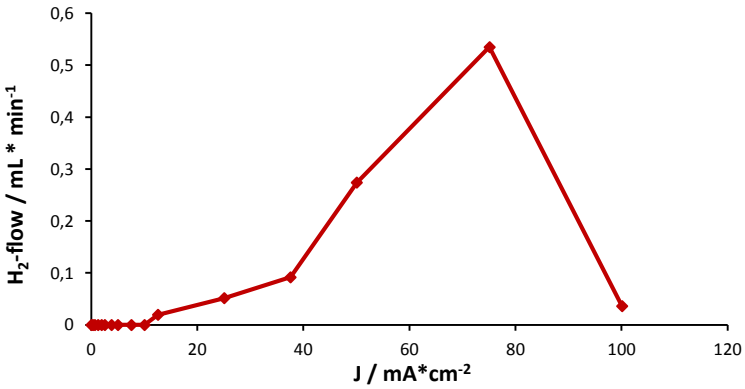

Figure 39: *Results of the online hydrogen detection measurement for MEA2; the hydrogen current at every DBFC current density step converted to hydrogen flow.*

The hydrogen detection measurement in

Figure ***39*** shows the good hydrolysis suppression of bismuth. At OCV and low current densities no hydrogen was detected. This is consistent with the theory of the suppression of surface hydride formation. At 10 mA/cm^2 a slow increase of the hydrolysis rate was observed. Then a massive increase to 0.5 mL/min at 75 mA/cm^2 occurred. This increase can be explained by the consumption of OH^- on the anode surface during the oxidation, which leads to the formation of a concentration gradient from the bulk solution to the surface. Therefore, the local pH on the anode surface decreases, which promotes hydrolysis as we discussed in the theoretical aspects in section 2.2.4. This effect occurs on Pt/C too, but since platinum can oxidize the formed hydrogen the hydrogen does not reach the detection system. Increasing the OH^- concentration in the fuel could alleviate the effect, but an excessively high pH creates problems with decreasing BO_2^- solubility. A lower mass specific energy density of the fuel would also be the result. Therefore, an optimum $[OH^-]/[BH_4^-]$ ratio needs to be found to reduce hydrolysis at high current densities but remaining good BO_2^- solubility and specific energy densities. The combination of pH optimization and the use of Bi could lead to a hydrolysis free system.

The low flowrate at 100 mA/cm^2 probably comes from the slow response time of the detection cell.

4.6.3 In-situ experiments with $Pt_{0.9}Bi_{0.1}/C$ as anode catalyst (MEA3)

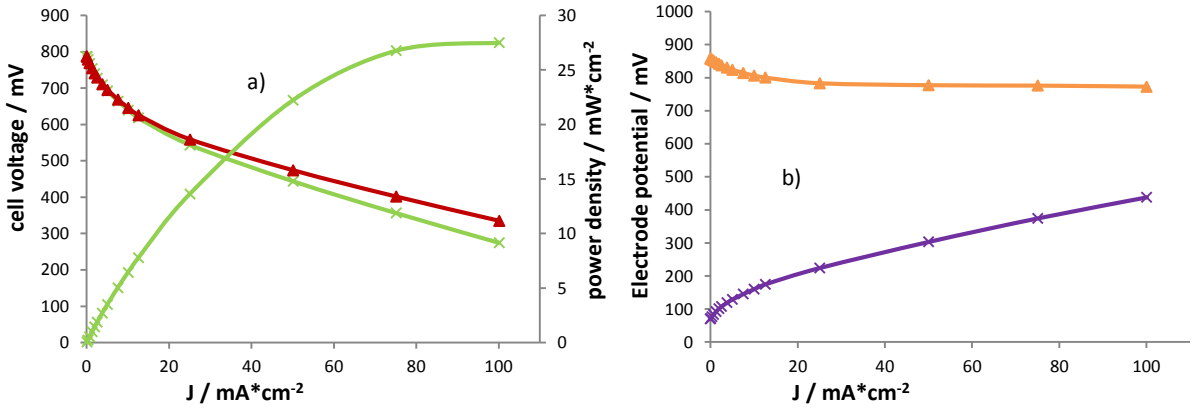

Figure 40: *Polarisation curve of MEA3 at 40°C: $Pt_{0.9}Bi_{0.1}/C$ anode with 1 mg/cm² Pt-loading vs. a MnO_2/C cathode; Tokuyama membrane; a) polarization curve; red line = I*R compensation b) anode and cathode polarization*

By looking at the polarisation curve of MEA3 one can see that a lower Bi content has positive effects on the performance, as it was expected. The OCV was 788 mV, which is an improvement of 55 mV in respect to the high Bi content catalyst. However, this value is not only attributed to a better anode performance. By comparing the OCPs of the anodes and cathodes in **Figure 40** b) and **Figure 38** b) one can see that the anode OCP only improves by 34 mV. The rest of the improvement can be attributed to a better cathode performance. This is because all were self-made rather than commercial cathodes. Nevertheless, a noticeable improvement in the anode kinetics could be achieved. While on the latter around 90 mV are lost only 75 mV are lost on the lower Bi content catalyst. Combined with the slightly better performance of the cathode during the $Pt_{0.9}Bi_{0.1}/C$ measurement, the overall kinetic loss amounts to about 140 mV.

Ohmic losses are small for MEA3 because the internal resistance was only 0.15 Ω. The losses generated by the slow mass transport in the liquid fuel are still visible because they are independent of the deployed catalyst.

Overall MEA3 yields 27 mW/cm². That means 11 mW/cm² are lost compared to Pt/C. But it is a good bargain if we compare the hydrolysis behaviour of $NaBH_4$ on Pt/C and $P_{0.9}Bi_{0.1}/C$.

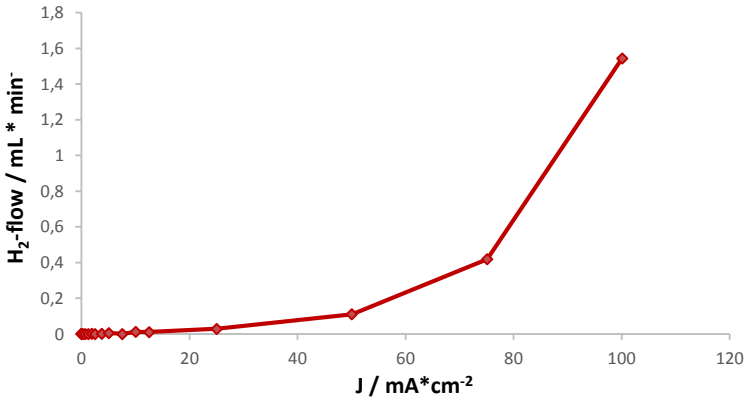

Figure 41: *Results of the online hydrogen detection measurement for MEA3; the hydrogen current at every DBFC current density step converted to hydrogen flow.*

While on Pt/C hydrolysis did occur at OCV and low current densities, hydrolysis did not occur on $P_{0.9}Bi_{0.1}$/C until high current densities, as represented in **Figure 41**. These results match those of the hydrogen detection measurement on MEA2 with $Pt_{0.8}Bi_{0.2}$/C. This means the lower Bi content has no negative effect on the suppression of hydrolysis at OCV conditions and low current densities.

The increase of the hydrogen flow rate starts slowly at 25 mA/cm^2 and then increases drastically at high current densities. At the points where the DBFC reaches its maximum power density the hydrolysis is greatly promoted. As a consequence, the efficiency at high power density is reduced. The reasons are the same as for $Pt_{08}Bi_{0.2}$/C and a thorough discussion can be found in section 3.6.2. As discussed the pH optimization could lead to a very promising DBFC system.

4.6.4 In-situ experiments with $Pt_{0.9}In_{0.1}$/C as anode catalyst (MEA4)

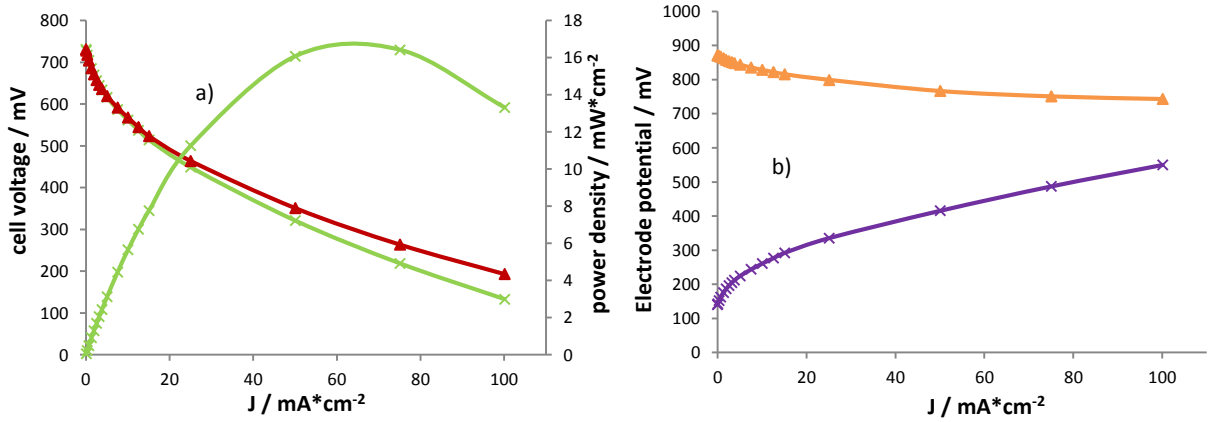

Figure 42: *Polarisation curve of MEA5 at 40°C: $Pt_{0.9}In_{0.1}$/C Anode with 1 mg/cm^2 Pt-loading vs. a MnO_2/C Cathode; Tokuyama membrane; a) polarization curve; red line = I*R compensation b) anode and cathode polarization*

The cathode of MEA 5 shows similar kinetic performances as the cathodes of MEA 2 and MEA 3.

By using $Pt_{0.9}In_{0.1}/C$ as anode catalyst the performance dropped drastically in comparison to $Pt_{0.9}Bi_{0.1}/C$. The kinetic losses are even greater than for MEA2 in **Figure 38**. While the OCV was comparable with 731 mV, the voltage drops for approx. 180 mV to reach 12.5 mA/cm^2. These losses originate from the high anode overpotential as can be seen in **Figure 42 b)**. 85 mV are lost from the open circuit potential to reach a linear potential drop. This is comparable to the losses of $Pt_{0.8}Bi_{0.2}/C$. The greater kinetic losses indicate the poor activity of the In modified catalyst.

The performance losses lead to a maximum power density of 16 mW/cm^2. That is a similar performance as $Pt_{0.8}Bi_{0.2}/C$ as anode catalysts. This shows that In has a greater effect on the kinetics of the BOR. Therefore, a further reduction of the indium content is advisable to reduce these kinetic limitations.

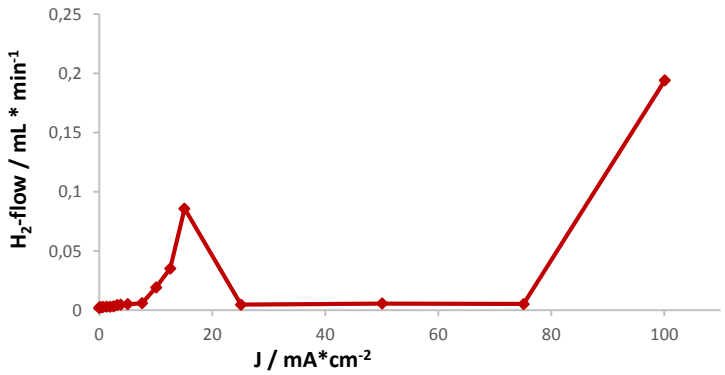

Figure 43: *Results of the online hydrogen detection measurement for MEA2; the hydrogen current at every DBFC current density step converted to hydrogen flow.*

The hydrogen detection measurement in **Figure 43** reveals, that a reduction of the In content is possible. Although the hydrogen flow increases to about 0.1 mL/min at 15 mA/cm^2 it sinks again shortly after that. The catalyst has the ability to oxidize hydrogen at increased anode potentials. This was already discussed for Pt/C in section 4.6.1.

At very high current densities 0.2 mL/min leave the DBFC. This means that due to the increasing pH gradient effect more hydrogen is created on the anode, which cannot be oxidized fast enough. Nevertheless, compared to the Bi modified catalysts indium has a more favourable effect on the borohydride hydrolysis properties. The stronger kinetic limitations of In need to be reduced though, to allow a practical application. Reduction of the In content could lead to a more favourable catalyst.

5 Conclusion and Outlook

This work provides a general overview of the current knowledge on the BOR was given and experimental results revealing new insights, were presented. Furthermore, a cell design was developed using an anion exchange membrane and a BH_4^- tolerant MnO_2 based cathode.

Using electrochemical methods as cyclic voltammetry and rotating disc electrode cyclic voltammetry the kinetic parameters for the BOR on the metals platinum, palladium and gold was determined. Bimetallic catalysts composed of these metals were investigated. It was shown that alloying platinum and gold in molar ratio of 1:1 gave a catalyst with excellent activity towards BOR. It was also proven that METMA-BH_4, DMETMA-BH_4 and TMPA-BH_4 can be used as fuels for a direct borohydride fuel cell. These compounds have an enhanced solubility in water and show a better long term stability than $NaBH_4$. Therefore, they are very promising for an application in DBFCs. Especially $Pt_{0.5}Au_{0.5}$/C combined with METMA-BH_4 exhibited desirable BOR behaviour. Pd/C also gave satisfactory results with METMA-BH_4 and TMPA-BH_4, but showed signs of gradual catalyst poisoning by the nitrogen species. This was not the case for $Pt_{0.5}Au_{0.5}$/C and METMA-BH_4. A DBFC system using these two compounds could lead to promising results. Further measurements in in-situ conditions need to be done to find the optimal fuel and catalyst.

The suppression of the hydrogen evolution on metal surfaces from the BH_4^- ion was very successful. By adding 10 to 20 mol% of Bi or In this reaction was inhibited at OCV conditions and for low current densities. Especially when using $Pt_{0.9}Bi_{0.1}$/C as anode catalyst the hydrolysis reaction was supressed with a power density loss of 10 mW/cm^2 compared to Pt/C. At current densities above 50 mW/cm^2 the hydrogen flow out of the cell increased to the values of Pt/C at OCV. This was attributed to the local decrease of $[OH^-]$ on the electrode surface.

Therefore, in future studies concerning inhibition with Bi or In the $[OH^-]$ should be increased. The low solubility of the by-product BO_2^- at higher pH values will pose an upper limit. Therefore, an optimum pH value has to be found.

To reduce the losses of power density a gradual reduction of Bi or In content in the catalysts will be needed to find an optimum where hydrolysis is supressed and the power density of the cell is satisfactory.

An optimization of the fuel mix would be a next step to further increase storage density and find reduce hydrolysis. For this purpose, taking the effect of the $[OH^-]/[BH_4^-]$ ratio and the poor solubility of BO_2^- into account will be necessary.

DBFC technology has proven to have great potential for niche- and stationary applications and this study showed how the problem of hydrolysis can be solved. A further development can lead

to a storage and conversion system with good storage densities and a liquid fuel, where existing infrastructure for transport could be used.

6 References

[1] J. P. Elder and a. Hickling, *Trans. Faraday Soc.*, vol. 58, p. 1852, 1962.

[2] M. V. Mirkin, *J. Electrochem. Soc.*, vol. 139, no. 8, p. 2212, 1992.

[3] M. Chatenet, M. B. Molina-Concha, and J.-P. Diard, *Electrochim. Acta*, vol. 54, no. 6, pp. 1687–1693, Feb. 2009.

[4] F. a. Coowar, G. Vitins, G. O. Mepsted, S. C. Waring, and J. a. Horsfall, *J. Power Sources*, vol. 175, no. 1, pp. 317–324, Jan. 2008.

[5] V. Kiran, T. Ravikumar, N. T. Kalyanasundaram, S. Krishnamurty, a. K. Shukla, and S. Sampath, *J. Electrochem. Soc.*, vol. 157, no. 8, p. B1201, 2010.

[6] E. Gyenge, M. Atwan, and D. Northwood, *J. Electrochem. Soc.*, vol. 153, no. 1, p. A150, 2006.

[7] D. a Finkelstein, N. Da Mota, J. L. Cohen, and H. D. Abruña, *J. Phys. Chem. C*, vol. 113, no. 45, pp. 19700–19712, 2009.

[8] E. Gyenge, *Electrochim. Acta*, vol. 49, pp. 965–978, 2004.

[9] U. Eberle, M. Felderhoff, and F. Schüth, *Angew. Chem. Int. Ed. Engl.*, vol. 48, no. 36, pp. 6608–30, Jan. 2009.

[10] K. G. Di Santo, E. Kanashiro, S. G. Di Santo, and M. A. Saidel, *Renew. Sustain. Energy Rev.*, vol. 52, pp. 1072–1082, 2015.

[11] S. Gupta and N. Hawtin, *Nature*, vol. 526, pp. S90-91, 2015.

[12] K. O'Malley, G. Ordaz, J. Adams, K. Randolph, C. C. Ahn, and N. T. Stetson, *J. Alloys Compd.*, vol. 645, pp. S419–S422, 2014.

[13] V. N. Emel'yanenko, M. A. Varfolomeev, S. P. Verevkin, K. Stark, K. Müller, M. Müller, A. Bösmann, P. Wasserscheid, and W. Arlt, *J. Phys. Chem. C*, p. acs.jpcc.5b10392, 2015.

[14] D. Geburtig, P. Preuster, A. Bösmann, K. Müller, and P. Wasserscheid, *Int. J. Hydrogen Energy*, pp. 1–8, 2015.

[15] G. Leitner, *Thermochim. acta*, vol. 391, pp. 159–168, 2002.

[16] C. W. Yoon and L. G. Sneddon, *J. Am. Chem. Soc.*, vol. 2, no. 0, pp. 13992–13993, 2006.

[17] P. Chen, Z. Xiong, J. Luo, J. Lin, and K. L. Tan, *Lett. to Nat.*, vol. 420, no. November, pp. 20–22, 2002.

[18] S. Hino, T. Ichikawa, N. Ogita, and H. Fujii, *Chem. Commun.*, pp. 3038–3040, 2005.

[19] Y. Okada, E. Sasaki, E. Watanabe, S. Hyodo, and H. Nishijima, *Int. J. Hydrogen Energy*, vol. 31, no. 10, pp. 1348–1356, 2006.

[20] M. Felderhoff, F. Schu, and B. Bogdanovic, *Chem. Commun.*, vol. 20, pp. 2249–2258, 2004.

[21] D. W. Rice, C. C. Stephenson, D. W. Rice, and C. Stephenson, *J. Am. Chem. Soc.*, vol. 77, pp. 1980–1983, 1980.

[22] I. Merino-Jimenez, M. J. Janik, C. Ponce de Leon, and F. C. Walsh, *J. Power Sources*, vol. 269, pp. 498–508, Dec. 2014.

[23] B. H. Liu, Z. P. Li, and S. Suda, *Electrochim. Acta*, vol. 49, no. 19, pp. 3097–3105, Aug. 2004.

[24] M. Chatenet, F. H. B. Lima, and E. A. Ticianelli, *J. Elecrtochem.Soc.*, vol. 157, pp. 1–8, 2010.

[25] F. H. B. Lima, A. M. Pasqualeti, M. B. Molina, M. Chatenet, and E. A. Ticianelli, *Electrochim. Acta*, vol. 84, pp. 202–212, 2012.

[26] M. Concha, M. Chatenet, E. A. Ticianelli, F. H. B. Lima, U. De S, and A. T. S, *J. Phys. Chem. C*,

pp. 12439–12447, 2011.

[27] G. Rostamikia and M. J. Janik, *Electrochim. Acta*, vol. 55, pp. 1175–1183, 2010.

[28] G. Rostamikia, A. J. Mendoza, M. A. Hickner, and M. J. Janik, *J. Power Sources*, vol. 196, no. 22, pp. 9228–9237, 2011.

[29] G. Rostamikia and M. J. Janik, *Energy Environ. Sci.*, vol. 3, pp. 1262–1274, 2010.

[30] I. Ohno and S. Haruyama, *J. Electrochem. Soc.*, vol. 132, pp. 2323–2330, 1985.

[31] M. Chatenet, F. Micoud, I. Roche, and E. Chainet, *Electrochim. Acta*, vol. 51, pp. 5459–5467, 2006.

[32] B. Y. J. A. Gardiner and J. M. I. Collat, *Inorg. Chem.*, vol. 4903, no. 8, pp. 1208–1212, 1965.

[33] J. A. Gardiner and J. W. Collat, *J. Am. Chem. Soc.*, vol. 1964, no. 6, pp. 1692–1700, 1965.

[34] F. G. Boyacı San, O. Okur, Ç. İyigün Karadağ, I. Isik-Gulsac, and E. Okumuş, *Energy*, vol. 71, pp. 160–169, Jul. 2014.

[35] M. G. Hosseini and M. Abdolmaleki, *Int. J. Hydrogen Energy*, vol. 38, no. 13, pp. 5449–5456, May 2013.

[36] S. Limpattayanate and M. Hunsom, *Renew. Energy*, vol. 63, pp. 205–211, Mar. 2014.

[37] Y. Lu, Z. Xu, H. A. Gasteiger, S. Chen, and K. Hamad-schifferli, *J. Am. Chem. Soc.*, pp. 12170–12171, 2010.

[38] B. Šljukić, J. Milikić, D. M. F. Santos, and C. a. C. Sequeira, *Electrochim. Acta*, vol. 107, pp. 577–583, Sep. 2013.

[39] C. Grimmer, R. Zacharias, M. Grandi, B. Pichler, I. Kaltenboeck, F. Gebetsroither, J. Wagner, B. Cermenek, S. Weinberger, A. Schenk, and V. Hacker, *J. Electrochem. Soc.*, vol. 163, no. 3, pp. 278–283, 2016.

[40] H. Dong, R. Feng, X. Ai, Y. Cao, H. Yang, and C. Cha, *J. Phys. Chem. B*, vol. 109, no. 21, pp. 10896–901, Jun. 2005.

[41] D. Šimkūnaitė, L. Tamašauskaitė-, and V. Jasulaitienė, *Chemija*, vol. 25, no. 3, pp. 171–184, 2014.

[42] P. Krishnan, T. H. Yang, S. G. Advani, and A. K. Prasad, *J. Power Sources*, vol. 182, no. 1, pp. 106–111, 2008.

[43] L. Gao and B. E. Conway, *Electrochim. Acta*, vol. 39, no. 11, 1994.

[44] M. Auinat and D. Starosvetsky, *J. Power Sources*, vol. 114, pp. 330–337, 2003.

[45] J. Huot and E. Boubour, *J. Power Sources*, vol. 65, pp. 81–85, 1997.

[46] Y. Sato and M. Takahashi, *J. Power Sources*, vol. 38, pp. 317–325, 1992.

[47] A. R. S. Kannan, S. Muralidharan, K. B. Sarangapani, V. Balaramachandran, and V. Kapali, *J. Power Sources*, vol. 57, pp. 93–98, 1995.

[48] M. Simões, S. Baranton, and C. Coutanceau, *Electrochim. Acta*, vol. 56, no. 1, pp. 580–591, Dec. 2010.

[49] S. Gabriel and J. Weiner, *Chem. Ber.*, vol. 21, pp. 2669–2679, 1888.

[50] N. V Plechkova and K. R. Seddon, *Chem. Soc. Rev.*, vol. 37, pp. 123–150, 2008.

[51] C. Grimmer, M. Grandi, R. Zacharias, S. Weinberger, A. Schenk, E. Aksamija, F. Mautner, B. Bitschnau, and V. Hacker, *J. Electrochem. Soc.*, vol. 163, no. 8, 2016.

[52] C. Grimmer, S. Nestl, J. Senn, and V. Hacker, *Int. J. Hydrogen Energy*, vol. 40, no. 4, pp. 2055–

2061, 2014.

[53] M. Reetz, WO 2003078056 A1, 2003.

[54] C. Hamann and W. Vielstich, *Elektrochemie*. Wiley VCH, 2005.

[55] H. Kimura and K. Tsuto, *Appl. Catal. A*, vol. 96, no. c, pp. 217–228, 1993.

[56] N. Takeno, *Geol. Surv. Japan Open File Rep.*, vol. 419, pp. 46–47, 2005.

[57] C. Grimmer, M. Grandi, R. Zacharias, B. Cermenek, H. Weber, C. Morais, T. W. Napporn, S. Weinberger, A. Schenk, and V. Hacker, *Applied Catal. B, Environ.*, vol. 180, pp. 614–621, 2016.

[58] Y. Zhai, J. Ge, and J. St-Pierre, *Electrochem. commun.*, vol. 66, pp. 49–52, 2016.

7 Attachments

7.1 RDE-CVs of Pt/C in presence of Ionic Liquids

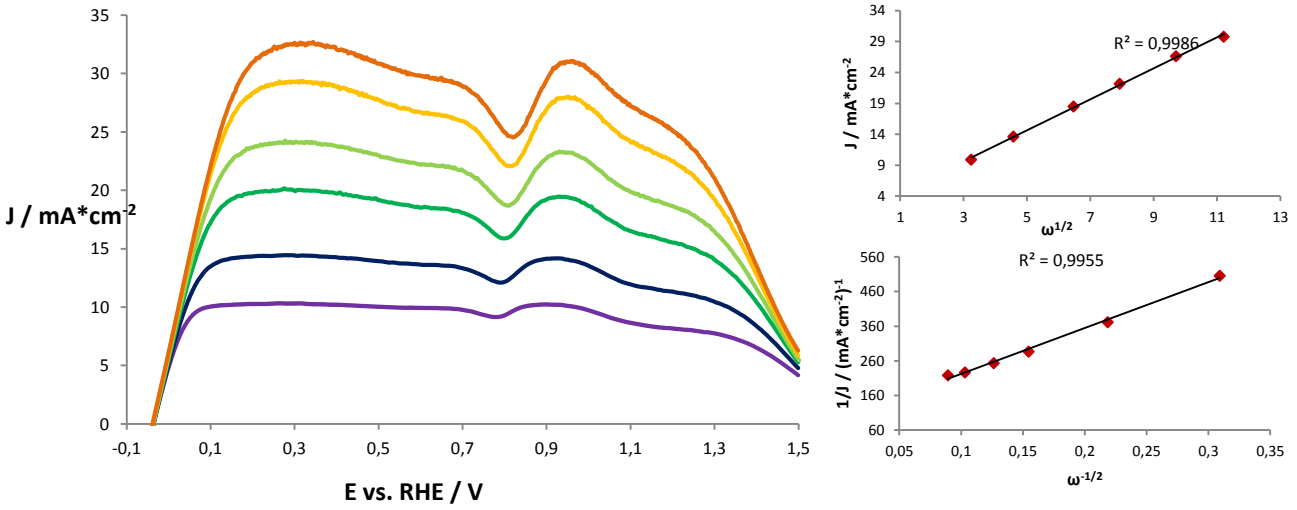

Figure 44: *Rotating disc electrode cyclic voltagrammogram, Levich and Koutecky-Levich plots of Pt/C (50 wt%) from Alfa Aesar in 5mM* ***METMA-BH₄*** *and 1M NaOH, 28 µg/cm², -0.05 to 1.5 V vs RHE, 10 mV/s; rotation rates are: 100, 200, 400, 600, 900 and 1200 rpm.*

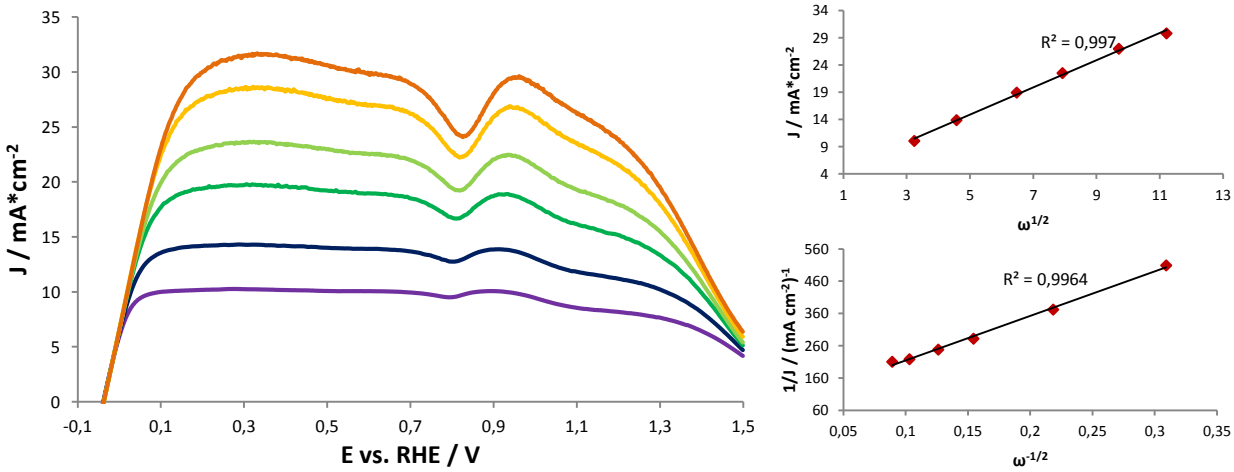

Figure 45: *Rotating disc electrode cyclic voltagrammogram, Levich and Koutecky-Levich plots of Pt/C (50 wt%) from Alfa Aesar in 5mM* ***DMETMA-BH₄*** *and 1M NaOH, 28 µg/cm², -0.05 to 1.5 V vs RHE, 10 mV/s; rotation rates are: 100, 200, 400, 600, 900 and 1200 rpm.*

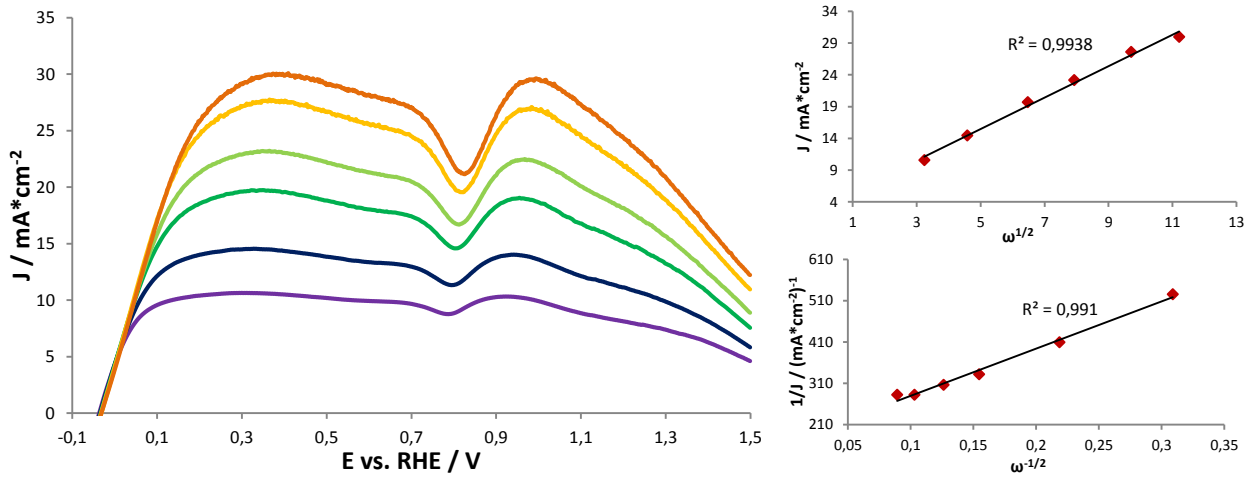

Figure 46: *Rotating disc electrode cyclic voltagrammogram, Levich and Koutecky-Levich plots of Pt/C (50 wt%) from Alfa Aesar in 5mM* ***TMPA-BH₄*** *and 1M NaOH, 28 µg/cm², -0.05 to 1.5 V vs RHE, 10 mV/s; rotation rates are: 100, 200, 400, 600, 900 and 1200 rpm.*

7.2 RDE-CV of Au/C in presence of ionic liquids

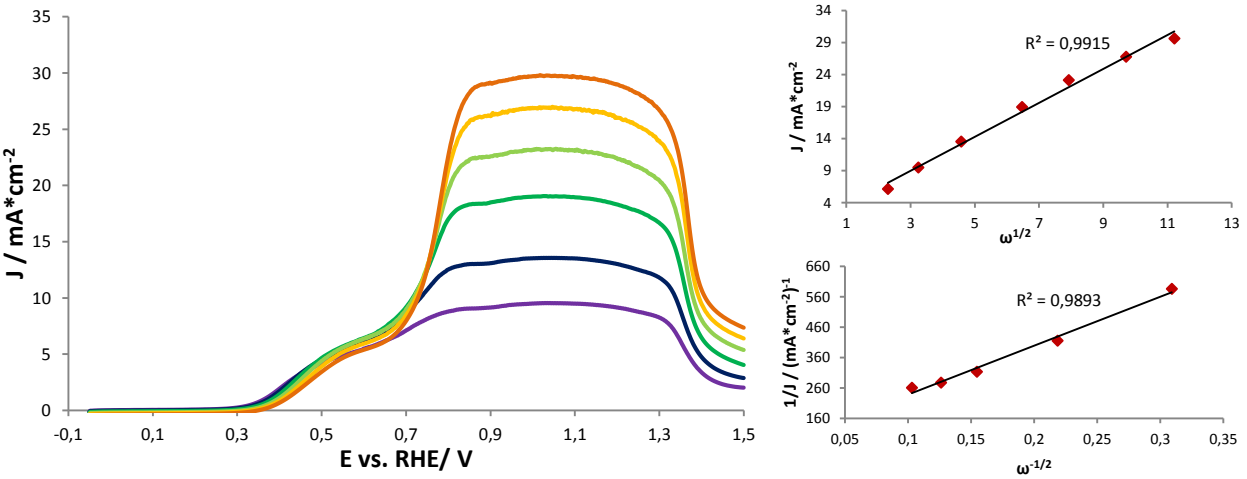

Figure 47: Rotating disc electrode cyclic voltagrammogram, Levich and Koutecky-Levich plots of Au/C (40 wt%) in 5mM **METMA-BH₄** and 1M NaOH, 56 µg/cm², -0.05 to 1.5 V vs RHE, 10 mV/s; rotation rates are: 100, 200, 400, 600, 900 and 1200 rpm.

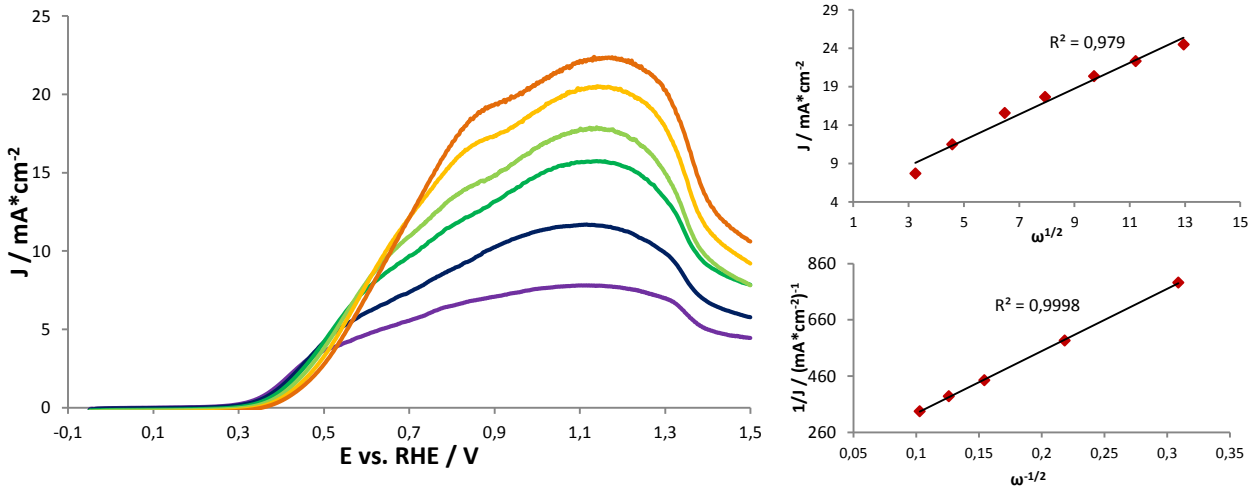

Figure 48: *Rotating disc electrode cyclic voltagrammogram, Levich and Koutecky-Levich plots of Au/C (40 wt%) in 5mM* ***DMETMA-BH₄*** *and 1M NaOH, 56 µg/cm², -0.05 to 1.5 V vs RHE, 10 mV/s; rotation rates are: 100, 200, 400, 600, 900 and 1200 rpm.*

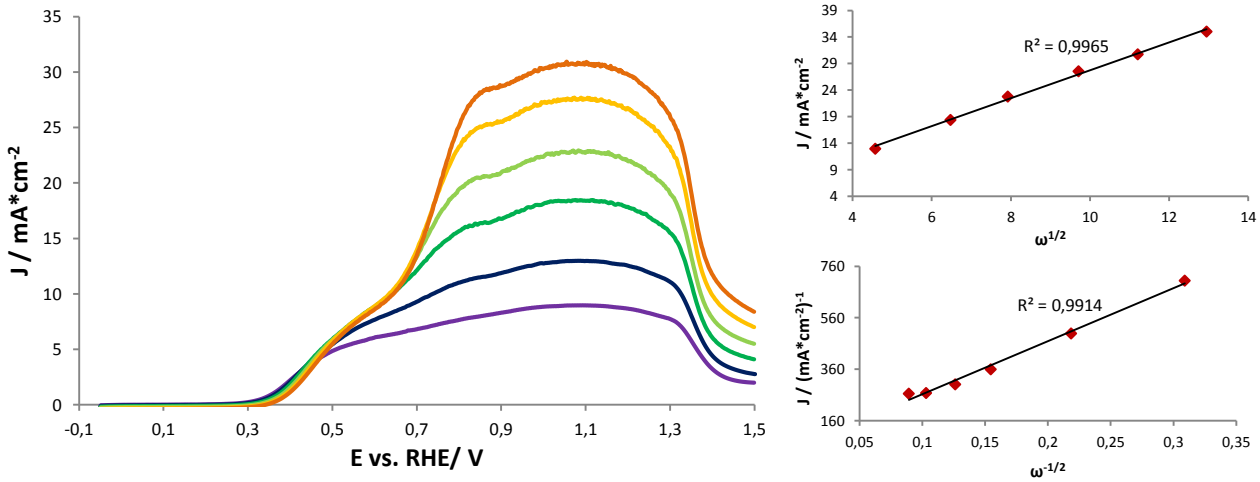

Figure 49: *Rotating disc electrode cyclic voltagrammogram, Levich and Koutecky-Levich plots of Au/C (40 wt%) in 5mM* ***TMPA-BH₄*** *and 1M NaOH, 56 µg/cm², -0.05 to 1.5 V vs RHE, 10 mV/s; rotation rates are: 100, 200, 400, 600, 900 and 1200 rpm.*

7.3 RDE-CV of Pd/C in presence of ionic liquids

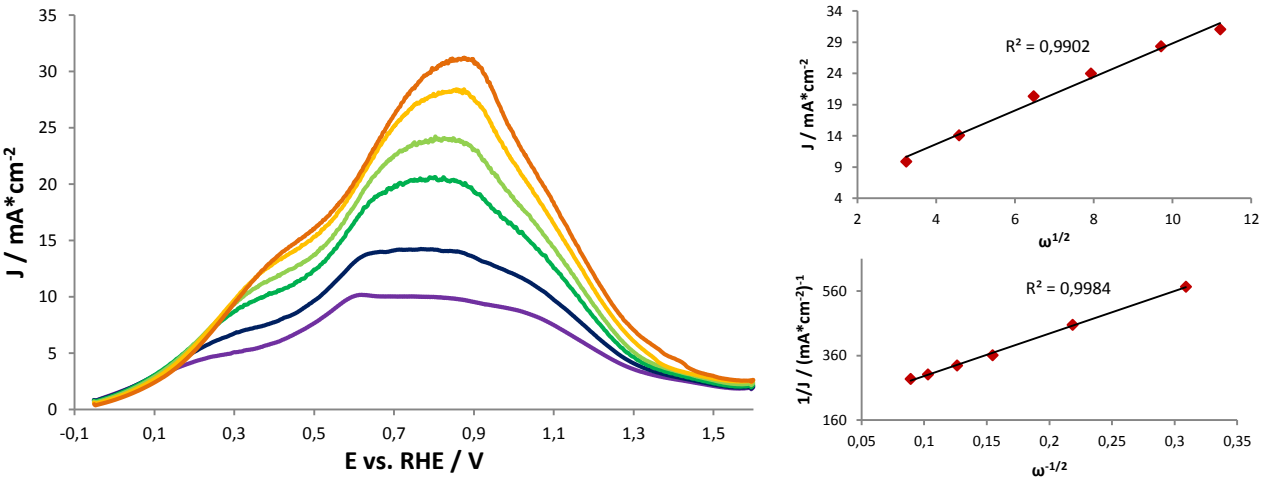

Figure 50: *Rotating disc electrode cyclic voltagrammogram, Levich and Koutecky-Levich plots of Pd/C (40 wt%) in 5mM* ***METMA-BH₄*** *and 1M NaOH, 28 µg/cm², -0.05 to 1.6 V vs RHE, 10 mV/s; rotation rates are: 100, 200, 400, 600, 900 and 1200 rpm.*

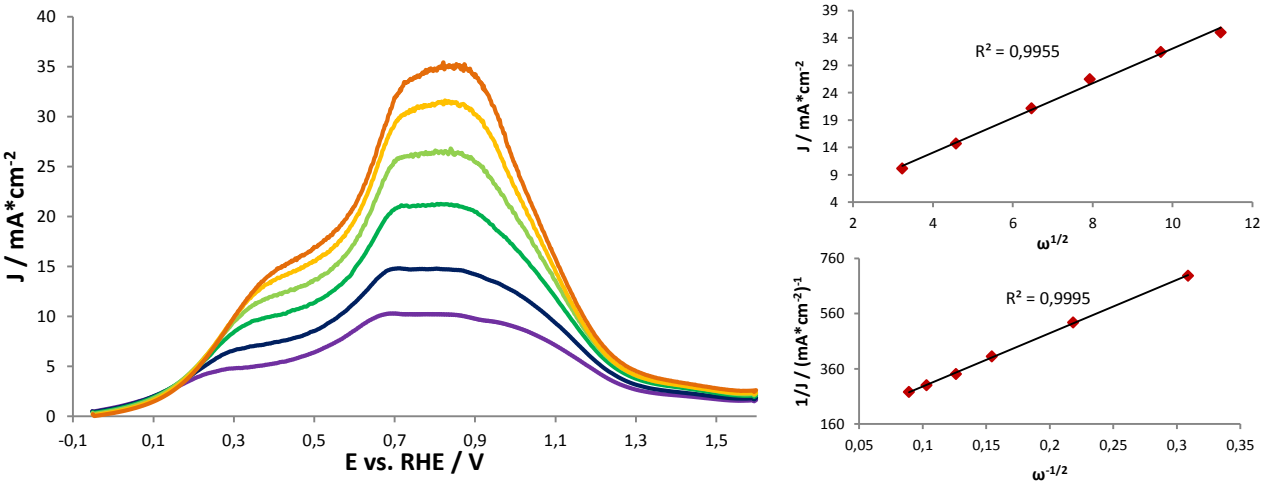

Figure 51: *Rotating disc electrode cyclic voltagrammogram, Levich and Koutecky-Levich plots of Pd/C (40 wt%) in 5mM* ***DMETMA-BH₄*** *and 1M NaOH, 28 µg/cm², -0.05 to 1.6 V vs RHE, 10 mV/s; rotation rates are: 100, 200, 400, 600, 900 and 1200 rpm.*

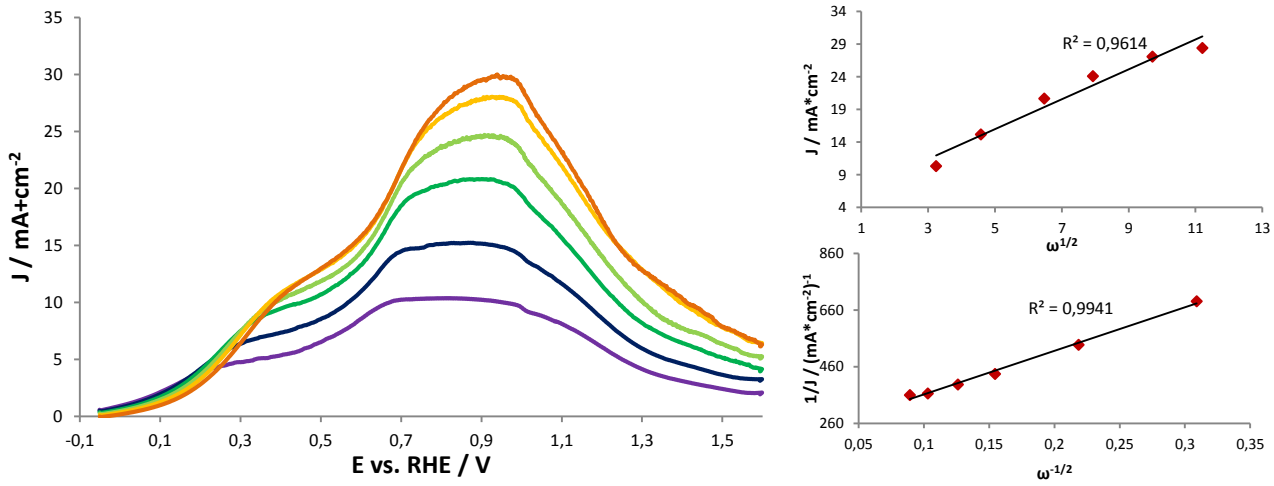

Figure 52: *Rotating disc electrode cyclic voltagrammogram, Levich and Koutecky-Levich plots of Pd/C (40 wt%) in 5mM* ***TMPA-BH₄*** *and 1M NaOH, 28 µg/cm², -0.05 to 1.6 V vs RHE, 10 mV/s; rotation rates are: 100, 200, 400, 600, 900 and 1200 rpm.*

7.4 RDE-CV of $Pt_{0.5}Au_{0.5}$/C in presence of ionic liquids

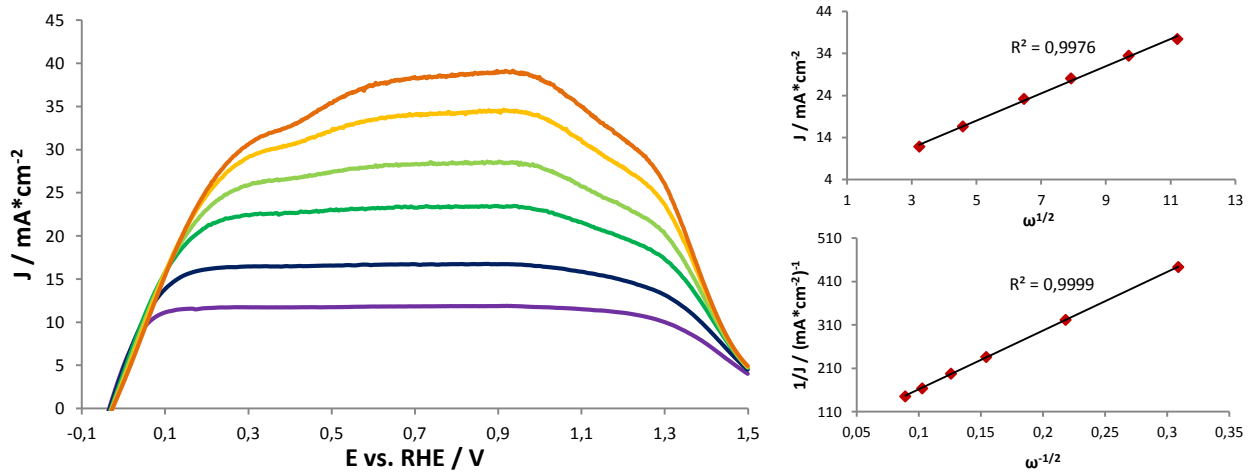

Figure 53: *Rotating disc electrode cyclic voltagrammogram, Levich and Koutecky-Levich plots of $Pt_{0.5}Au_{0.5}$/C (40 wt%) in 5mM* ***METMA-BH₄*** *and 1M NaOH, 42 µg/cm², -0.05 to 1.5 V vs RHE, 10 mV/s; rotation rates are: 100, 200, 400, 600, 900 and 1200 rpm.*

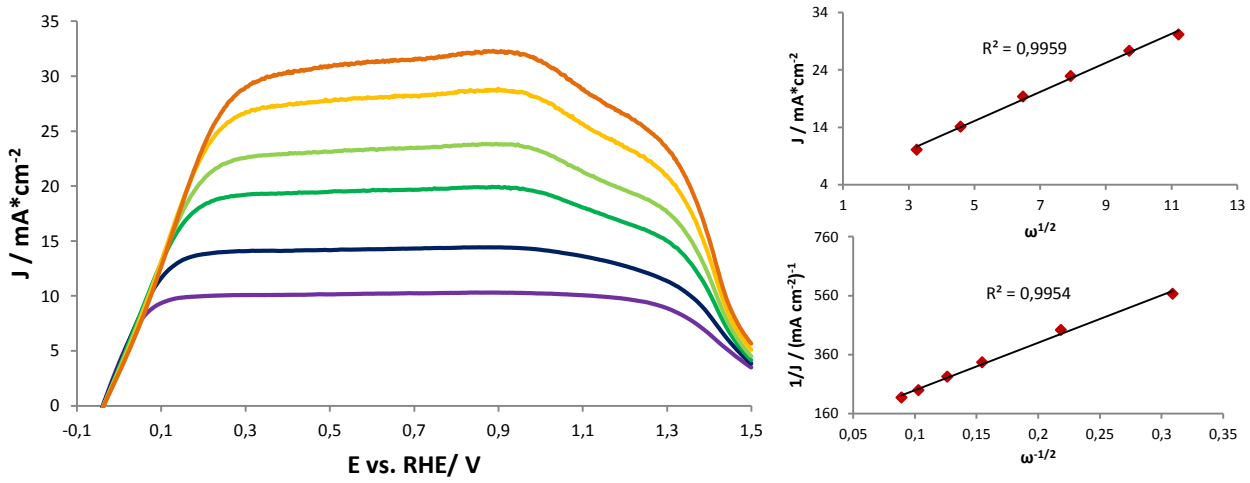

Figure 54: *Rotating disc electrode cyclic voltagrammogram, Levich and Koutecky-Levich plots of $Pt_{0.5}Au_{0.5}$/C (40 wt%) in 5mM* ***DMETMA-BH₄*** *and 1M NaOH, 42µg/cm², -0.05 to 1.5 V vs RHE, 10 mV/s; rotation rates are: 100, 200, 400, 600, 900 and 1200 rpm.*

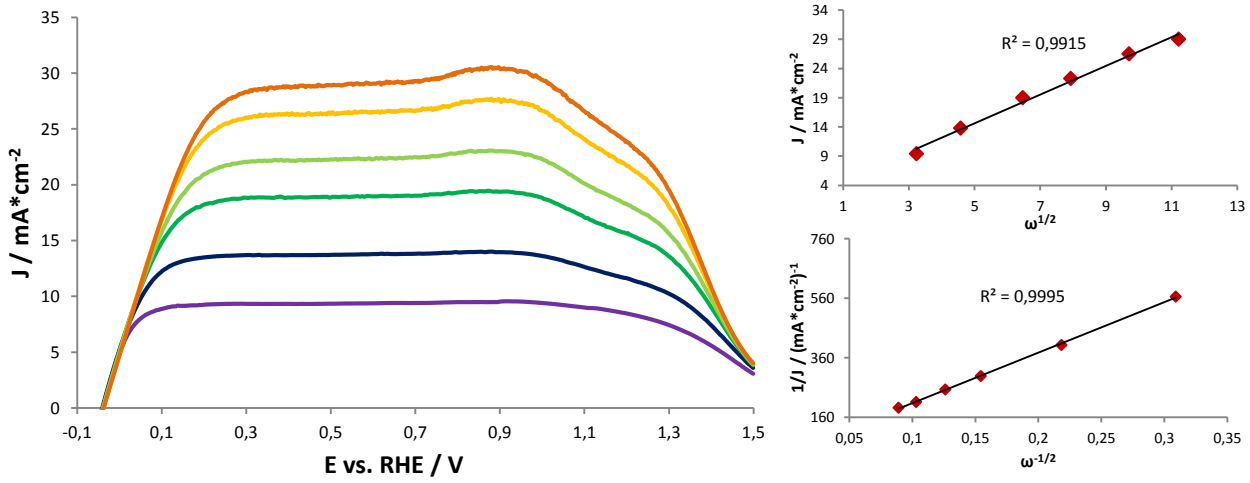

Figure 55: *Rotating disc electrode cyclic voltagrammogram, Levich and Koutecky-Levich plots of $Pt_{0.5}Au_{0.5}$/C (40 wt%) in 5mM* ***TMPA-BH₄*** *and 1M NaOH, 42 µg/cm², -0.05 to 1.5 V vs RHE, 10 mV/s; rotation rates are: 100, 200, 400, 600, 900 and 1200 rpm.*

7.5 Mass transport normed RDE-CV of Pt/C in presence of $NaBH_4$

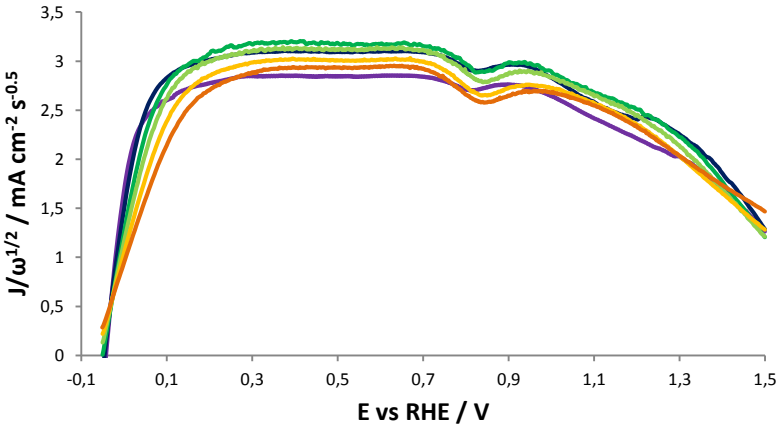

Figure 56: *Mass transport normed RDE-CV of Pt/C (50%) in 5mM $NaBH_4$ and 1M NaOH, 28 µg/cm², -0.05 to 1.5 V vs RHE, 10 mV/s; rotation rates are: **100**, **200**, **400**, **600**, **900** and **1200** rpm.*

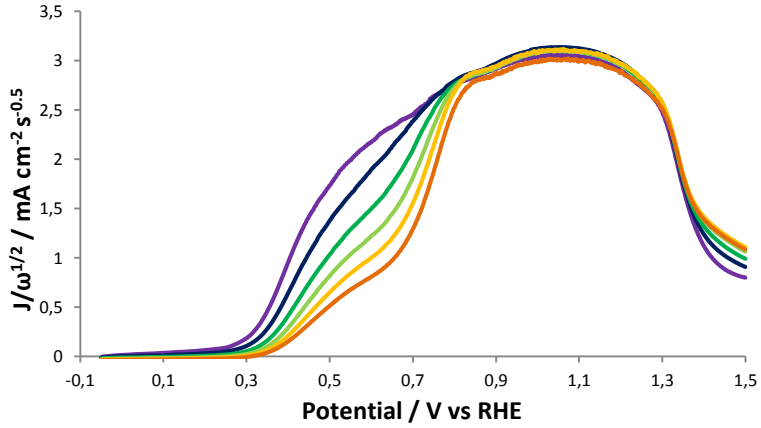

Figure 57: *Mass transport normed RDE-CV of Au/C (40%) in 5mM $NaBH_4$ and 1M NaOH, 56 µg/cm², -0.05 to 1.5 V vs RHE, 10 mV/s; rotation rates are: **100**, **200**, **400**, **600**, **900** and **1200** rpm.*